AD NUMBER

AD900487

NEW LIMITATION CHANGE

TO

Approved for public release, distribution unlimited

FROM

Distribution authorized to U.S. Gov't. agencies only; Test and Evaluation; 24 MAY 1972. Other requests shall be referred to Naval Ordnance Laboratory, Attn: Code 241, Silver Spring, MD 20910.

AUTHORITY

NOL, per DTIC Form 55

NOLTR 72-102

BLAST AND FRAGMENT HAZARDS FROM BURSTING HIGH PRESSURE TANKS

By
J. F. Pittman

17 MAY 1972

NOL

NAVAL ORDNANCE LABORATORY, WHITE OAK, SILVER SPRING, MARYLAND

NOLTR 72-102

BLAST AND FRAGMENT HAZARDS FROM BURSTING HIGH PRESSURE TANKS

Prepared by:
J. F. Pittman

ABSTRACT: Five pressure vessels that are used in the flight hardware of spacecraft were inflated until they burst. Airblast and fragment parameters were measured to evaluate the hazards from the accidental rupture of such tanks during their handling, checkout, and use. Tank volumes ranged up to 6 ft^3, skin thicknesses up to 0.368 inches, and burst pressures up to 8,000 psi.

Airblast results showed that tank rupture generated shockwave overpressures and impulses at high enough levels to be a significant hazard to personnel and equipment. Rupture blast energy could not be equated to a single TNT blast yield. The tanks burst into as many as 60 fragments, some weighing several pounds. These fragments attained maximum velocities of about 1400 ft/sec.

AIR/GROUND EXPLOSIONS DIVISION
EXPLOSIONS RESEARCH DEPARTMENT
NAVAL ORDNANCE LABORATORY
SILVER SPRING, MARYLAND

NOLTR 72-102 17 May 1972

Blast and Fragment Hazards From Bursting High Pressure Tanks

Thin-walled pressure vessels make up a large portion of the flight hardware of missile systems. The hazards resulting from their accidental rupture during tests, checkouts, and use must be assessed for safety considerations and planning purposes. This report describes work done to determine the available energy and potential damage from an unplanned rupture.

This task was funded by the Safety Office, NASA, Kennedy Space Center as NOL Task #577/NASA, Work Unit X01. The experimental work was carried out at the Naval Ordnance Laboratory's Stump Neck Test Facility at Indian Head, Maryland. The mention of proprietary items in this report constitutes neither criticism nor endorsement of such products by the Naval Ordnance Laboratory.

ROBERT WILLIAMSON II
Captain, USN
Commander

C. J. ARONSON
By direction

CONTENTS

		Page
1.	Introduction	1
1.1	Background	1
1.2	Scope of the Experiment and Objectives	1
2.	Experimental Procedures	4
2.1	Test Site and Firing Arena	4
2.2	Tank Pressurization	4
2.2.1	Pressurization System	4
2.2.2	Pressure System Operation	10
2.2.3	History of the Pressurization of Tanks A and B	12
2.2.4	Pressurization of Tanks C and D	12
2.2.5	Pressurization of Tank E	12
2.3	Instrumentation	15
2.3.1	Blast Instrumentation	15
2.3.2	Fragment Velocity System	17
2.3.3	Photography of the Anthropomorphic Dummies	19
2.3.4	Sequence of Operations	19
3.	Blast Measurements	21
3.1	Theory and Background	21
3.2	Blast Gage Layout	21
3.3	Pressure-time Histories	21
3.4	Blast Results	38
3.4.1	Pressure Results from Tanks A and B	38
3.4.2	Pressure Results from Tank C	41
3.4.3	Pressure Results from Tanks D and E	41
3.5	Positive Shockwave Durations	48
3.5.1	Durations for Tanks A and B	48
3.5.2	Durations for Tank C	48
3.5.3	Durations for Tanks D and E	52
3.6	Positive Shockwave Impulse	52
3.6.1	Impulse from Tanks A and B	52
3.6.2	Impulse from Tank C	52
3.6.3	Impulse from Tanks D and E	58
4.	Fragmentation Results	61
4.1	Setup for Fragment Samples	61
4.2	Fragment Recovery	62

CONTENTS (Cont'd)

	Page
4.2.1 Fragments from Tank A	62
4.2.2 Fragments from Tank B	62
4.2.3 Fragments from Tank C	65
4.2.4 Fragments from Tank D	65
4.2.5 Fragments from Tank E	65
4.3 Fragment Velocities	70
4.3.1 Velocities of Tank A Fragments	70
4.3.2 Velocities of Tank B Fragments	75
4.3.3 Velocities of Tank C Fragments	78
4.3.4 Velocities of Tanks D and E Fragments	78
5. Anthropomorphic Dummies	86
6. Discussion	87
6.1 Tank Pressurization	87
6.2 Summary of Blast Measurements	87
6.3 Fragmentation	95
6.3.1 Fragment Density	95
6.3.2 Fragment Velocities	96
6.4 Qualitative Damage	98
7. Conclusions	100
REFERENCES	101
ACKNOWLEDGEMENTS	102
APPENDIX A	118
APPENDIX B	124

ILLUSTRATIONS

Figure	Title	
2.1	Experimental Set up for Tanks A, B, C, and D	5
2.2	Arena Construction	6
2.3	The High Pressure System	7
2.4	Discharge Volume vs Pump Supply Pressure	9
2.5	10,000 psi Line Gage Calibration	11
2.6	Pressure vs Time for Tank C	13
2.7	Pressure vs Time for Tank D	14
2.8	Pressure vs Time for Tank E	16
2.9	Strobe Unit (2 Required)	18
3.1	Field Layout for Tank D; 6 ft^3 Tank	22
3.2	Pressure Time Histories from Tank A	23

ILLUSTRATIONS (Cont'd)

Figure	Title	Page
3.3	Pressure Time Histories from Tank B	26
3.4	Pressure Time Histories from Tank C	29
3.5	Pressure Time Histories from Tank D	32
3.6	Pressure Time Histories from Tank E	35
3.7	Pressure Time Histories from 8.2-lb TNT Spheres	37
3.8	Side-on Overpressures from Tank A; 1.34 ft^3 Burst at 625 psi	39
3.9	Side-on Overpressure from Tank B; 1.68 ft^3 Burst at 600 psi	40
3.10	Face-on Pressures from Tank A; 1.34 ft^3 Burst at 625 psi	42
3.11	Face-on Pressures from Tank B; 1.68 ft^3 Burst at 600 psi	43
3.12	Side-on Overpressures from Tank C; 0.235 ft^3 Burst at 8,000 psi	44
3.13	Face-on Pressures from Tank C; 0.235 ft^3 Burst at 8,000 psi	45
3.14	Side-on Overpressures from Tanks D and E; 6 ft^3 Burst at 8,000 psi	46
3.15	Face-on Pressure from Tank D; 6 ft^3 Tank Burst at Nominal 8,000 psi	47
3.16	Side-on Positive Duration from Tank A; 1.34 ft^3	49
3.17	Side-on Positive Duration from Tank B; 1.68 ft^3	50
3.18	Side-on Positive Duration from Tank C; 0.235 ft^3	51
3.19	Side-on Positive Duration from Tank D; 6 ft^3	53
3.20	Side-on Positive Duration from Tank E; 6 ft^3	54
3.21	Side-on Positive Impulse from Tank A; 1.34 ft^3	55
3.22	Side-on Positive Impulse from Tank B; 1.68 ft^3	56
3.23	Side-on Positive Impulse from Tank C; 0.235 ft^3	57
3.24	Side-on Positive Impulse from Tank D; 6 ft^3	59
3.25	Side-on Positive Impulse from Tank E; 6 ft^3	60
4.1	Fragments from Tank A	63
4.2	Fragments from Tank B	64
4.3	Fragments from Tank C	66
4.4	Fragments from Tank D	67
4.5	Approximate Location of Fragments for Tank D	68
4.6	Fragments from Tank E	69
4.7	Approximate Location of Fragments for Tank E	71
4.8	Ground Camera Photo of Tank A Rupture	72
4.9	Tower Camera Photo of Tank A Rupture	73
4.10	Tower Camera Geometry	74
4.11	Ground Camera Photo of Tank B Rupture	76
4.12	Tower Camera Photo of Tank B Rupture	77
4.13	Ground Camera Photo of Tank C Rupture	79
4.14	Tower Camera Photo of Tank C Rupture	80
4.15	Tower Camera Photo of Tank D Rupture	81
4.16	Ground Camera Photo of Tank D Rupture	82

ILLUSTRATIONS (Cont'd)

Figure	Title	Page
4.17	Tower Camera Photo of Tank E Rupture	84
4.18	Ground Camera Photo of Tank E Rupture	85
6.1	Peak Airblast Overpressures from an 8,000 psig Tank Rupture vs Distance in Tank Radii	88
6.2	TNT Equivalence of the Air Blast from an 8,000 psig Tank Rupture Based on Peak Shock Overpressure	89
6.3	Positive Shockwave Impulse from an 8,000 psig Tank Rupture vs Distance in Tank Radii	91
6.4	Peak Airblast Overpressure from a 600 psig Tank Rupture vs Distance in Tank Radii	92
6.5	TNT Equivalence of the Airblast from a 600 psig Tank Rupture Based on Peak Shock Overpressure	93
6.6	Positive Shock Wave Impulse from a 600 psig Tank Rupture vs Distance in Tank Radii	94
6.7	Calculated and Measured Fragment Velocities	97
A-1	Shock Overpressure vs Distance for Exploding Pressure Vessel; 6 ft at 8,000 psi	120
A-2	Space-Time Paths for Explosion of 8,000 psi Air Sphere	121
A-3	Pressure-Time Records for Explosion of 8,000 psi Air Sphere	122
A-4	Calculated Shock Overpressures from 1.34 ft Tank Burst at 460 psi	123
B-1	Basic Geometry for the Calculations	139
B-2	Geometry for Mass Correction	140
B-3	Fragment Radius and Velocity vs Time	141
B-4	Fragment Radius and Velocity vs Time	142
B-5	Fragment Radius and Velocity vs Time	143

TABLES

Table	Title	
1.1	Tank Data	2
3.1	Blast Data from 24" Cylinder; Tank A	103
3.2	Blast Data from 29" Cylinder; Tank B	104
3.3	Blast Data from 0.235 ft^3 Vessel; Tank C	105
3.4	Blast Data from 6 ft^3 Vessel; Tank D	106
3.5	Blast Data from 6 ft^3 Cycled Vessel; Tank E	107
3.6	Blast Data from 8.2-lb TNT Spheres	108
4.1	Fragmentation Data from Tank A	110
4.2	Panel Hits	111
4.3	Fragmentation Data from Tank B	112
4.4	Fragmentation Data from Tank C	113

TABLES (Cont'd)

Table	Title	Page
4.5	Fragmentation Data from Tank D	114
4.6	Fragmentation Data from Tank E	115
4.7	Times of Strobe Flashes	116
4.8	Measured Fragment Velocities	117

1. Introduction

1.1 Background

Thin walled pressure vessels constitute a large portion of the flight hardware of missile systems. The Kennedy Space Center (KSC) is concerned with the integrity of such systems and any hazards that result from their tests, checkouts, and eventual use. The KSC must be able to determine the available energy and potential damage should a pressure vessel rupture. Such data are used for planning purposes and for safety considerations such as the protection of personnel and facilities.

The energy available from pressure vessel rupture can be determined from a formula based on the isentropic expansion of the gas from rupture pressure to ambient atmospheric pressure. A simple method to relate this energy to damaging shock wave overpressures and impulses does not exist; nor can we determine the velocity of tank fragments and their energy from such simple calculations.

This report describes a series of experiments that are designed to produce empirical data on which hazard estimates can be based. The appendices of this report describe the beginnings of theoretical efforts that can be developed into methods to predict blast parameters and fragment velocities from rupturing vessels.

1.2 Scope of the Experiment and Objectives

Five pressure vessels, or tanks, were destructively tested by inflating them with nitrogen until they burst. Blast and fragment data were obtained. In addition three anthopomorphic dummies were placed near the tanks and their response to the blast and fragments photographed. Particular information for each test tank is presented in Table 1.1. The tanks are labeled A through E in the order in which they were fired. They will be so identified throughout this report.

Experimental objectives were:

a) to measure the blast parameters generated by the rupture of nitrogen-filled pressure vessels, attempt to express these results in terms of TNT equivalence, and compare the results with the potential energy in the stored nitrogen.

TABLE 1.1 TANK DATA

Tank Letter Designator	Vessel Type	Vessel Shape	Dimensions	Serial Number	Pressure Data		
					Operate	Burst (Design)	Burst (Actual)
A	Aerozine 50 Fuel Tank	Cylinder with Hemi-spherical ends	Length = 24 inches Diameter = 13 inches Volume = 1.34 feet^3 Weight = 8.5 pounds	100311010010	188 psig	460 psig	625 psig
B	Oxidizer Tank	Same as Tank A	Length = 29 inches Diameter = 13 inches Volume = 1.68 feet^3 Weight = 10.2 pounds	100311020016	138 psig	460 psig	600 psig
C	Helium Tank	Sphere	Diameter = 9.2 inches Volume 0.235 feet^3 Weight = 6.3 pounds	10048ME 00057	4,150 psig	7,500 psig	8,000 psig
D	Helium Pressure Vessel	Sphere	Diameter = 27 inches Volume = 6 feet^3 Weight ≅ 171 pounds	00407ACB 0025	3,250 psig	8,000 psig	8,000 psig
E*	Helium Pressure Vessel	Sphere	Diameter = 27 inches Volume = 6 feet^3 Weight ≅ 170 pounds	00407ACB 0001	3,250 psig	8,000 psig	8,130 psig

* This vessel was pressure cycled prior to rupture

All tanks were made of the same material, titanium, 6 aluminum, 4 Vanadium alloy.

b) to determine the size, weight, distribution, and initial velocity of fragments resulting from tank rupture.

c) to photograph the response of anthropomorphic dummies to the effects of the bursting pressure vessels.

2. Experimental Procedures

2.1 Test Site and Firing Arena

The experiments were conducted at the Naval Ordnance Laboratory's Stump Neck Test Facility near Indian Head, Maryland. The experimental setup of the firing arena, shown in Figure 2.1, was constructed at the bottom of a dry pond. Since our instrument trailer was located only 200 feet from ground zero, the 10-foot high banks of the pond protected it from fragments.

The setup was constructed inside a 40-foot diameter arena whose walls were made from 30 celotex panels. Each panel was made from 12 sheets of celotex banded to suitable wood frames (Figure 2.2). A 5.4-foot opening was left in the arena wall for an entrance and for the ground camera station.

A reenforced concrete firing pad was poured flush with the ground in the center of the arena. This pad was 4' x 4' x 1.5'. A 3" pipe led through the pad to a centrally located 10" x 10" x 10" hole in the top center of the pad. High pressure tubing was fed through the 3" pipe to a junction where connections to the test tanks were made. The junction suffered little damage with this arrangement and the same junction was used for the first four tanks.

Other equipment shown includes the three blast-gage lines, the camera station, the dummies, and the reflecting screen. Location and function of these equipments will be discussed later under the appropriate heading.

2.2 Tank Pressurization

2.2.1 Pressurization System

All tanks were pressurized with N_2. The main components in the pressurization system, shown in Figure 2.3, are described below.

The heart of the pressurization system was a one-cylinder Corblin high-pressure pump, Model A4C-600, capable of pumping approximately 0.25 lbs. of N_2 per minute at a pressure of 9,000 psi. A 20-horsepower, 220 V. 3-phase motor was used to drive the pump. An independent 30 Kw generator was used, in turn, to supply power for the motor-pump unit. The input (supply) pressure to the pump was allowed to vary between 1,500 and 2,000 psi and was dependent upon the number

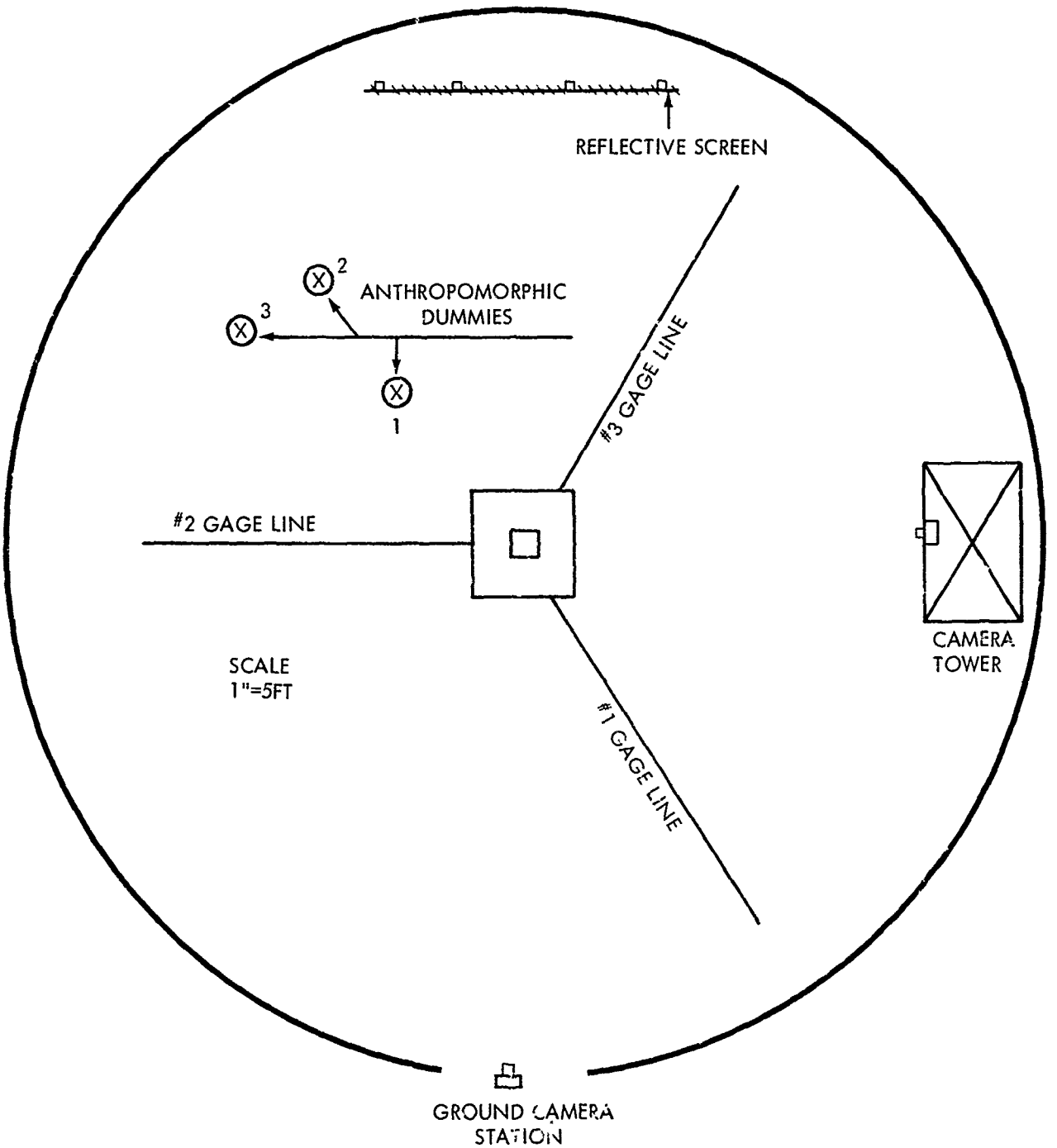

FIG. 2-1 EXPERIMENTAL SETUP FOR TANKS A, B, C, AND D

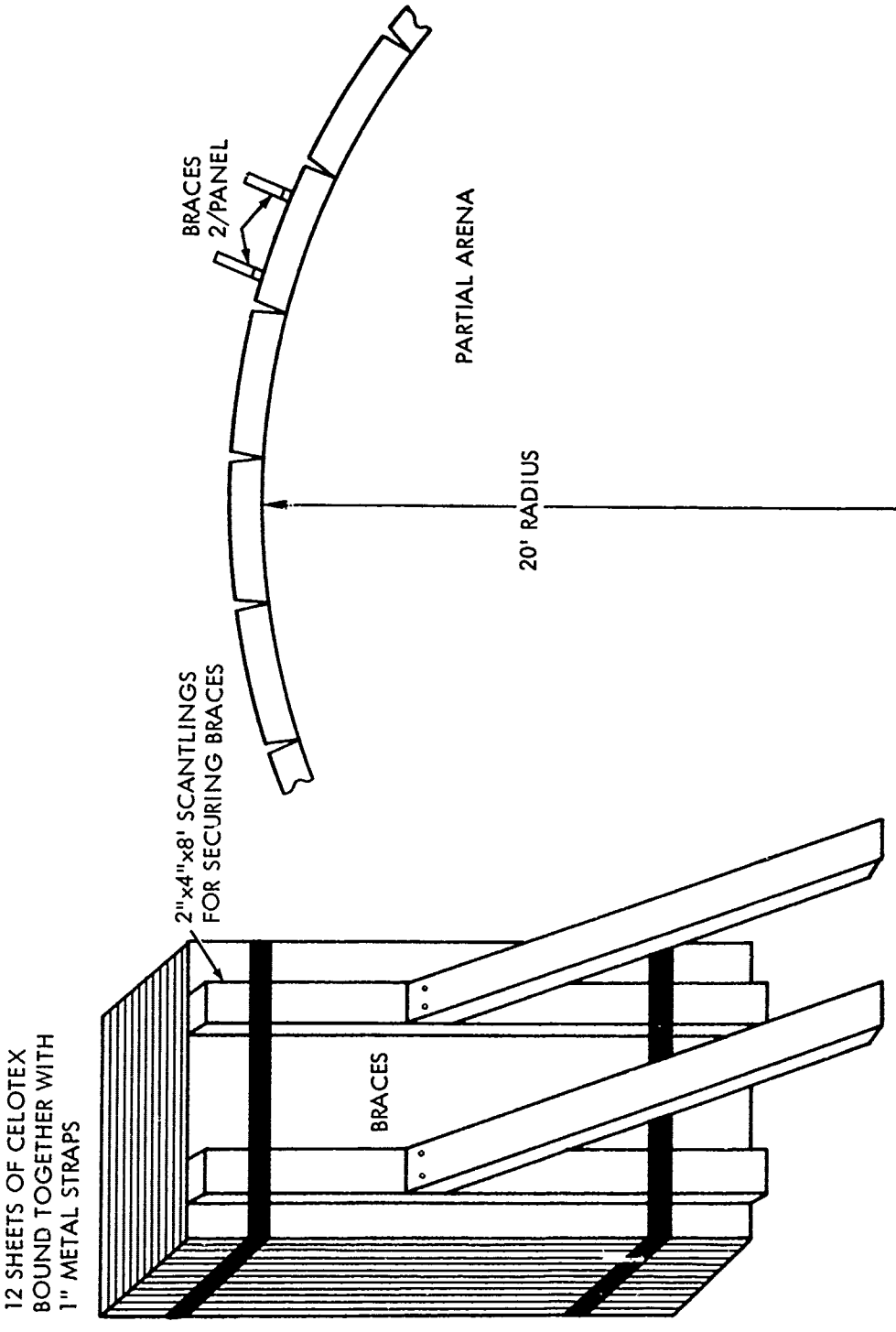

FIG. 2-2 ARENA CONSTRUCTION

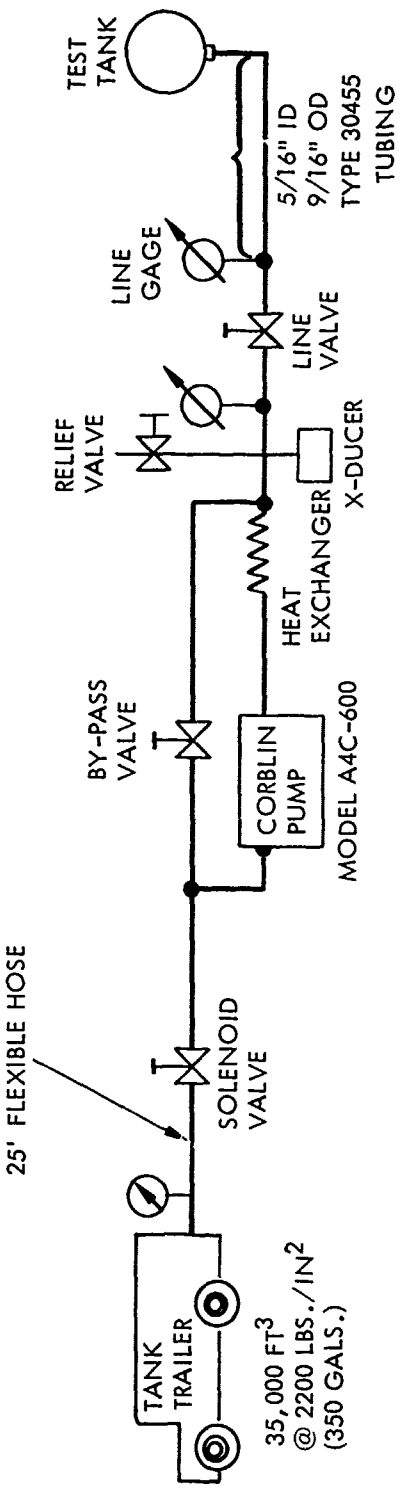

FIG. 2-3 THE HIGH PRESSURE SYSTEM

of valves opened (tanks used) in the supply trailer at any given time. Figure 2.4 shows the relationship between the supply pressure and the volume of gas the pump is capable of pumping at a discharge pressure of 9,000 psi.

The N_2 gas supply was provided by a compressed gas tank-trailer having a capacity of 35,000 $ft.^3$ (350 gals.). Each of the 33 tanks in the trailer emptied into a common manifold through individual valves. The discharge from the manifold was, in turn, controlled by a master valve. The average tank pressure varied between 2,200 and 2,600 psi and was dependent upon the temperature of the tanks. However, at night when the tests were conducted the pressure sometimes dropped to as low as 2,100 psi. It was found that several of the individual tank valves leaked, and as the pressure in the tanks associated with them decreased it was nearly impossible to raise the pressure in the manifold much above 2,000 psi unless a large number of tank valves were opened simultaneously. Experience showed that a manifold pressure of 1,500 to 2,000 psi was quite satisfactory for the proper operation of the pump.

The trailer was connected through a 25-foot length of flexible hose to an electric solenoid valve at the pump site. This valve was used to isolate the supply trailer from the rest of the system at tank rupture time and thus prevented undue loss of N_2 before the hand operated valves could be closed.

The compressed gas at the discharge side of the pump was passed through a water-cooled heat exchanger where the temperature was reduced to a few degrees above ambient. The gas was then fed to the test tank through approximately 180 feet of 5/16" ID x 9/16" OD stainless steel tubing, coupled at 20-foot intervals. The tubing was rated at 40,000 psi burst pressure. The orifice in the couplings was 7/32" in diameter. Except for the line valve located at the pump site these were the only constrictions in the line between the pump and the test tank.

Pressure sensing units were connected into the system for each of the five tests (Fig. 2.3). Two were standard high pressure bourdon-type dial gages while the third was a bridge-type bonded strain gage having an overall accuracy better than 1%. The bourdon-type dial gages had been calibrated shortly before the test series was begun and again immediately afterwards, and their accuracy was of the order of 1/2% of full scale. Two complete sets of pressure measuring units were used to bracket the expected burst pressures of the

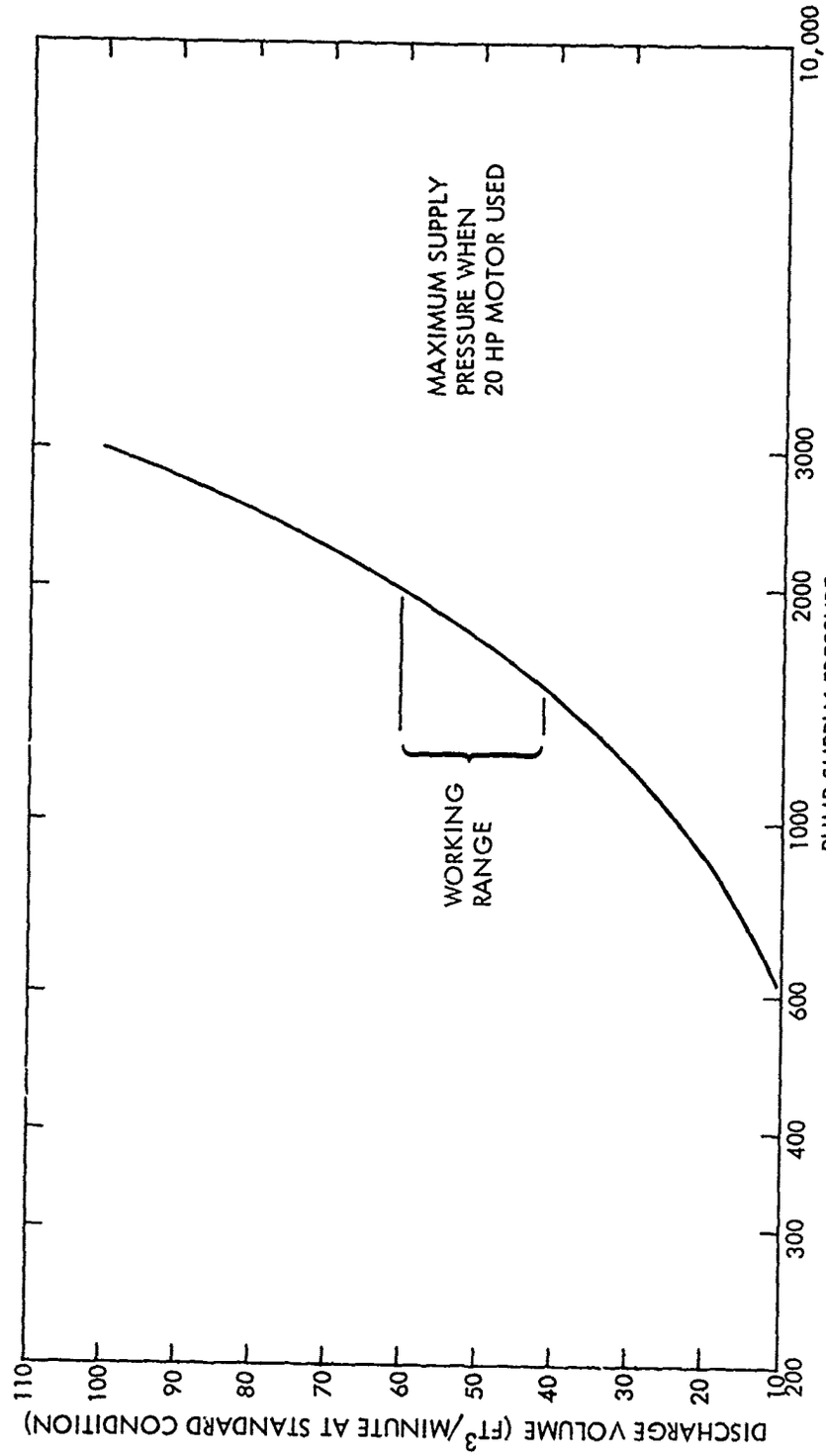

FIG. 2-4 DISCHARGE VOLUME VS PUMP SUPPLY PRESSURE
(DISCHARGE PRESSURE = 9,000 PSI)

test tanks. One set consisted of a 0 - 500 psi transducer in conjunction with a 0 - 1,000 psi bourdon dial gage and was used with the two lower pressure tanks. For the higher pressure tanks, the gages were changed to ones having a full-scale capacity of 10,000 psi. The standard dial gages had 100-pound graduations and could be read to within 50 psi very easily. A calibration curve for the 10,000 psi line gage is shown in Fig. 2.5. Full scale output of the strain gage transducers was about 30 mv and required amplification to enable them to drive a Brush Pen Recorder. The vertical amplifier of a Tektronix scope was used for this purpose. Gage output was not recorded for tanks A and B since burst pressure exceeded the strain gage's rating.

2.2.2 Pressure System Operation

The two low-pressure test tanks (tanks A and B from Table 1.1) were pressurized directly from the supply tank trailer, bypassing the pump. Pressurization was accomplished by opening the line valve (Fig. 2.3) slowly and monitoring the pressure shown on the line gages. Gas was admitted slowly to insure that the indicated gage pressure was the actual pressure in the test tank. The valve was periodically closed during the pressure run to check for leaks and to be sure that the tank pressure and the gage pressure were the same.

At installation, tanks A and B were pretested at 200 psi to check the integrity of the complete system. This check was made 3 to 4 hours prior to the data run to allow corrections to be made.

The burst pressure of tanks C, D, and E was higher than the tank-trailer pressure. Hence, the pump was used to raise the pressure to the tank's bursting point. The pressurization sequence was as follows. First, the test tank was pressurized to pump-supply-pressure directly from the trailer. Meanwhile the pump was operating in an idling mode. Following this initial pressurization, the pump was cut in and the tank pressure permitted to rise. Pressure pulsations from the pump made accurate reading of the dial gage impossible. Therefore, the line valve was closed slowly until the pulsations smoothed out. As with the other tanks, the pressure cycle was interrupted periodically to insure that the tank pressure was the same as that being read on the line gage. This procedure also allowed the bonded strain gage to be constantly calibrated throughout the pressure cycle.

The pressure system was checked at the installation of these tanks by raising the pressure to 2,000 psi. This was done 3 to 4 hours prior to the data run.

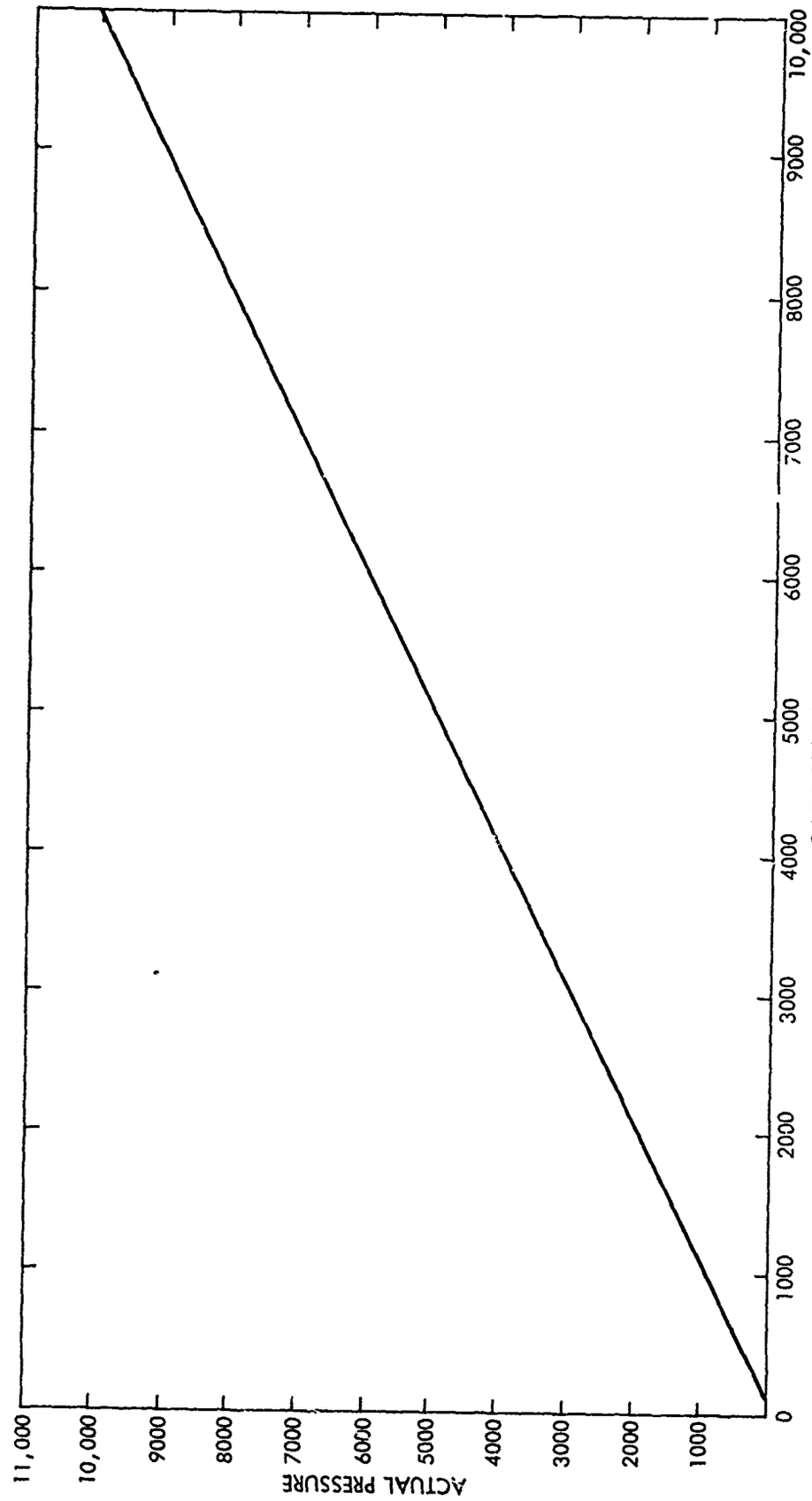

FIG. 2-5 10,000 PSI LINE GAGE CALIBRATION

2.2.3 History of the pressurization of Tanks A and B

When all systems were ready, tank A was slowly pressurized to 460 psi at which point a leak developed in a tank coupling. The tank was bled down and a new coupling installed. Tank pressure was then raised to 500 psi where a leak developed. The leak sealed itself when pressure was reduced slightly. A third pressure run was made and again the leak became evident at 500 psi. The leak was again self-curing when pressure was reduced. The tank was then taken into the laboratory and dismantled. We discovered that the flange bolts could be tightened several turns after removal of the safety wire. Examination of the teflon gasket under the flange showed that it was extruding under pressure and causing the leak.

At this point, the tank had been pressurized to 460 psi once and to 500 psi twice. Yet there was little evidence of permanent deformation. The thick coat of white paint that we had sprayed on the tank was not cracked.

The tank was reassembled with the flange bolts snugged down. The tank was then pressurized without incident until it burst at 625 psi.

Prior to test, the flange bolts on tank B were snugged down. This tank was pressurized to its burst pressure of 600 psi without incident. Total time to pressurize tank B from 0 to burst was 21 minutes, about 29 psi/minute pressure increase.

2.2.4 Pressurization of Tanks C and D

Tank C was connected and raised to its burst pressure of 8,000 psi without incident. For this and the remaining tanks, tank pressure vs time was recorded. This information for tank C is plotted in Figure 2.6.

Tank D was also inflated to its burst pressure of 8,000 psi without incident. Tank pressure vs time during the inflation cycle is shown in Figure 2.7.

2.2.5 Pressurization of Tank E

Tank E was cycled 55 times. A cycle consisted of raising the tank pressure from 4,000 to 5,000 psi, holding at 5,000 psi for 15 seconds, and then reducing pressure to 4,000 psi. The time required

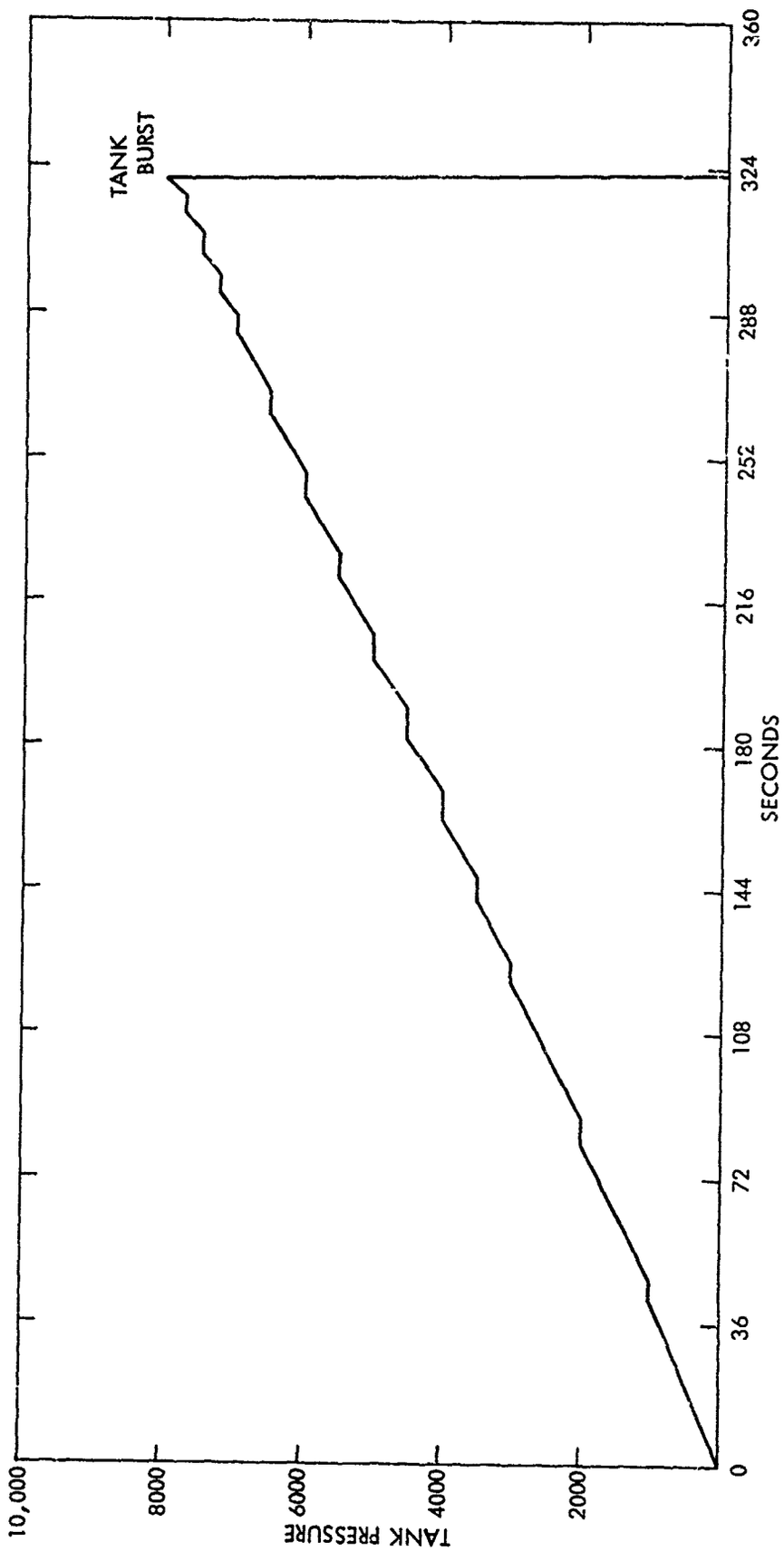

FIG. 2-6 PRESSURE VS TIME FOR TANK C

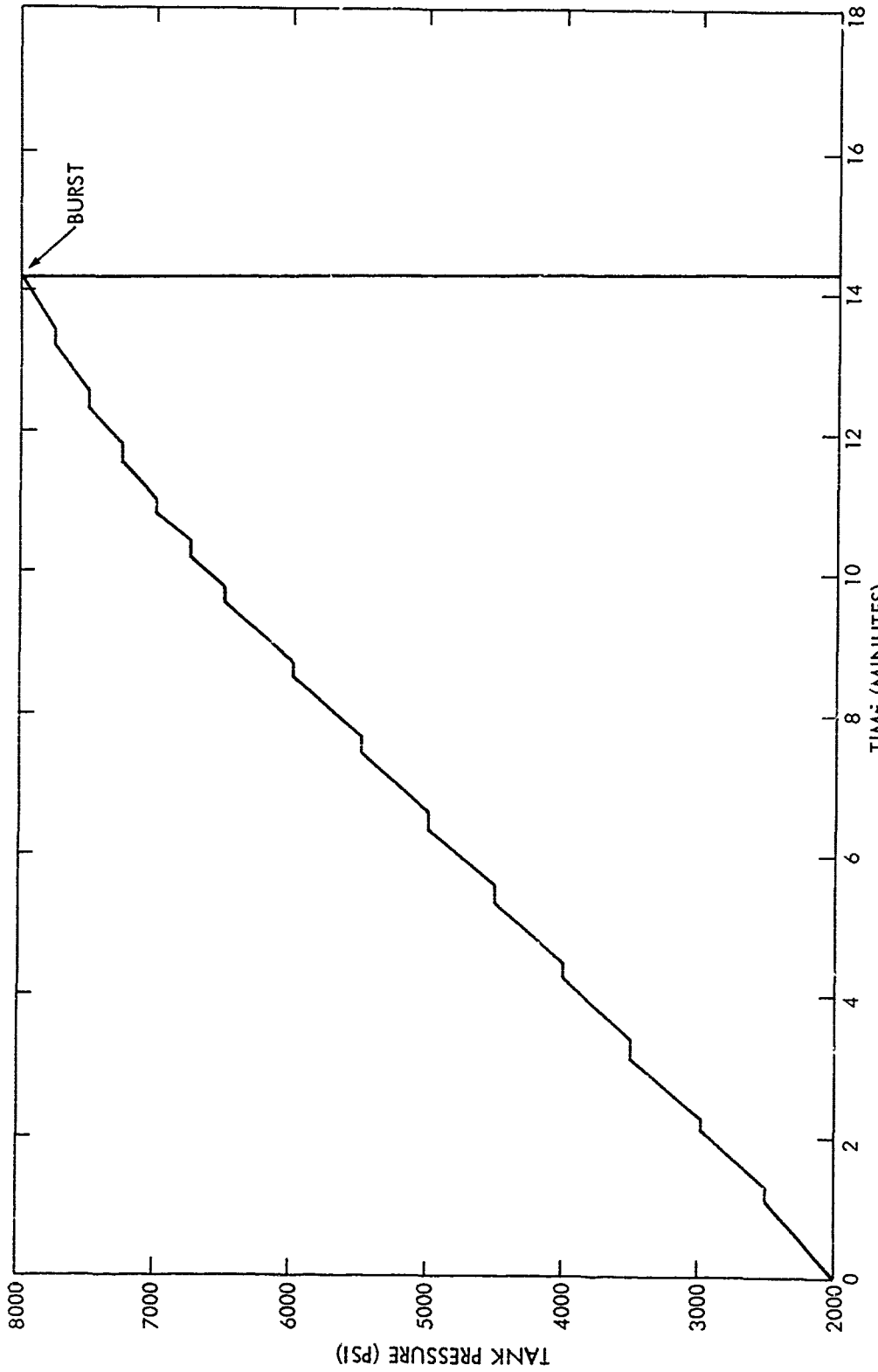

FIG. 2-7 PRESSURE VS TIME FOR TANK D

for one cycle averaged about 7 minutes. At the end of the 32nd cycle the operation was halted for 28 minutes so that camera film could be changed. During this period, tank pressure was reduced to 3,000 psi to provide a greater measure of safety for personnel working in the vicinity of the tank.

During the reduction portion of the cycle, the N_2 was exhausted into the supply trailer to conserve gas.

Following the 55th cycle, tank pressure was increased to start the final inflation to rupture. At 5,200 psi, a leak appeared and the pressure was reduced. The leak was self-healing as the pressure decreased below 5,000 psi. Inspection showed that the seal on top of the tank was leaking. (Tanks D and E had openings at both top and bottom.) The top assembly was removed, cleaned, and a new "C" ring installed. (The "C" ring is a metal ring with a C-shaped cross section. Sealing is produced when the ring expands against two mating surfaces.) Pressure was again increased with a leak again appearing at about 5,200 psi. Operations were halted for the night and a new seal assembly was fabricated the following day. This assembly used the more conventional double neoprene "O" ring seals.

The test was resumed the following evening and no leaks appeared. However, at 5,250 psi, a signal light indicated that the breakwire around the tank had parted. The pressure was reduced to 3,000 psi and the breakwire tested. The breakwire was still intact and we assumed that a voltage transient had activated the signal light. Inflation was resumed and the burst pressure of 8,130 psi was reached without further incident. The final inflation pressure vs time for tank E is shown in Figure 2.8.

2.3 Instrumentation

2.3.1 Blast Instrumentation

The blast instrumentation system is built around piezoelectric gages whose outputs are recorded by cathode-ray oscilloscopes and rotating drum cameras. The oscilloscopes and auxiliary equipment used for time bases, synchronization, and power are housed in a special instrumentation trailer. This and similar systems have been used at NOL over the past several years and are described in reference (1).*

Both side-on and face-on pressures were measured using three gage types. The side-on gages were either Atlantic Research Corporations model LC-33 gages or Susquehanna Instruments model ST-7 gages. The face-on gages (Atlantic Research Corporation Model LC-71) were mounted in 18-inch round aluminum baffles oriented normal to the direction of the shock flow.

*References are found on page 101

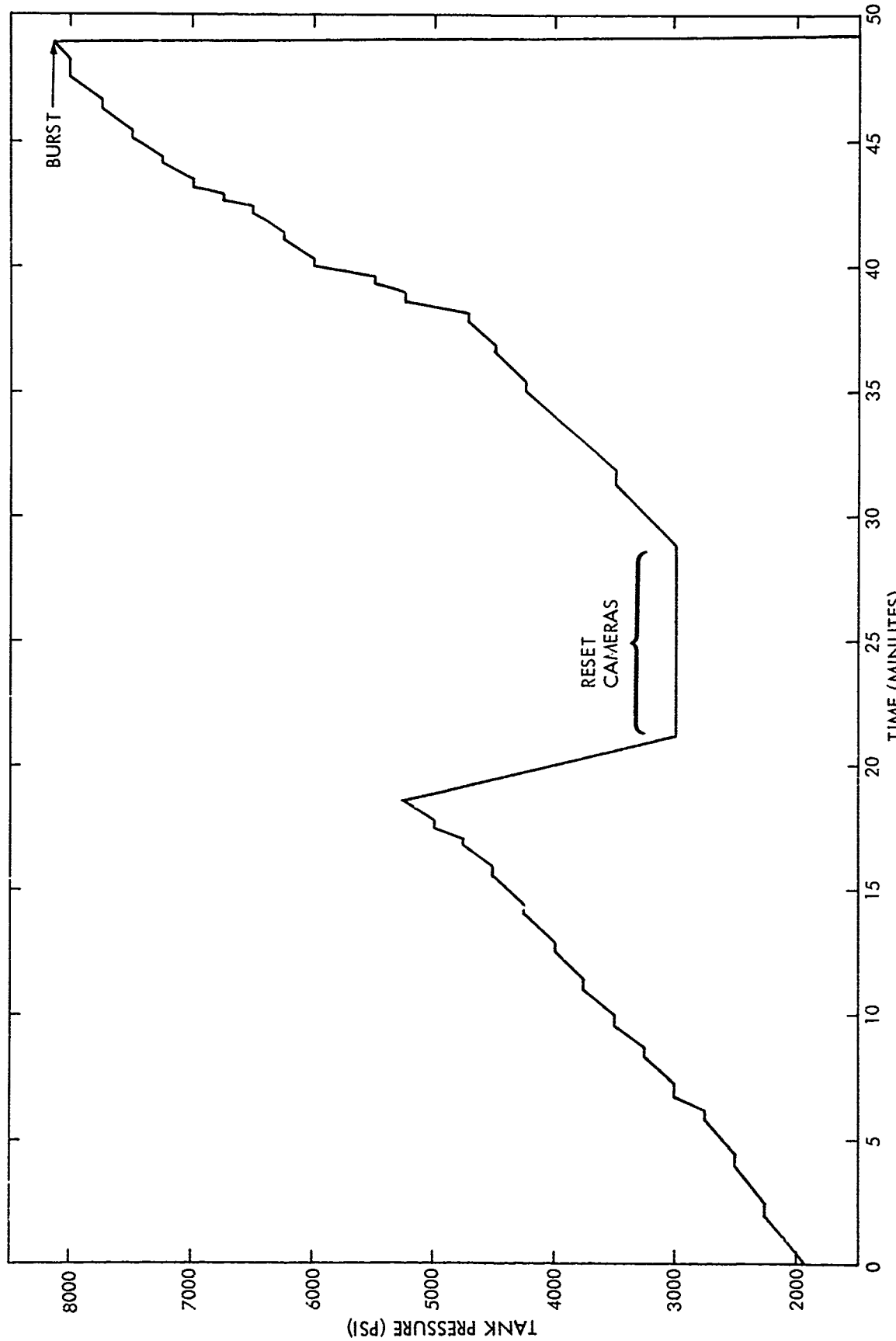

FIG. 2-8 PRESSURE VS TIME FOR TANK E

Signals from the LC-33 and LC-71 gages were transmitted via anti-noise coaxial cable to charge amplifiers mounted in the instrument trailer. Signals from the ST-7 gages were fed to charge amplifiers located at the gages. The voltage outputs from all charge amplifiers were displayed on cathode-ray oscilloscopes. Rotating drum cameras with a suitable time base produced permanent pressure-time records. The frequency response of the system was from below 0.2 hz to about 80 Khz.

In operation, the equipment was setup and ready with cameras open during the inflation cycle. The oscilloscopes were unblanked at tank rupture by a signal from a trigger unit initiated by a breakwire around the tank.

2.3.2 Fragment Velocity System

Attempts to measure fragment velocities involved two techniques. One method used breakwires and electronic counters. The first breakwire was wrapped around the tank under test and signaled tank rupture. The second breakwire was supported by an 8-gage wire frame formed to the tank shape but everywhere nominally 1 ft larger in radius. At tank rupture, the first breakwire interrupted a current to signal an electronic counter to start. The first fragment to travel the 1 ft separation broke the second wire. This again interrupted a current to signal the counter to stop. To avoid errors in the counters due to trigger level settings, trigger signal shapers were used between both the start wire and stop wire signals and the appropriate counter input.

The second technique used to measure fragment velocities involved a stroboscopic photographic system. Briefly, this system used two camera stations. Each station consisted of a single 4" x 5" camera and an electronic flash tube. The tube was flashed four times at measured intervals. The first flash occurred at tank rupture, with the three succeeding pulses occurring at later, appropriately spaced intervals. The strobe unit is diagrammed in Figure 2.9.

One of the cameras was placed at ground level and photographed against the background formed by a reflecting screen. Limiting the size of the light source in conjunction with the above screen produced a true shadow-graph system similar to that described in reference (2). Thus in most cases, the shock generated by the bursting tank was photographed by one or more of the flashes. With this system, however, only the shadow of the fragment against the screen was photographed.

A second camera was located on a tower above and off to the side of the tank. This camera photographed tank fragments directly against a low reflecting background.

In equipment tests, the flash tubes fired at the preset times within ± 0.3%. To be sure that they operated properly at tank rupture,

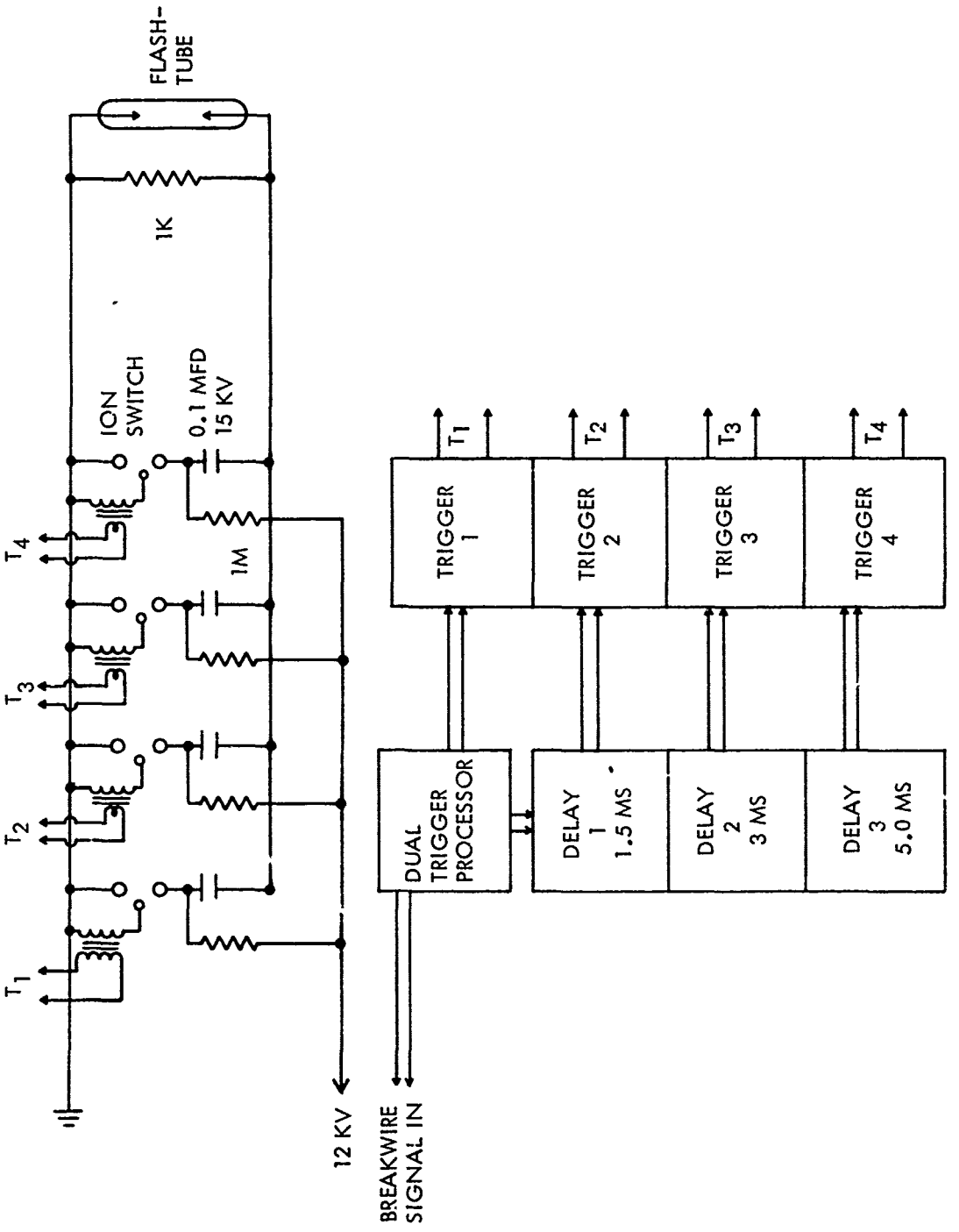

FIG. 2-9 STROBE UNIT

we monitored the light output by placing a photocell near each flash tube. The photocell outputs were recorded on a dual beam oscilloscope with a suitable time base.

The system was operated as follows. When the internal tank pressure reached the specified working level during the inflation cycle, the camera shutters were opened remotely. At tank rupture, the first breakwire signal triggered the flasher system shown in Figure 2.9. At the same time the camera shutter closing solenoids were energized, and the shutters closed 18 milliseconds after tank rupture. The time from tank rupture to the last strobe flash was always less than 18 milliseconds.

Since the camera shutters remained open for several minutes, the experiments were done on moonless nights.

Both systems did not function on every tank rupture. However, one or the other system always operated so that fragment velocities were measured on every test.

2.3.3 Photography of the Anthropomorphic Dummies

The reactions of the anthropomorphic dummies to tank rupture were photographed using 16-mm Mitchell cameras operating at 24 frames/second. Since the experiments were done at night, light was supplied by photoflood lamps. These lamps were turned on at tank rupture to avoid fogging the strobe camera film. To shorten turn-on time, the filaments of the photoflood lamps were preheated to a dull red glow. The photofloods reached 90% of full brightness in about 50 milliseconds after tank rupture -- 20 milliseconds relay closure-time and 30 milliseconds for the lamp filaments to reach incandescence. Thus, the dummies were photographed within two frames after tank rupture.

2.3.4 Sequence of Operations

A typical sequence of events for instrumenting tank rupture follows:

a) When the pressure in the tank under test reached its operating pressure, the following operations were done manually:

1) Open strobe camera shutters
2) Check ready position of all electronics
3) Open drum camera shutters on blast recording equipment
4) Start Mitchell cameras

b) At tank rupture, the following operations were initiated automatically by the first breakwire signal:

1) Unblank oscilloscopes in pressure instrumentation

2) Initiate fragment velocity screen to start fragment velocity counter.
3) Trigger first strobe flash.
4) Turn on photofloods.
5) Energize strobe camera solenoid for shutter closure

c) After tank rupture but less than 0 + 1 millisecond, fragment velocity screen pulse stops fragment velocity counter.

d) At 0 + 1.5 milliseconds, second strobe pulse triggers.

e) At 0 + 3.0 milliseconds, third strobe pulse triggers.

f) At 0 + 5.0 milliseconds, fourth and last strobe pulse triggers.

g) At 0 + 18 milliseconds, strobe camera shutters close.

h) At 0 + 50 milliseconds, photoflood lamps reach 90% of maximum brightness.

i) Equipment turned off manually at about 0 + 1 minute.

3. Blast Measurements

3.1 Background and Theory

The purpose of the blast measurements was to determine an empirical explosion energy output; hopefully, a single TNT energy equivalent to aid in estimating the damage potential from such accidental tank ruptures.

The expected side-on airblast overpressures were calculated to aid in experimental planning. The calculations used the one-dimensional hydrocode from reference (3). Results of these calculations are given in Appendix A. The hydrocode used, called WUNDY, gives the results for a free air situation. Since the tanks were ruptured near the ground all measurements were made in the mach region. Therefore, a reflection coefficient of 1.5 was used when comparing theory and measurements. This will be discussed further in the presentation of the data.

Nominal 8.2-lb TNT spheres were fired to validate our TNT predictions and to generate data to directly compare with the data generated by the rupture of the high pressure helium tanks.

All the tanks were placed with their center of mass 16" above the ground. The TNT spheres were fired with their center of mass 12" above the ground. The TNT spheres were fired at this level to assure that the blast measurements were made in the mach region.

3.2 Blast Gage Layout

The blast gages were located along three equally spaced radial lines extending from Ground Zero (GZ). This set up is shown in Figure 3.1. Gage distances are those used for tanks D and E. A similar set up was used for tanks A, B, and C except that the distances from GZ to the gages were reduced. Nominal gage distances for tanks A, B, and C were 3.5, 5.6, and 12.0 ft from GZ. All gages were 6 inches above the ground.

3.3 Pressure-Time Histories

Tracings of the pressure-time histories are shown in Figures 3.2 through 3.6 for tanks A through E, respectively. The traces are similar to those from the TNT charge shown in Figure 3.7. There are incidences of double peaks and other perturbations on tank-rupture records, particularly from the gages nearest GZ. Records from the positions furthest from the charge are usually free from such perturbations indicating that the shock wave has smoothed by the time it has propagated this distance.

Shockwave arrival times are different from the different gage lines. This shows a lack of symmetry for the shock front that is further borne out in the pressure differences shown in section 3.4.

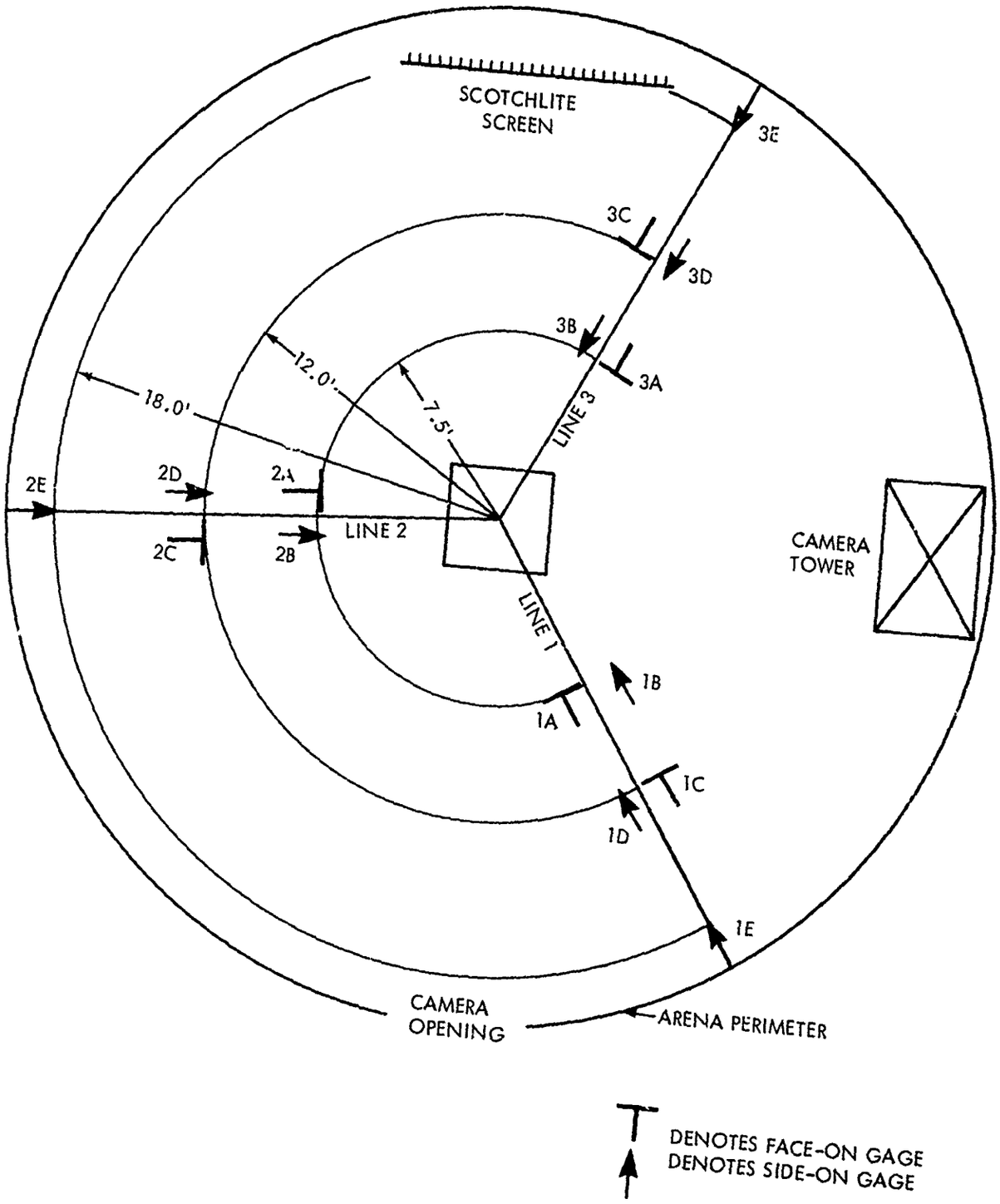

FIG. 3-1 FIELD LAYOUT FOR TANK D; 6FT^3 TANK

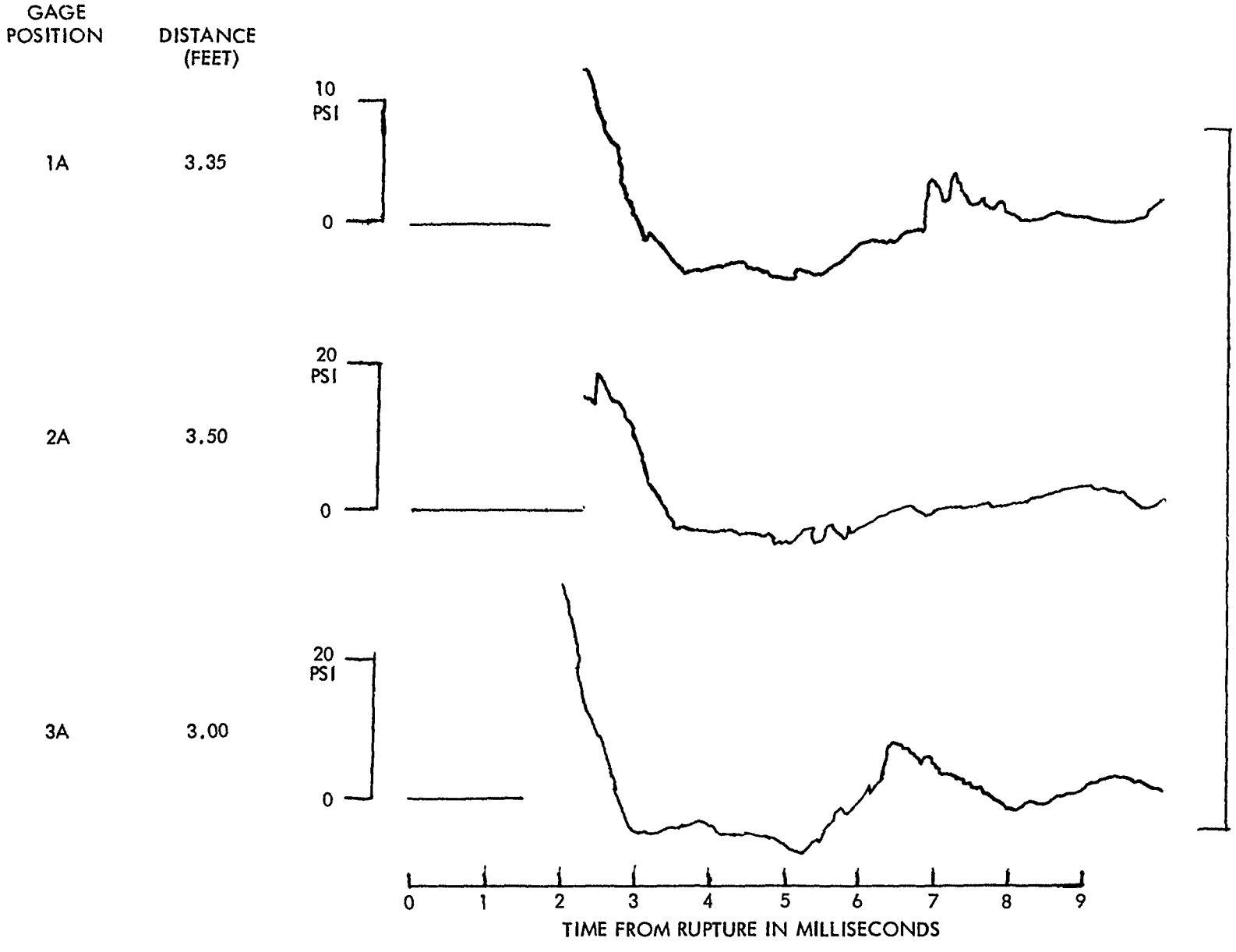

FIG. 3.2 PRESSURE-TIME HISTORIES FROM TANK A.

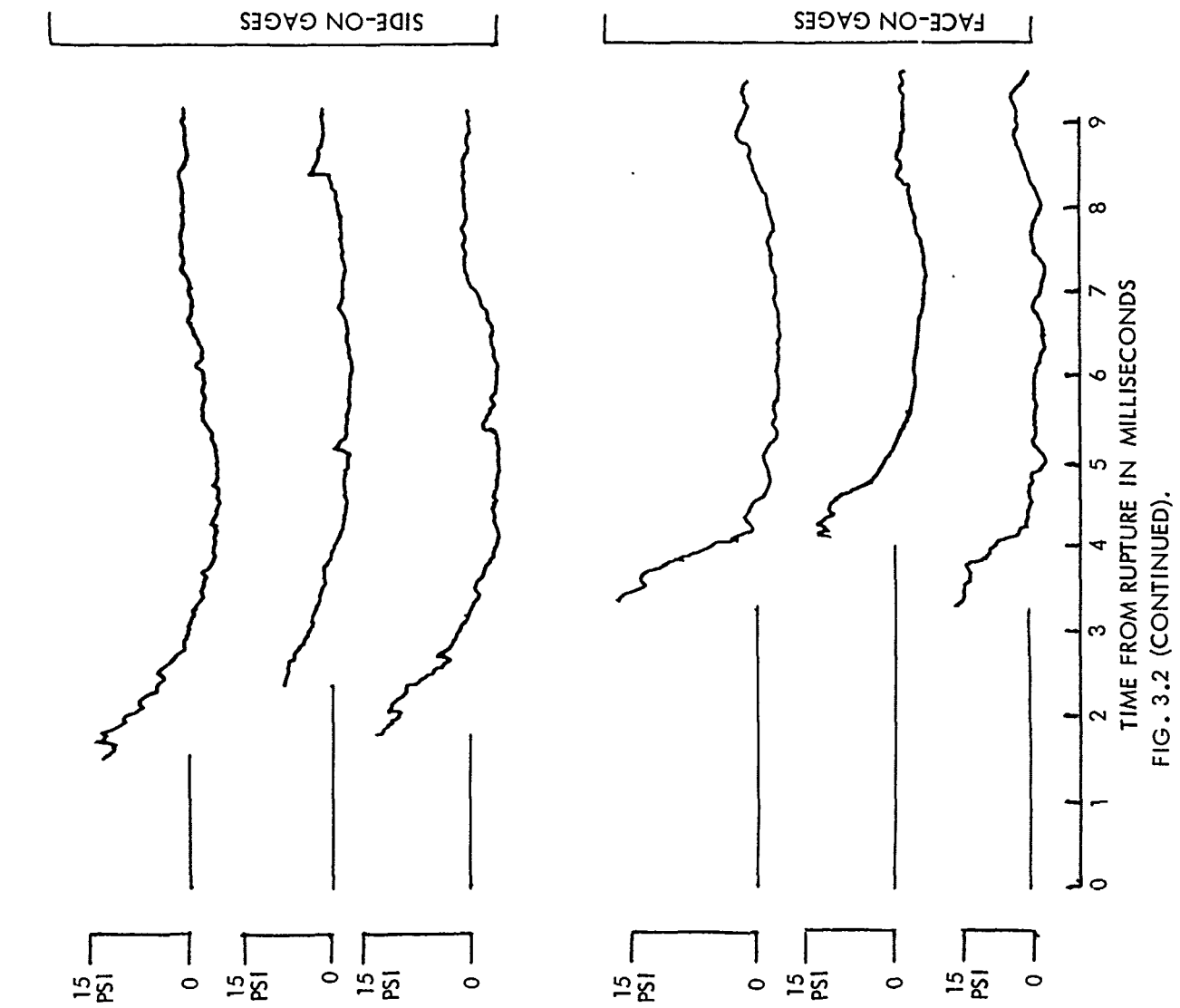

FIG. 3.2 (CONTINUED).

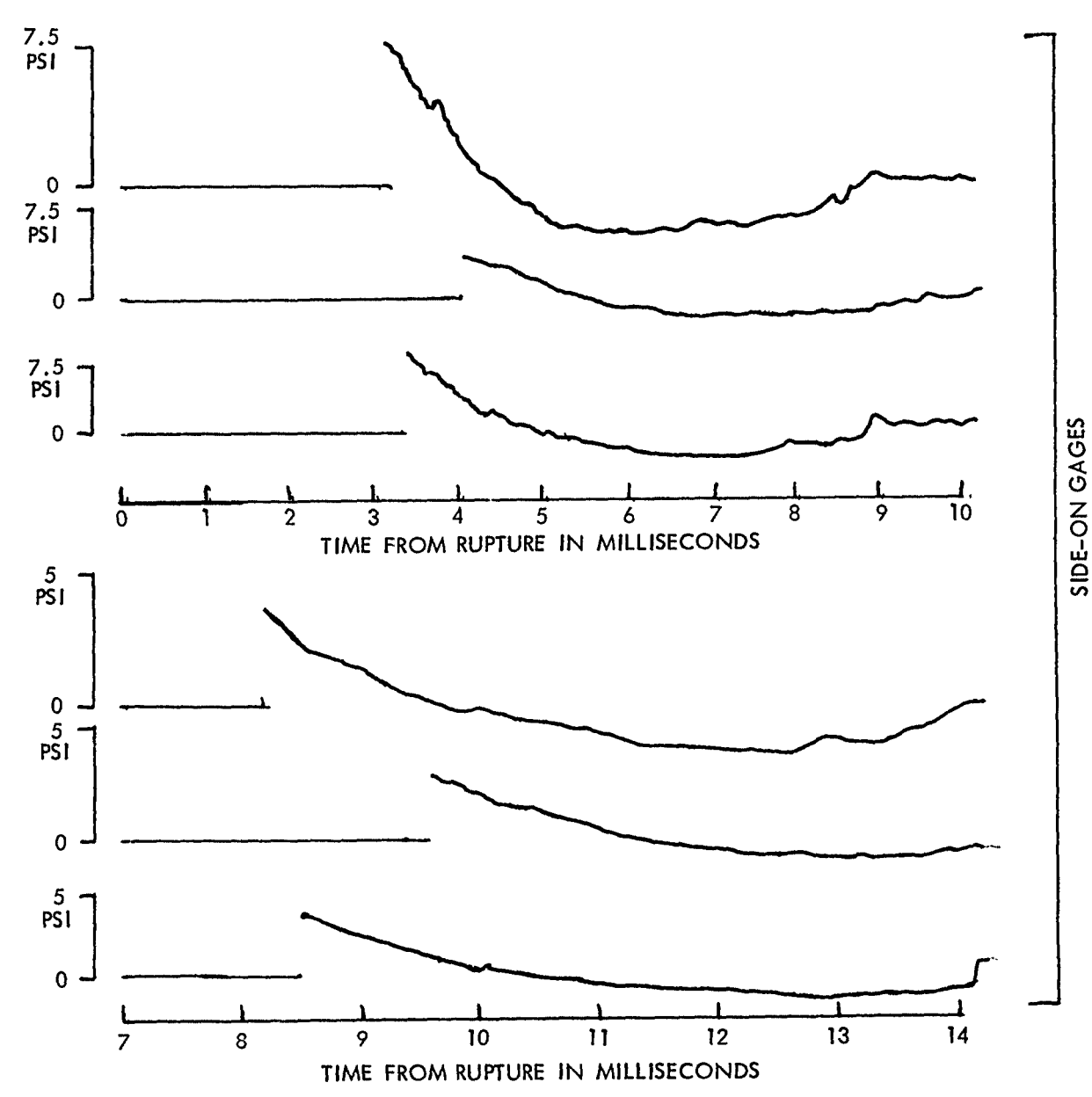

FIG. 3.2 (CONTINUED)

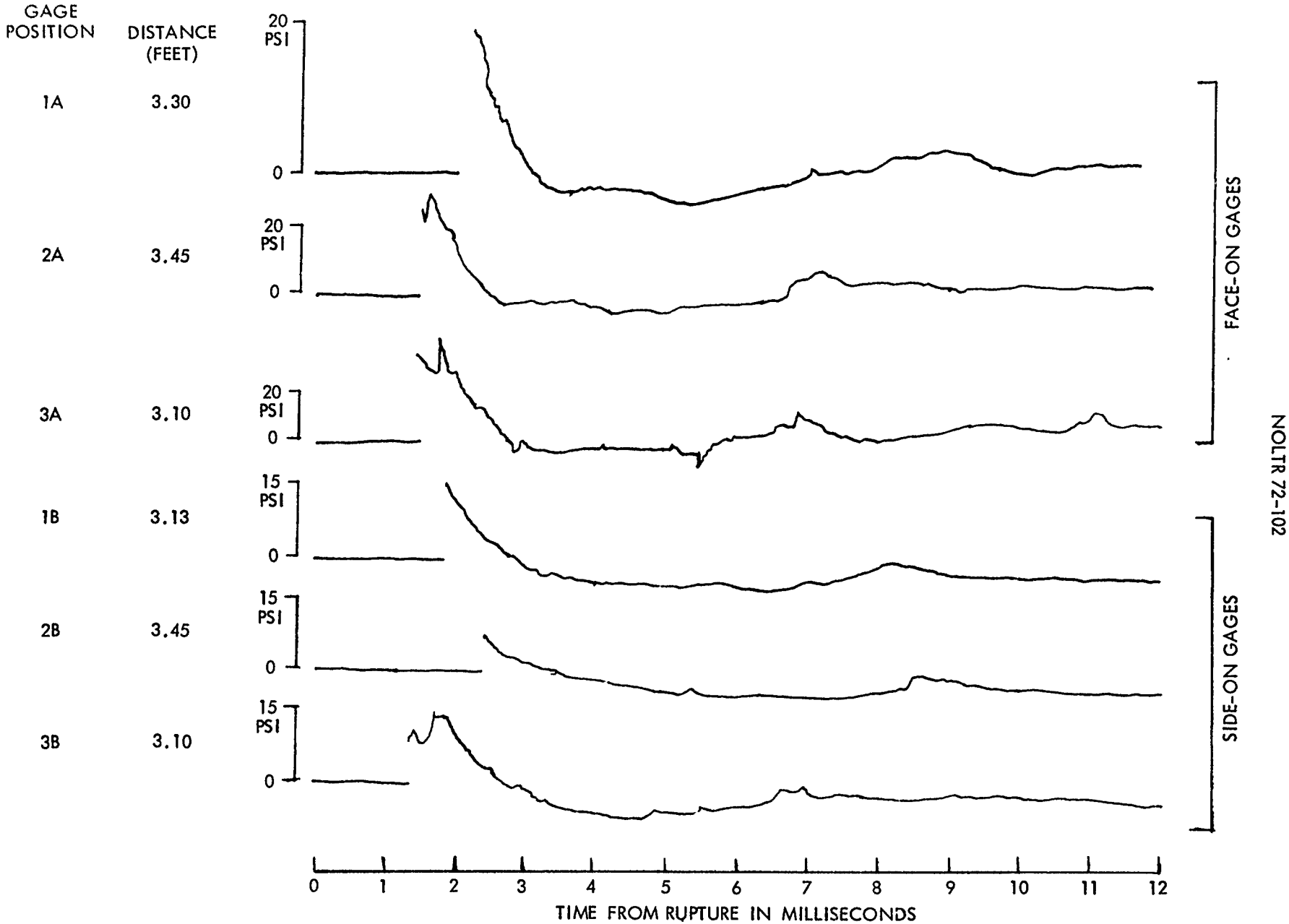

FIG. 3.3 PRESSURE-TIME HISTORIES FROM TANK B

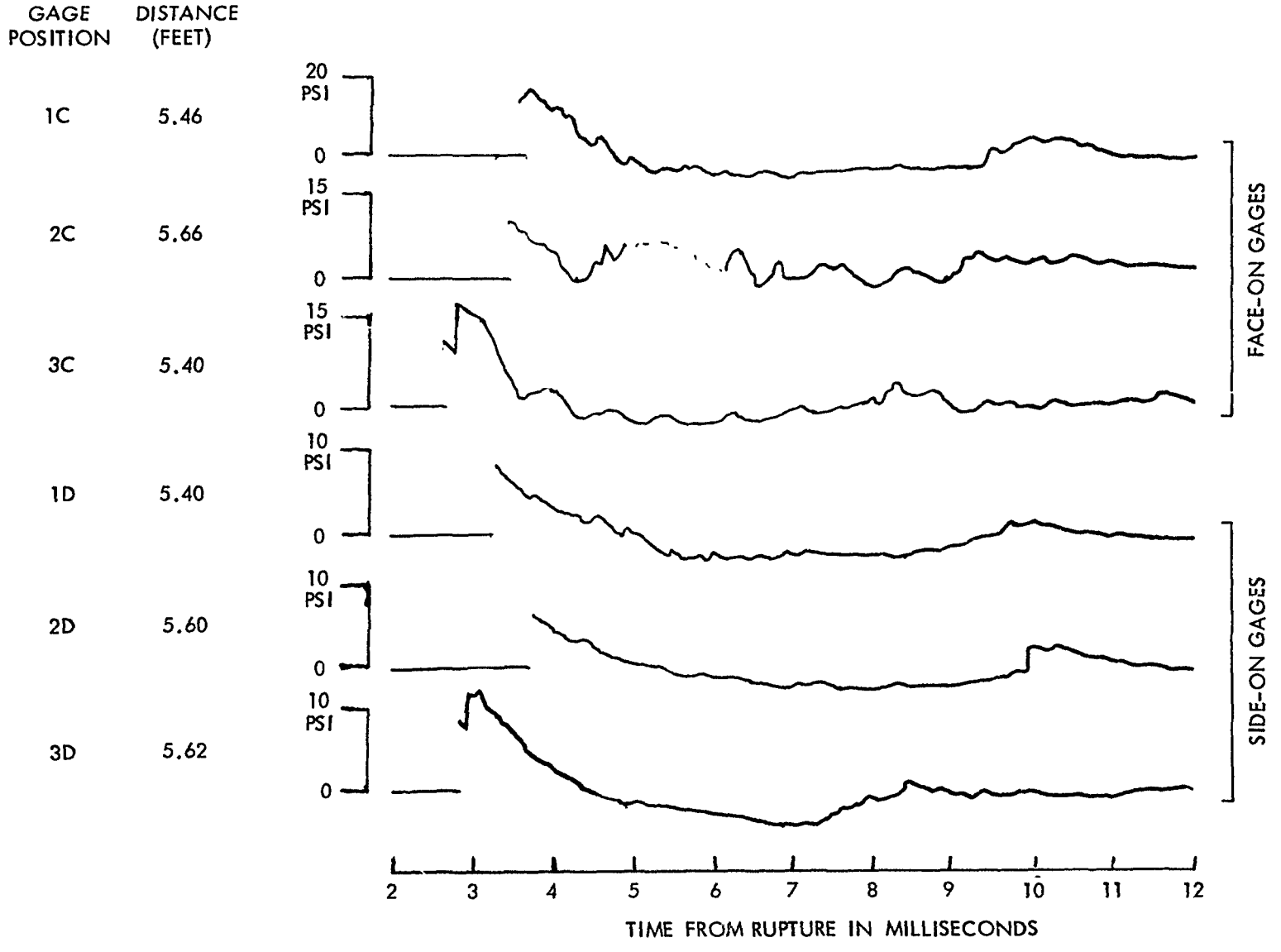

FIG. 3.3 (CONTINUED)

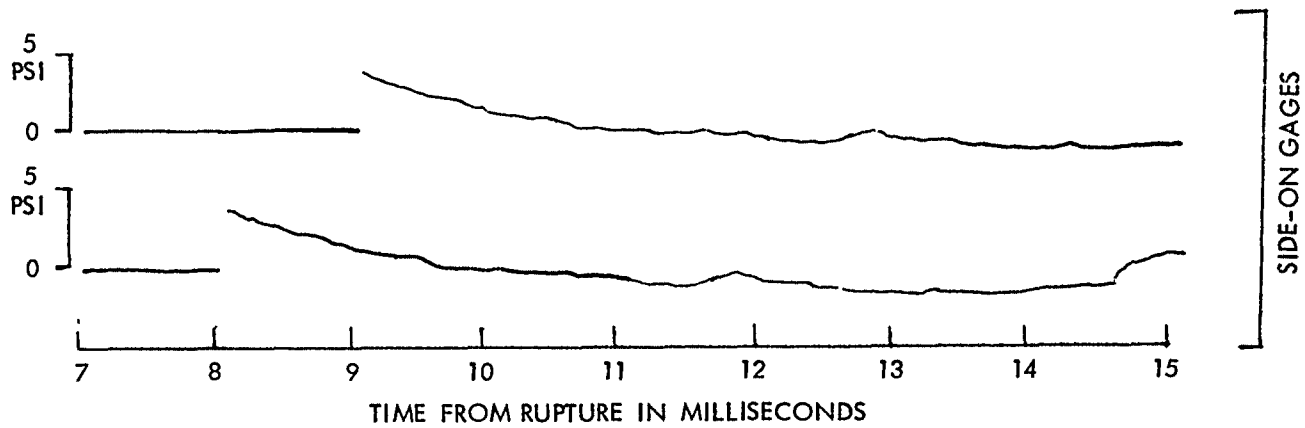

FIG. 3.3 (CONTINUED)

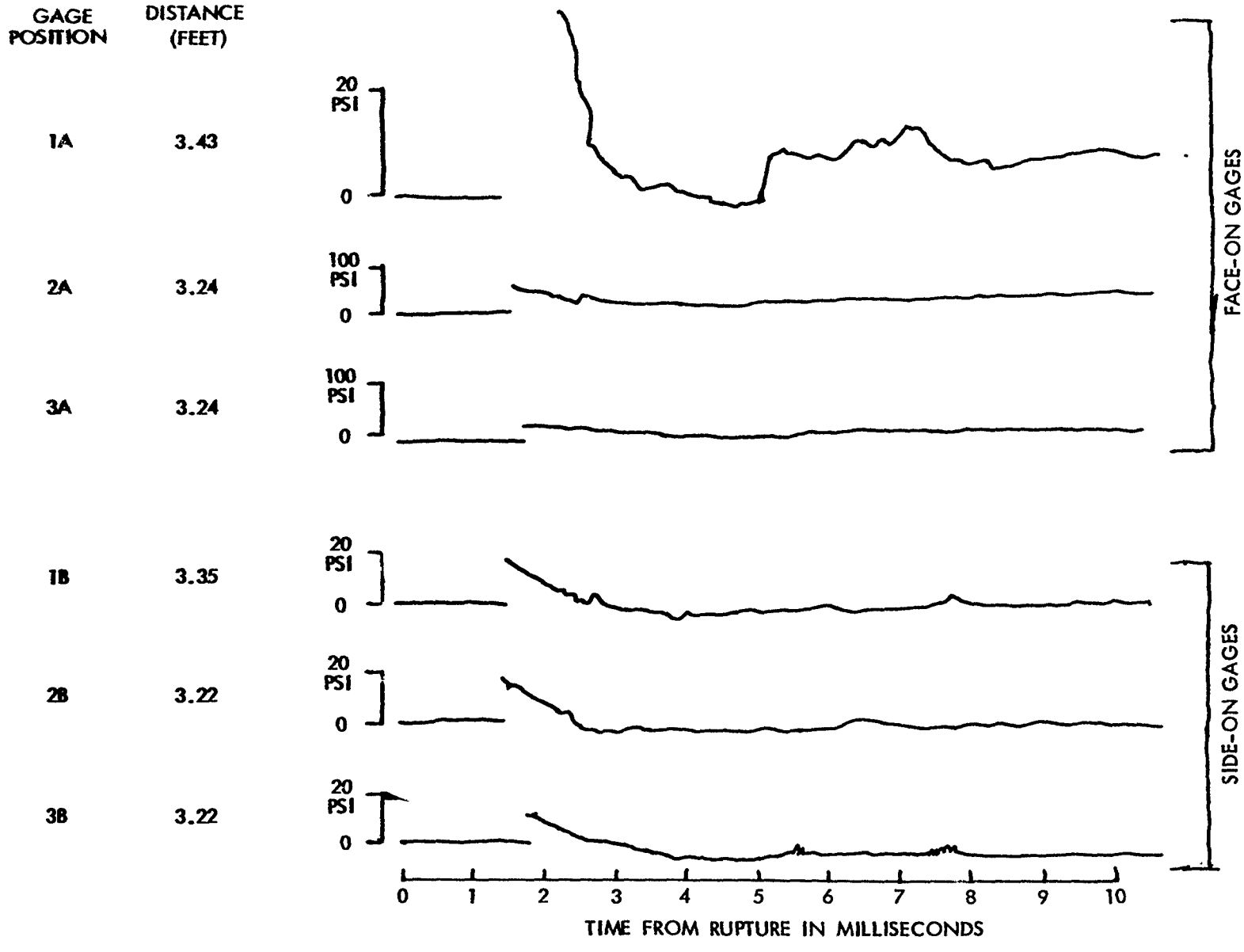

FIG. 3.4 PRESSURE-TIME HISTORIES FROM TANK C

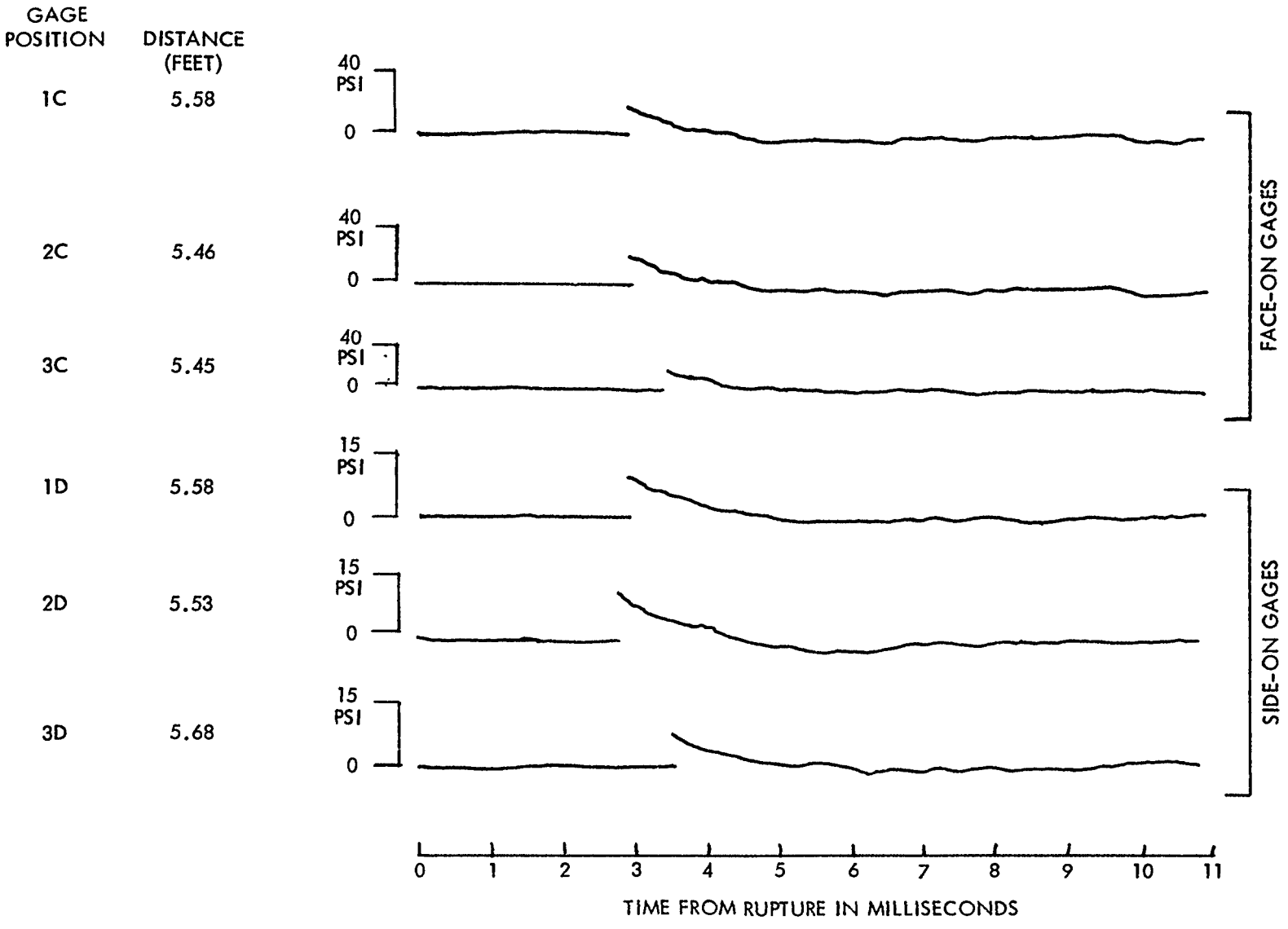

FIG. 3.4 (CONTINUED)

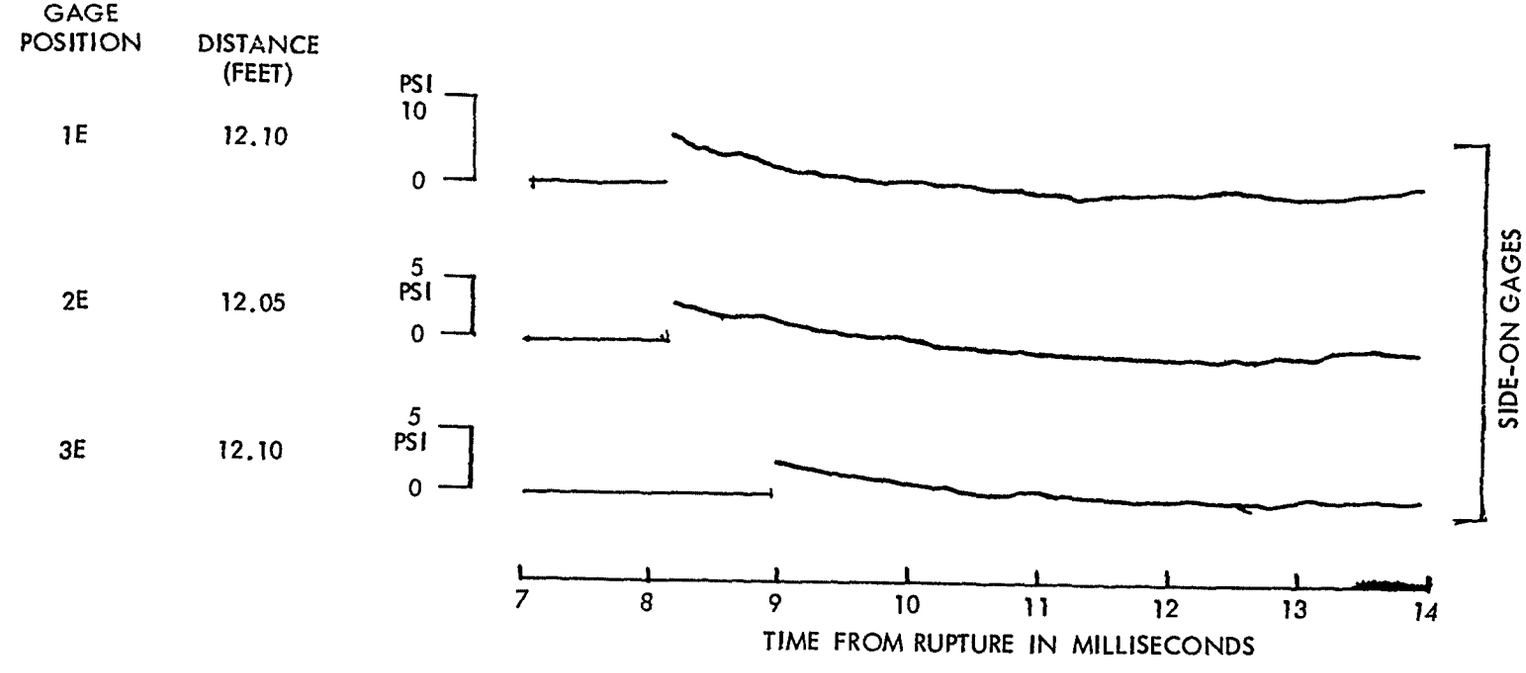

FIG. 3.4 (CONTINUED)

GAGE POSITION	DISTANCE (FEET)
1A	6.77
2A	7.42
3A	7.12
1B	6.92
2B	7.59
3B	7.17

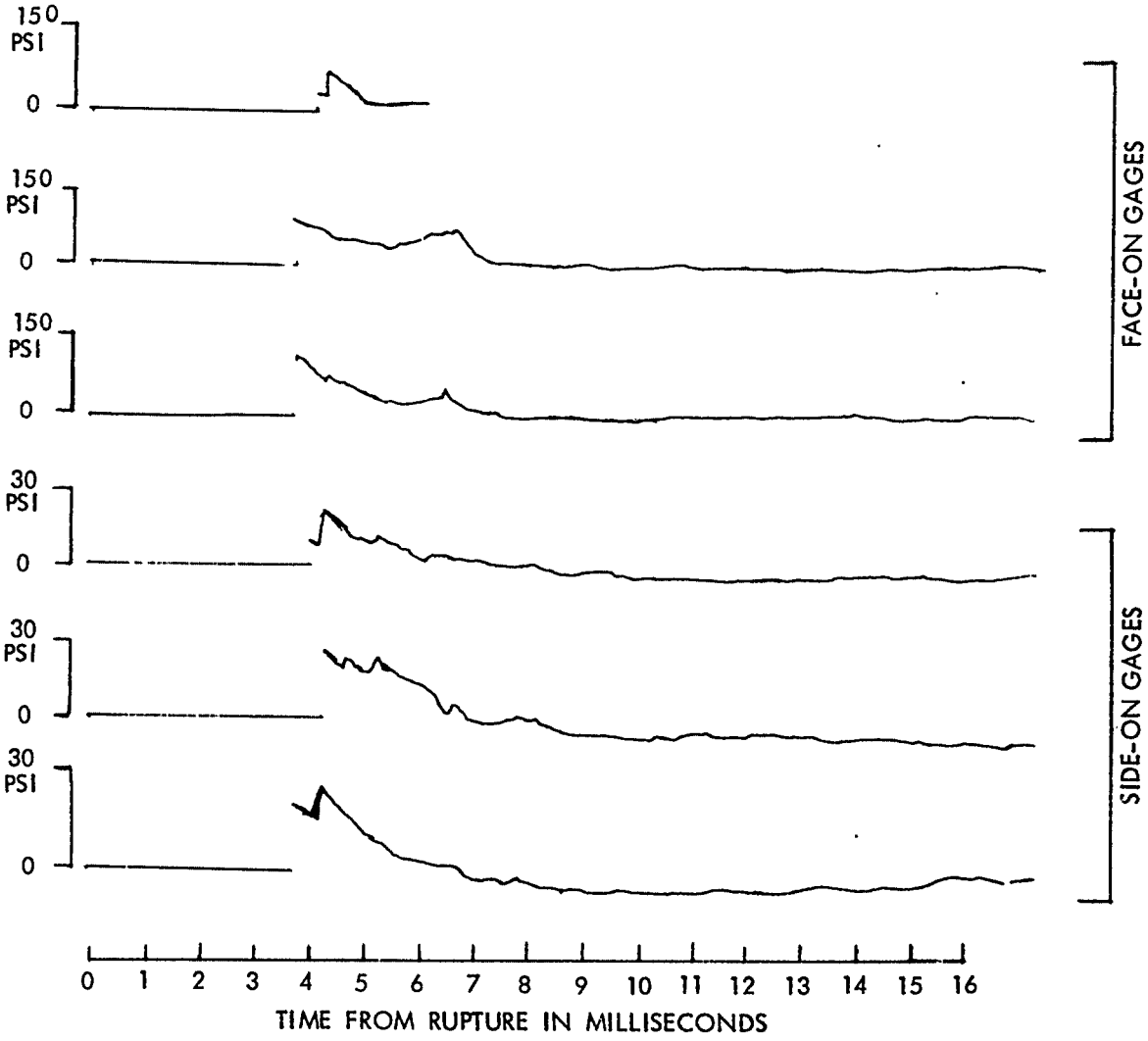

FIG. 3.5 PRESSURE-TIME HOSTORIES FROM TANK D

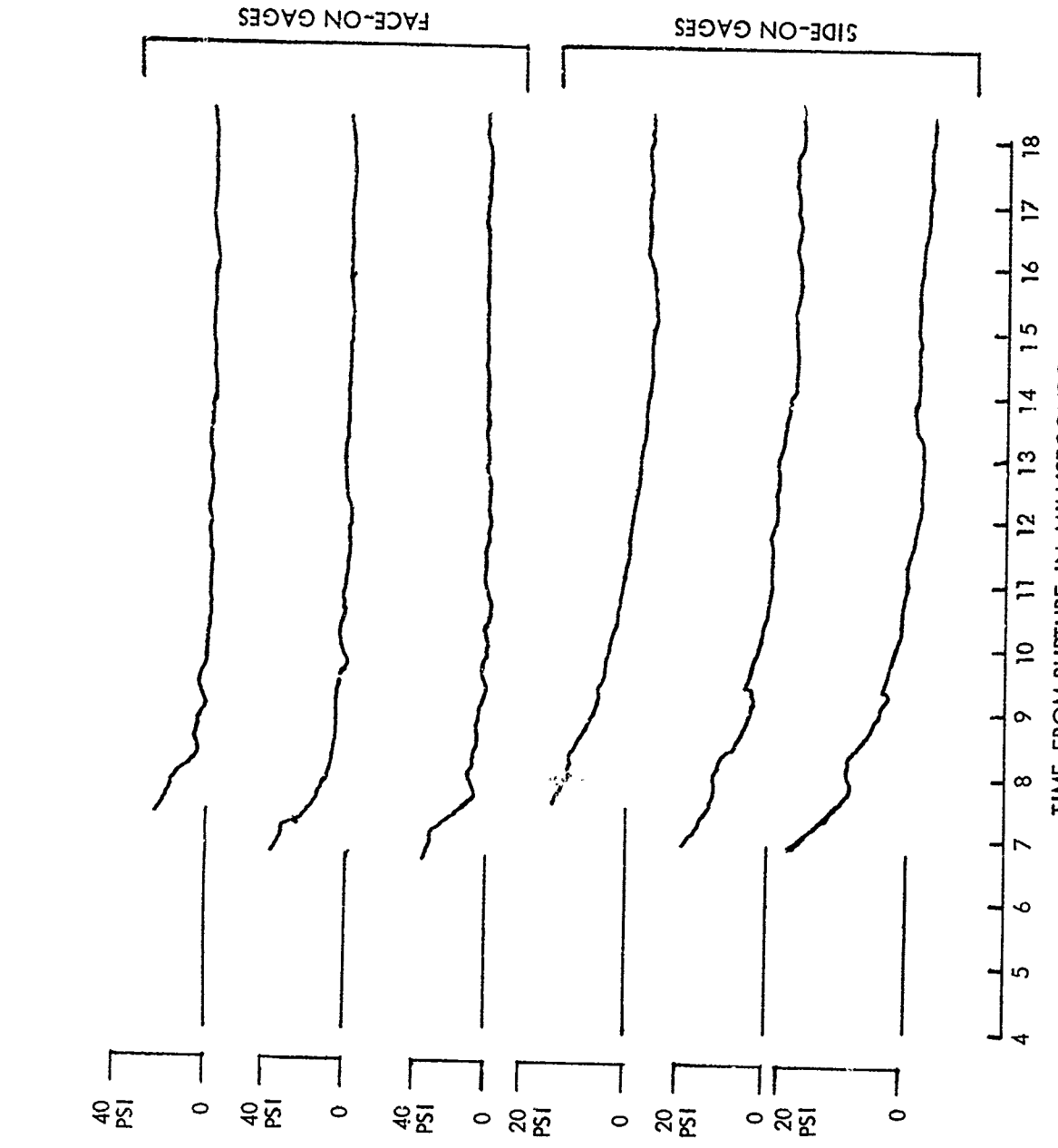

FIG. 3.5 (CONTINUED)

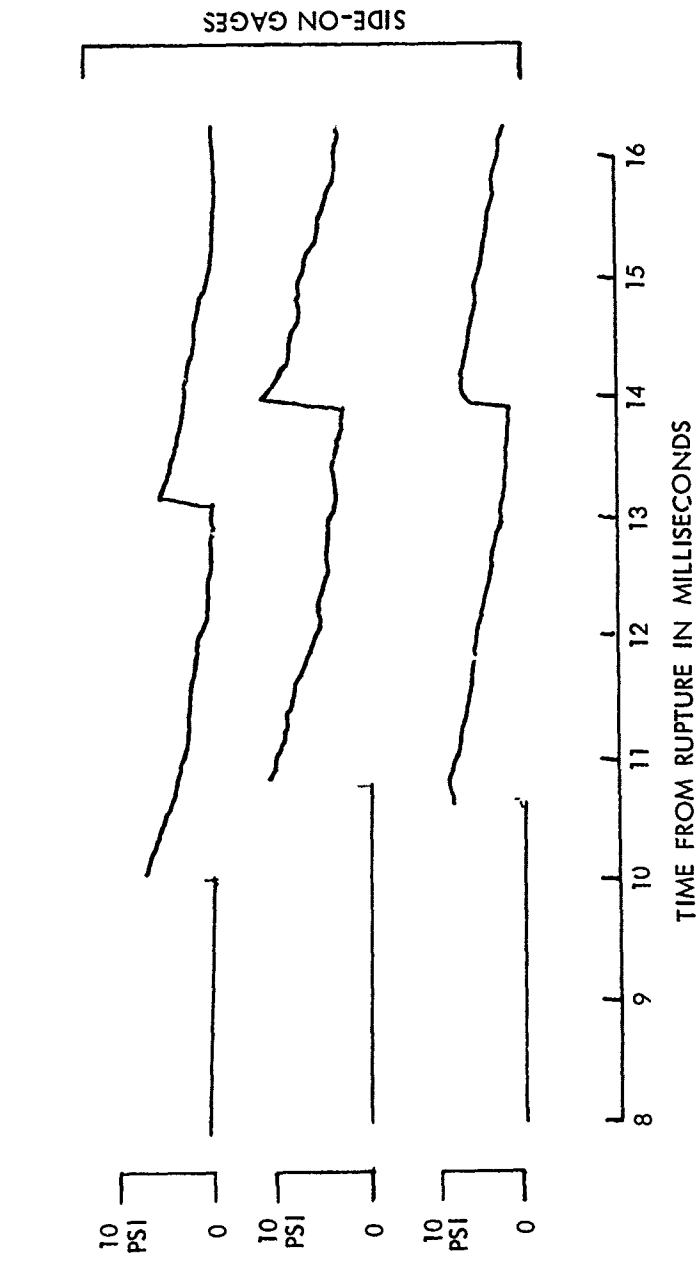

FIG. 3.5 (CONTINUED)

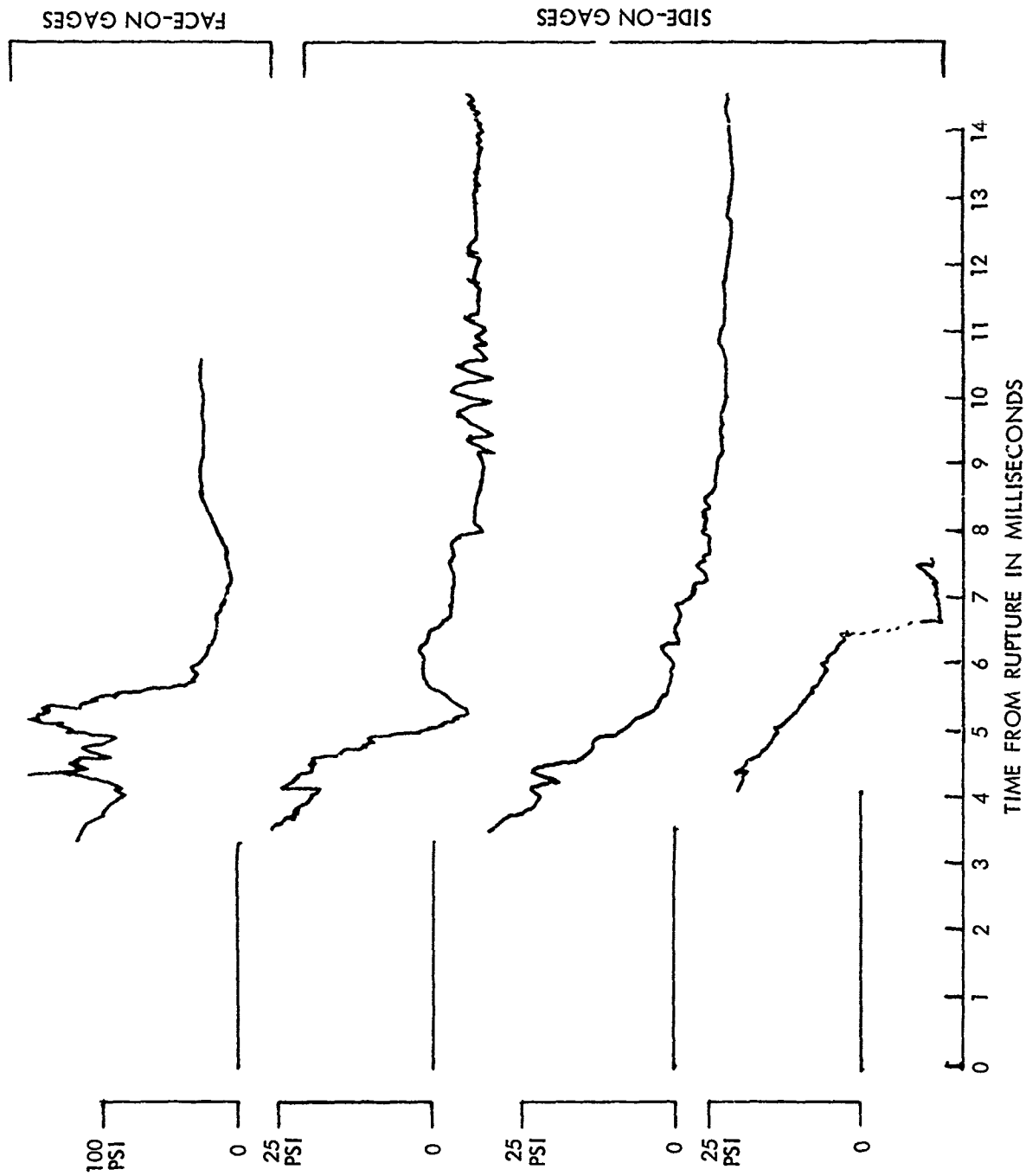

FIG. 3.6 PRESSURE-TIME HISTORIES FROM TANK E

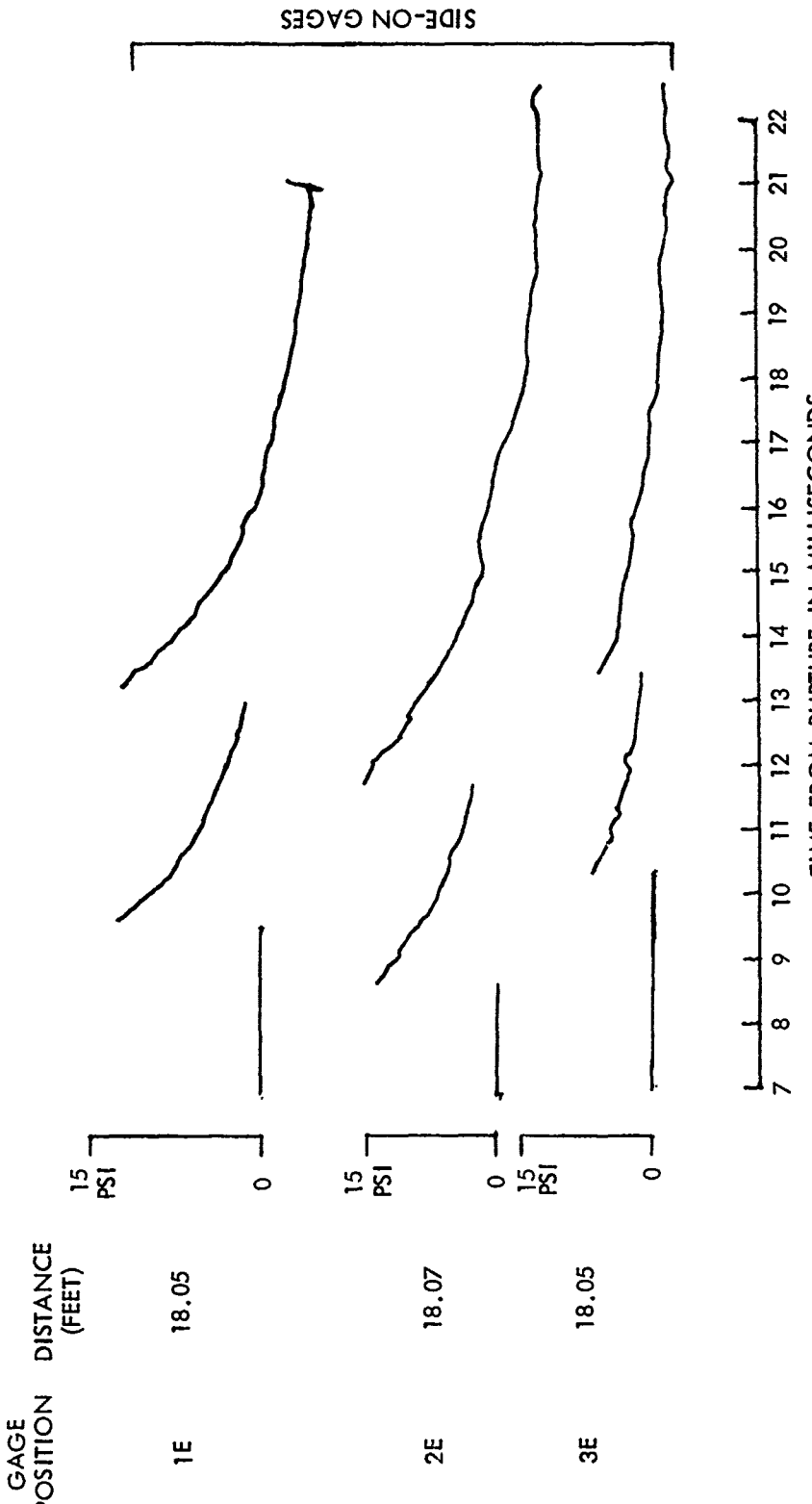

FIG. 3.6 (CONTINUED)

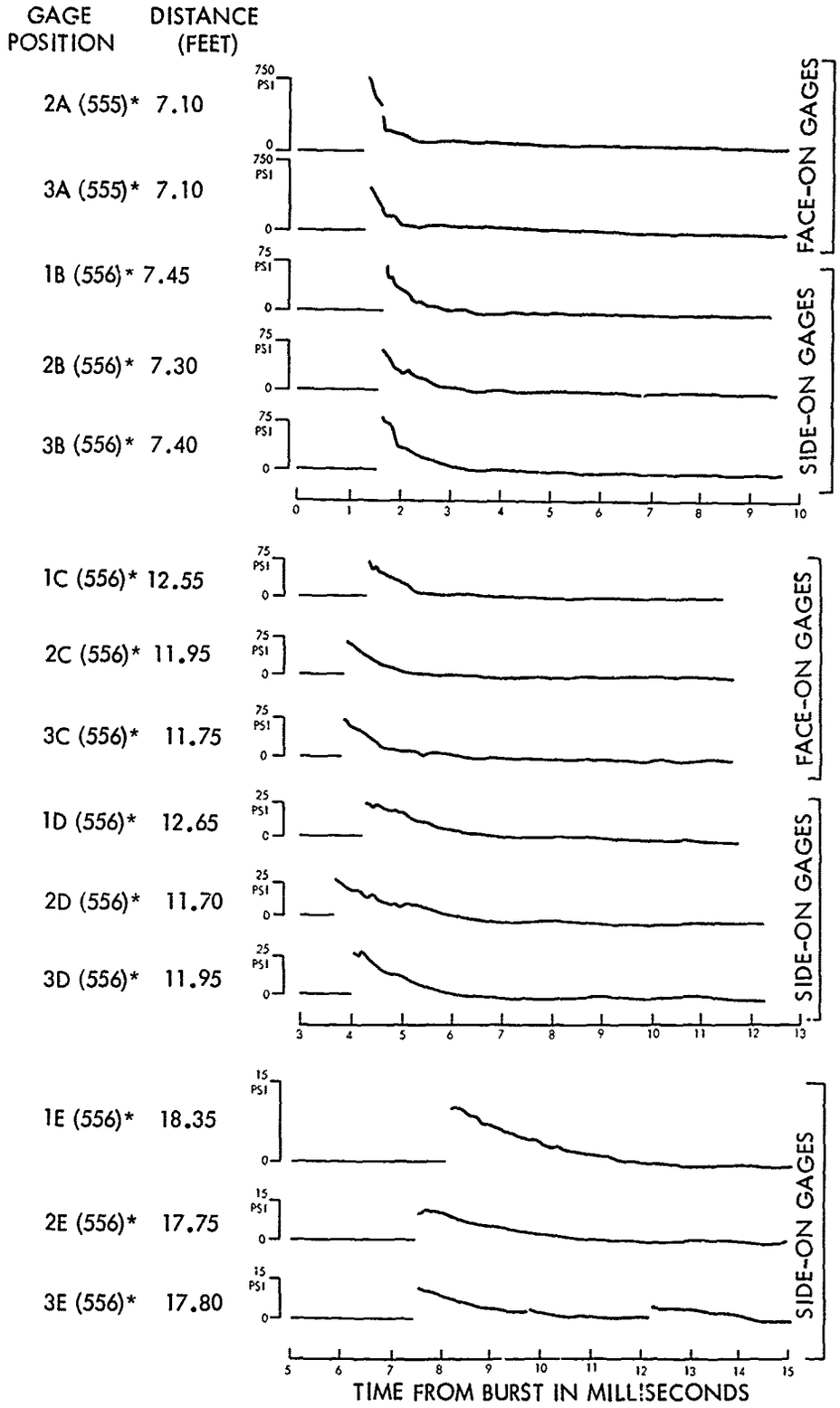

*REFERS TO SHOT NUMBER FROM TABLE 3-6

FIG. 3-7 PRESSURE-TIME HISTORIES FROM 8.2-LB. TNT SPHERES

Gages at the 18 ft positions (tanks D and E) were two feet nearer the charge than the celotex arena wall. Therefore, there is a strong reflection from the wall. This reflection is the second shock shown on the records from Tanks D and E for the 18 ft position. (Figures 3.5 and 3.6).

3.4 Blast Results

3.4.1 Pressure Results from Tanks A and B

Blast data generated by the rupture of Tanks A and B are given in Tables 3.1 and 3.2. Side-on pressure data are presented in Figures 3.8 and 3.9. The predicted TNT curve was obtained from the calculated data in reference (4) by adjusting for ground reflection. Specifically, a ground reflection coefficient of 1.5 was assumed. The reference (4) data were scaled to 0.138 pounds TNT by reducing distances by $(1.5)^{1/3}$ $(0.138)^{1/3}$ or 0.592. These data are shown in Figure 3.8. The measured TNT data was scaled from the 8.2 lb TNT data shown in Table 3.6. The figure 0.138 pounds of TNT comes from a calculation based on the isentropic expansion of the gas in the tank from burst pressure to ambient (14.7 psi). The detonation energy of TNT was assumed to be 1018 calories/gram. A similar isentropic calculation for the Tank B rupture pressure and volume yields a TNT equivalent of 0.169 pounds of TNT. The data for Tank B are shown in Figure 3.9. The predicted TNT curve in Figure 3.9 was generated by multiplying the distances in the reference (4) data by $(1.5)^{1/3}$ $(0.169)^{1/3}$ or 0.633.

The predictions for the tank rupture pressures were obtained from the calculated values shown in Appendix A by appropriate allowance for ground reflection. Again, a reflection coefficient of 1.5 was assumed. Thus distances for a given pressure were multiplied by $(1.5)^{1/3}$ or 1.145.

Two things are immediately apparent from Figures 3.8 and 3.9. The pressure decay slopes are different for the curve based on tank-rupture pressures and the TNT based curve. Secondly, pressures along different radii from GZ are not equal showing a lack of symmetry. Therefore, a single value for the TNT equivalency of the tank rupture energy does not describe the phenomena.

The predicted curve was based on a burst pressure of 460 psig; inserting the correct burst pressure in the calculations will increase the predicted side-on pressures from tank rupture by about 15% in the pressure range of interest. Further, no allowance was made in the calculations for the reduction of energy available to the shock resulting from the energy expended in tank rupture and fragment acceleration. Including this factor for conventional explosions results in a reduction of side-on pressure in the high pressure region. The inclusion of this "Mass Effect" in the tank calculations may give similar results. The quantitative effect is not known in the absence of such calculations (Ref. (5)).

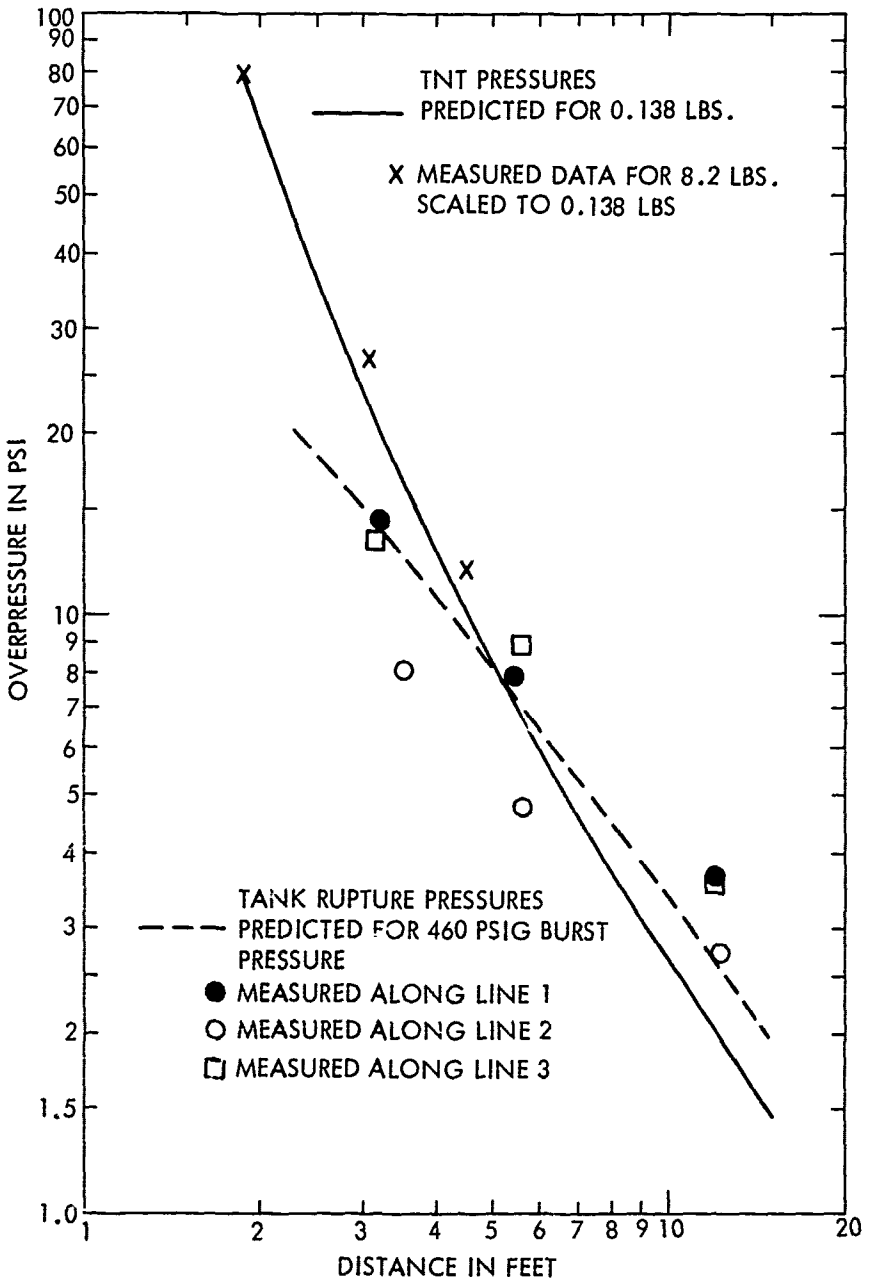

FIG. 3-8 SIDE-ON OVERPRESSURES FROM TANK A; 1.34 FT^3 BURST AT 625 PSI

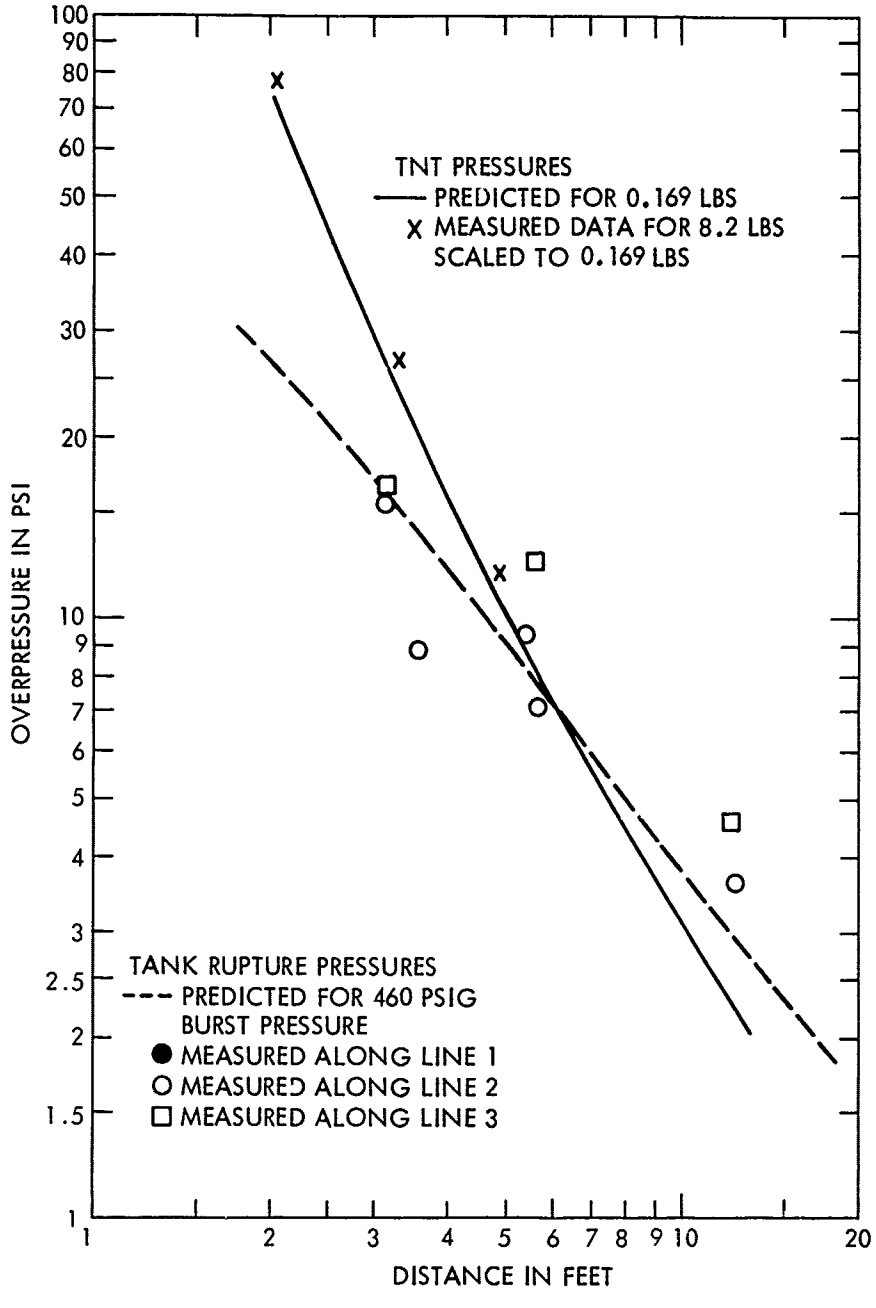

FIG. 3-9 SIDE-ON OVERPRESSURES FROM TANK B; 1.68 FT^3 TANK BURST AT 600 PSI

Face-on pressures are shown in Figures 3.10 and 3.11 for Tanks A and B. The TNT curve was generated from reference (4) data using the same scale factors as for the side-on pressures. Pressures were calculated using the equation for normally reflected pressures given in reference (6).

3.4.2 Pressure Results from Tank C

Data from this tank are presented in Table 3.3 and Figures 3.12 and 3.13. The predicted TNT curve was based on a yield of 0.324 lbs and a reflection coefficient of 1.5. Thus the TNT curve was obtained by decreasing the distances for the calculated one-pound data given in reference (4) by $(1.5)^{1/3} \times (0.324)^{1/3}$ or 0.79. No TNT charges of equivalent size were fired since the 8.2-lb TNT data found in Table 3.6 can be scaled down for comparison. The predicted curve for tank rupture pressures was obtained from the 6-ft^3 vessel predictions in Appendix A as follows. Since the burst pressure of the tanks were equal, distances for equal pressures were reduced by the ratio of the tank radii $\frac{4.6}{13.5}$ or 0.34. The tank rupture pressure predictions did not allow for the energy losses due to tank rupture and acceleration. An accounting for this energy in the calculations will lower side-on pressures nearest the tank; the amount is unknown until such calculations are made.

The measured tank rupture data again show a lack of symmetry about GZ and a different slope from that of the predicted TNT curve. Thus a single TNT energy equivalent does not adequately describe the data.

Similar comments are appropriate to the face-on pressures shown in Figure 3.13. The differences between measured data and predicted TNT data are accentuated. This comes about because the ratio between side-on and reflected pressures is pressure dependent. It varies from a low of 2 as side-on pressures approach zero to 8 as they become infinitely large.

3.4.3 Pressure Results from Tanks D and E

Pressure data from the rupture of these two tanks are presented in Tables 3.4 and 3.5 and Figures 3.14 and 3.15.

The predicted TNT curve in Figure 3.14 is based on the 1-lb free air data in reference (4). A ground reflection coefficient of 1.5 was assumed. Thus the predictions for 10.1 lbs of TNT were obtained by multiplying the distances for 1 lb by the scale factor $(1.5)^{1/3}$ $(10.1)^{1/3}$ or 2.48. (The tank rupture energy based on isentropic expansion is equivalent to 10.1 lbs of TNT.) Measured 8.2-lb TNT data were scaled to 10.1 lbs by increasing distances $\left(\frac{10.1}{8.2}\right)^{1/3}$ or 1.07.

The predicted tank rupture-pressures were obtained by multiplying the Wundy code calculations by a suitable factor to account

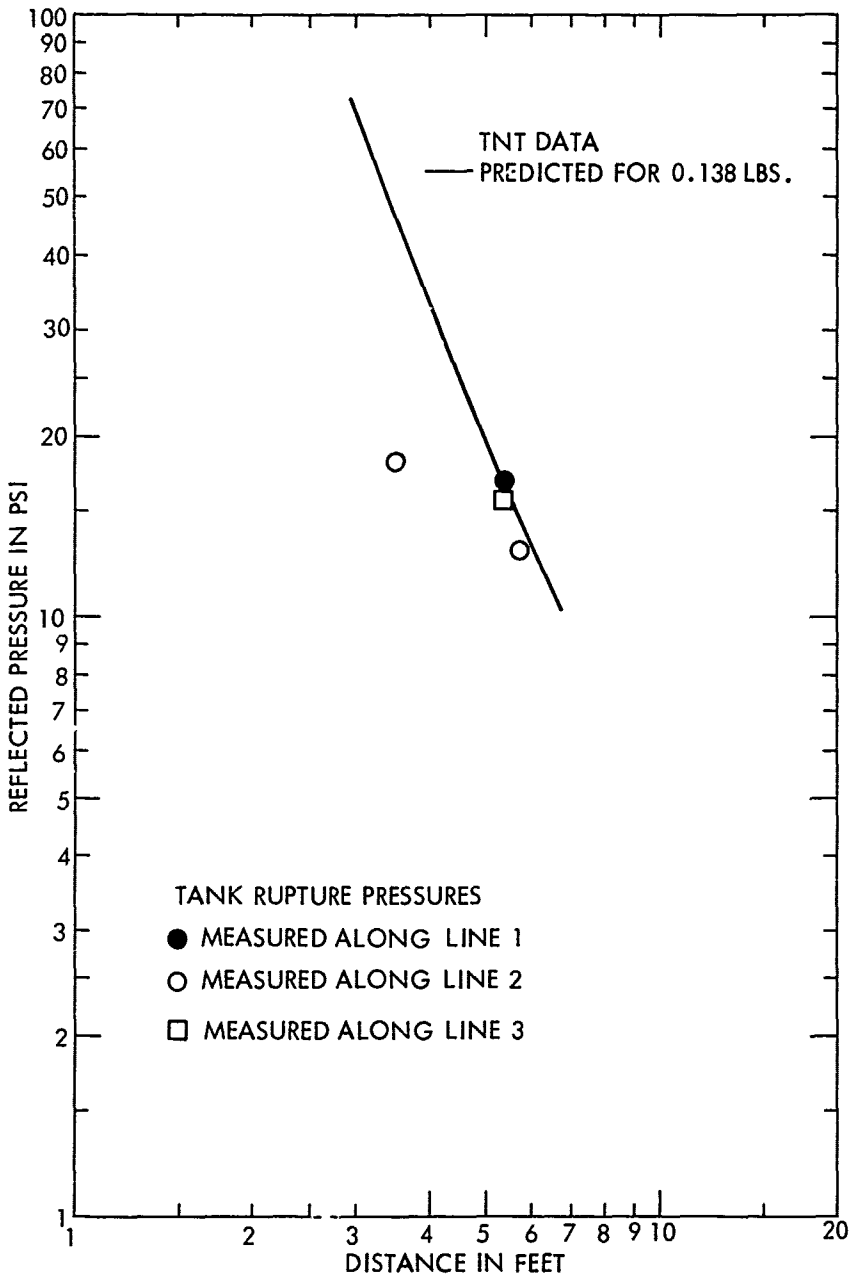

FIG. 3-10 FACE-ON PRESSURES FROM TANK A; 1.34 FT^3 BURST AT 625 PSI

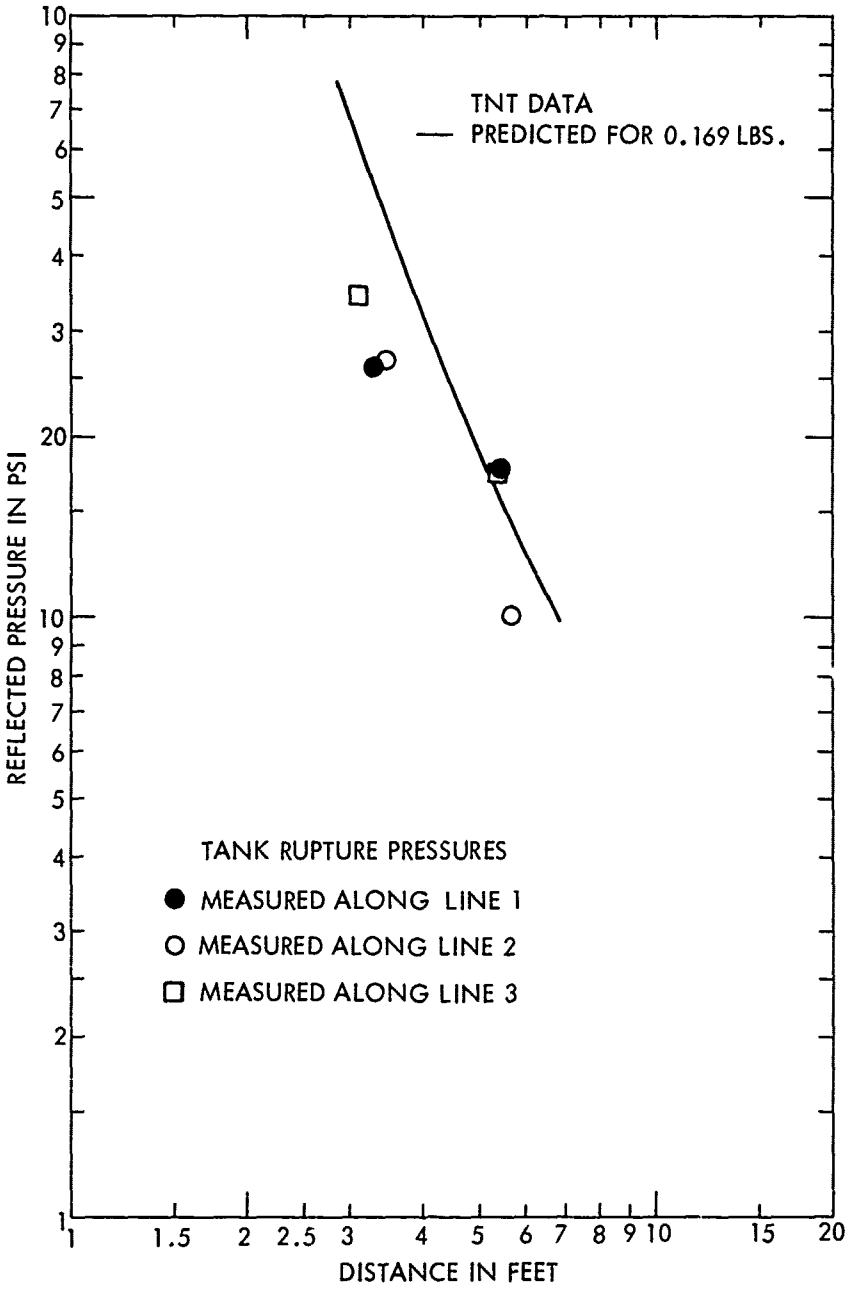

FIG. 3-11 FACE-ON PRESSURES FROM TANK B; 1.68 FT^3 BURST AT 600 PSI

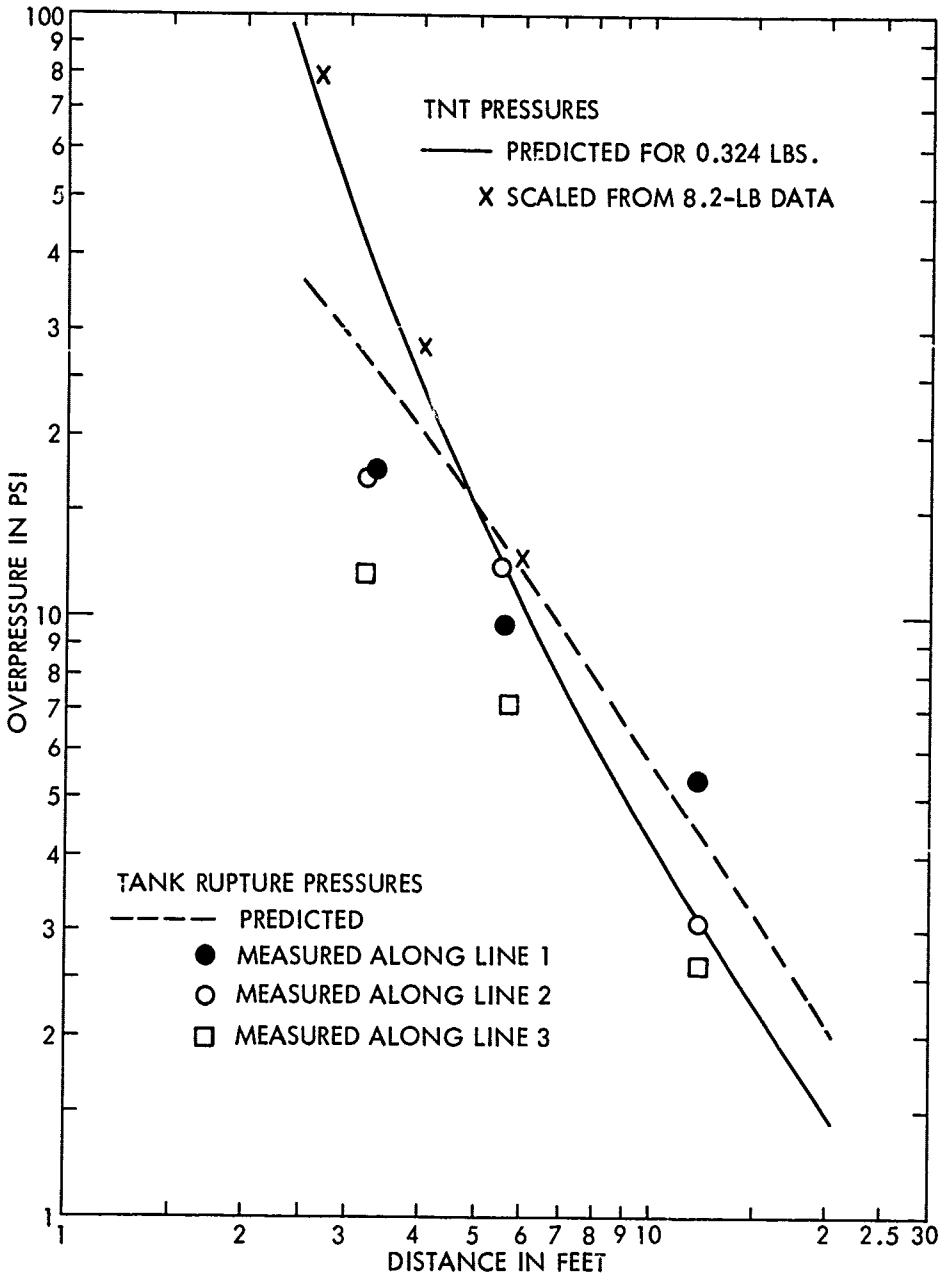

FIG. 3-12 SIDE-ON OVERPRESSURES FROM TANK C; 0.235 FT^3 BURST AT 8,000 PSI

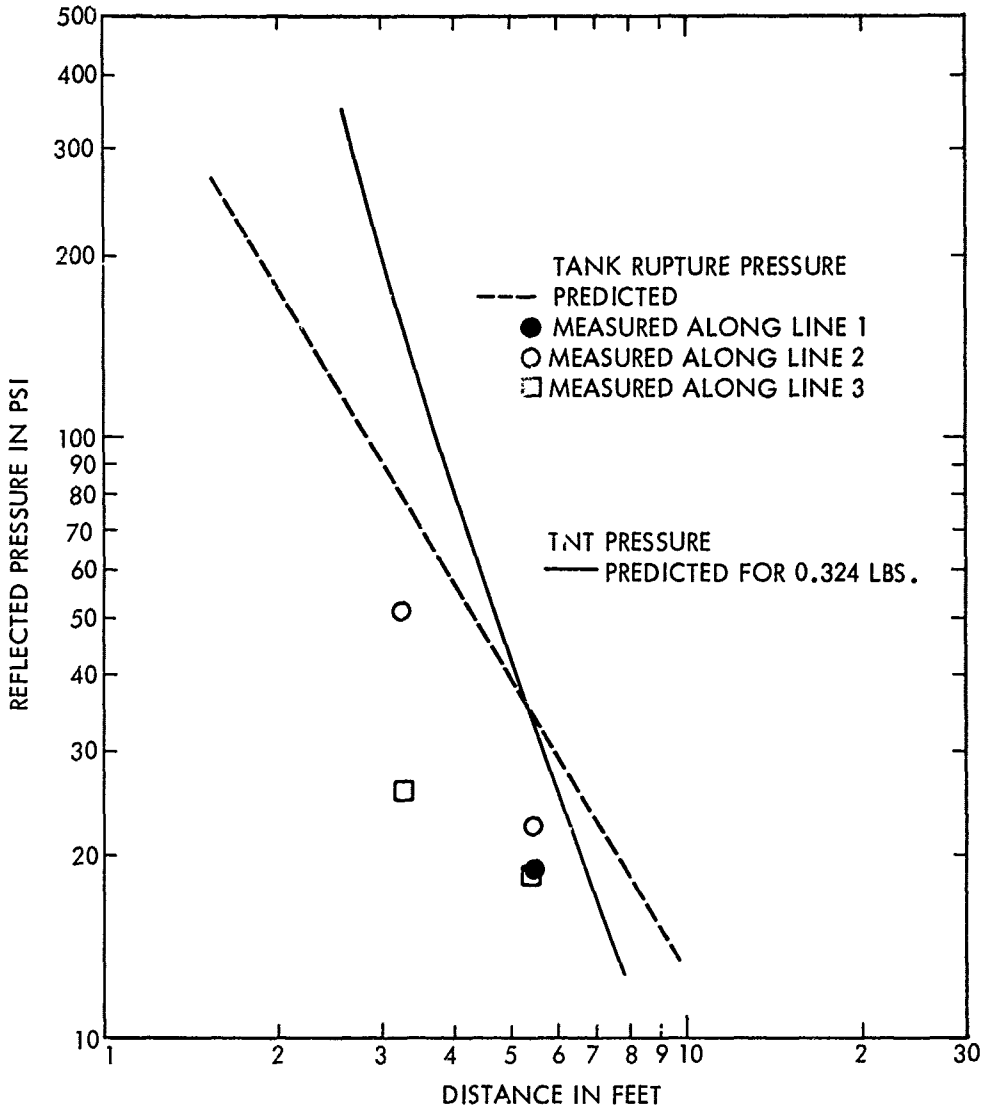

FIG. 3-13 FACE-ON PRESSURES FROM TANK C; 0.235 FT^3 TANK BURST AT 8,000 PSI

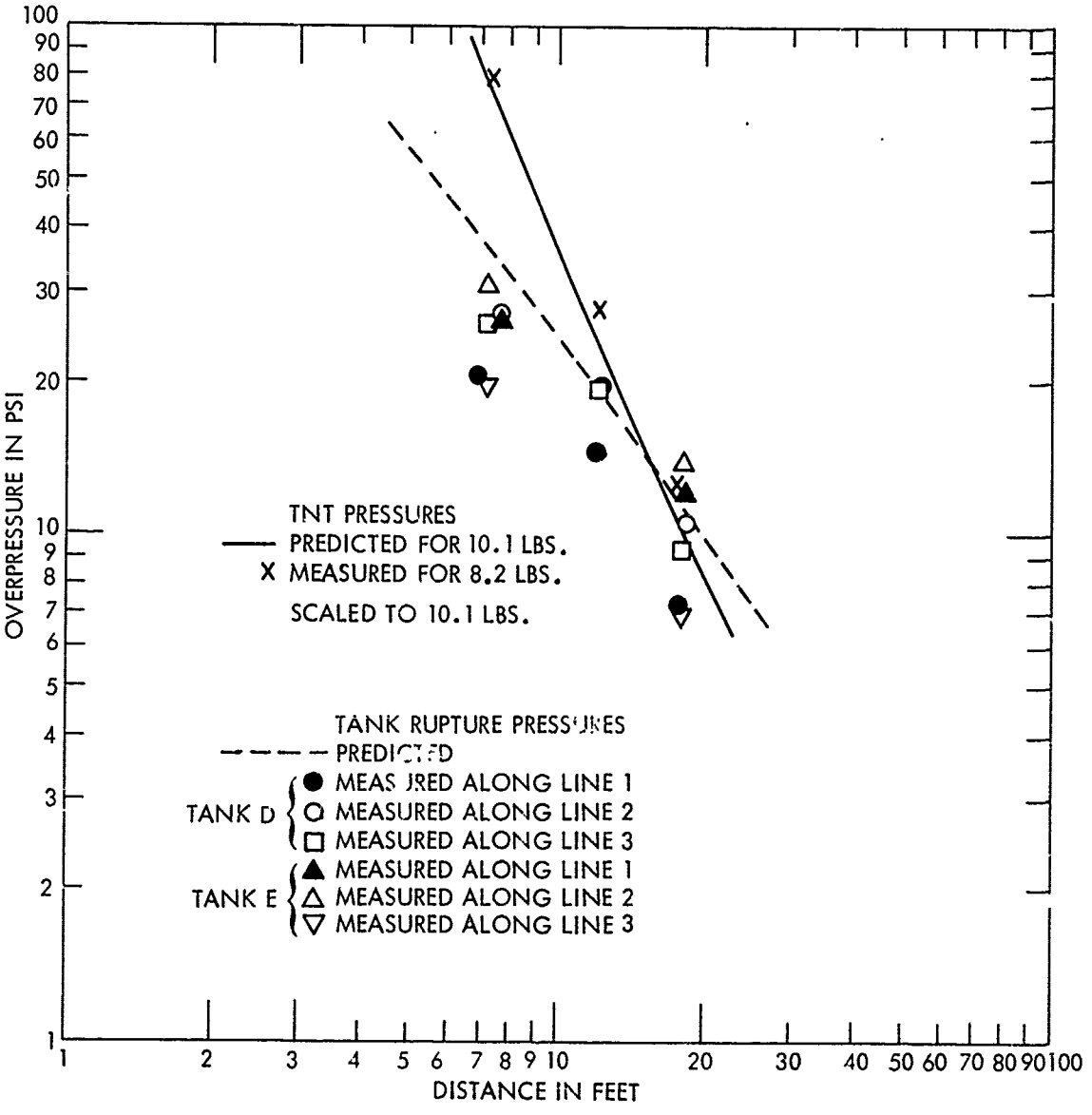

FIG. 3-14 SIDE-ON OVERPRESSURES FROM TANKS D AND E; 6 FT^3 BURST AT 8,000 PSI

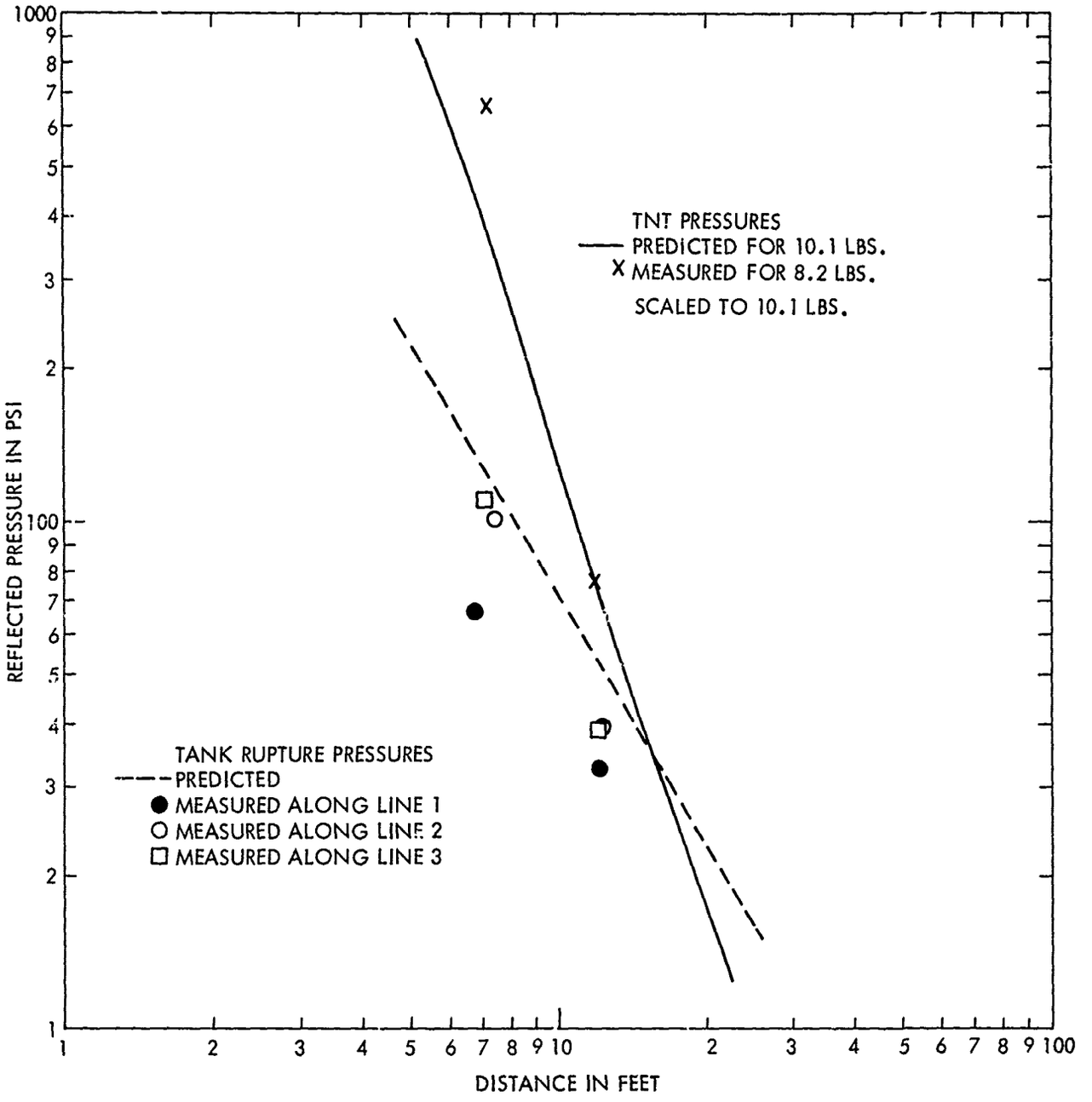

FIG. 3-15 FACE-ON PRESSURES FROM TANK D; 6 FT^3 TANK BURST AT 8,000 PSI

for pressure enhancement due to the ground proximity. As with TNT, a reflection coefficient of 1.5 was assumed. Therefore the scale factor is $(1.5)^{1/3}$ or 1.145. Again, the effects of the pressure vessel's mass was not considered. Inclusion of the mass effect in the side-on pressure calculations for tank rupture would give results similar to those predicted for tanks A, B, and C.

Figure 3.14 shows the measured tank rupture pressures from tank D to be in reasonable agreement with those from tank E. Again, the shock strength is not symmetrical about GZ. There is also a difference between the slopes of the predicted TNT curve and that obtained from the tank rupture data. Thus, no single TNT equivalence value can be used to describe the tank rupture data.

Similar comments apply to the face-on pressures shown in Figure 3.15. The differences between predicted face-on and measured face-on pressures are greater than those for the side-on case. Again, this comes about because the ratio of face-on to side-on pressures is pressure dependent.

3.5 Positive Shockwave Durations

3.5.1 Durations for Tanks A and B

Figures 3.16 and 3.17 present the positive shock wave durations from Tanks A and B. Predicted TNT values were scaled from reference (6) data to the isentropic expansion energy equivalents of 0.138 lbs and 0.169 lbs TNT for Tanks A and B respectively. Both distances and durations were multiplied by 0.592 for Tank A and 0.633 for Tank B. The origin of these scale factors is given in Section 3.4.1. The measured 8.2-lb TNT data were scaled for Tank A by multiplying measured distances and durations by the factor $\left(\frac{0.138}{8.2}\right)^{1/3}$ or 0.256 and to Tank B by the factor $\left(\frac{0.169}{8.2}\right)^{1/3}$ or 0.275.

Figures 3.16 and 3.17 show that tank rupture durations are longer than those from TNT. Because the tank rupture durations are much longer close-in, they generate a curve with a shallower slope than does TNT.

3.5.2 Durations for Tank C

Figure 3.18 presents the positive shock wave durations generated by the rupture of Tank C. Predicted TNT values are those from reference (6) scaled to 0.324 lbs TNT burst near a reflecting surface with 1.5 reflection coefficient. Thus both distances and durations were multiplied by $(1.5)^{1/3}$ $(0.324)^{1/3}$ or 0.79. Measured 8.2-lb TNT data were scaled to 0.324 lbs by multiplying both durations and distances by $\left(\frac{0.325}{8.2}\right)^{1/3}$ or 0.34.

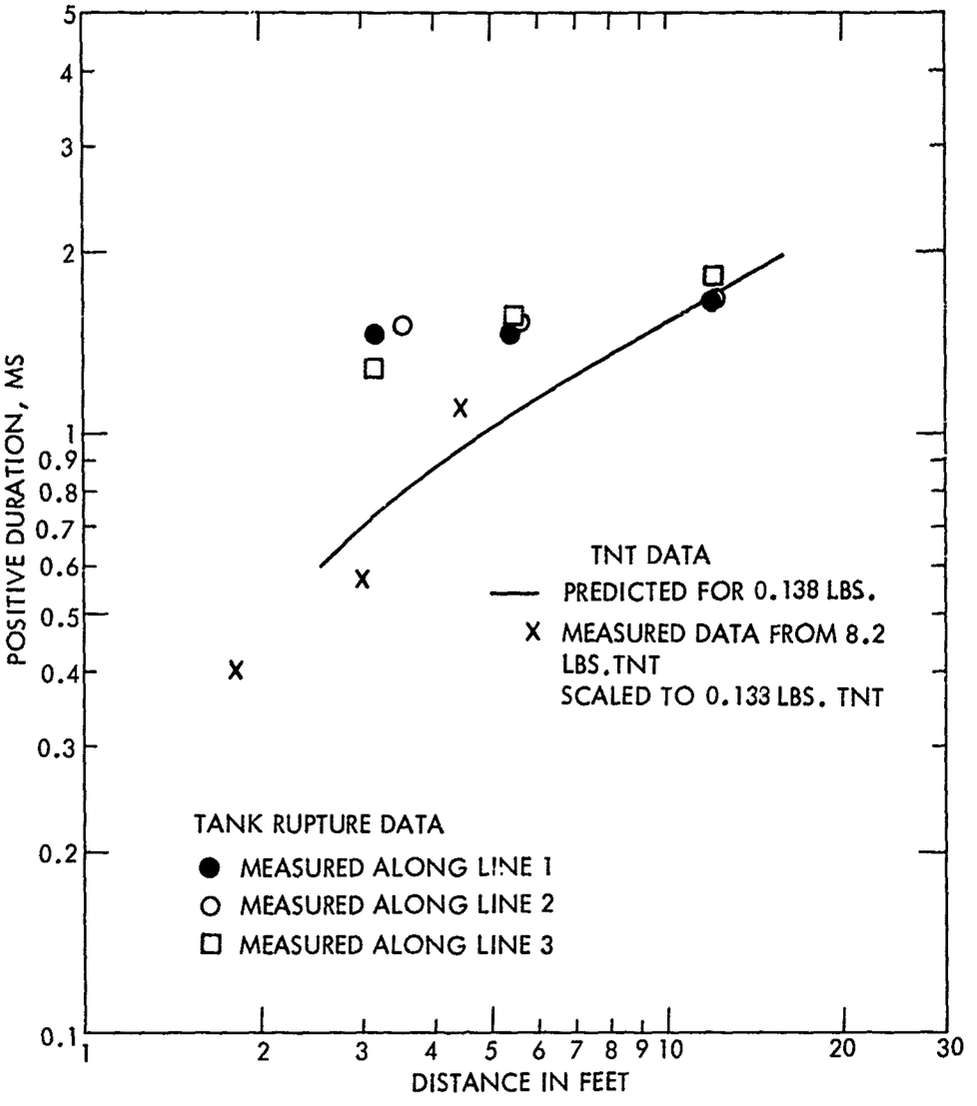

FIG. 3-16 SIDE-ON POSITIVE DURATION FROM TANK A; 1.34 FT^3

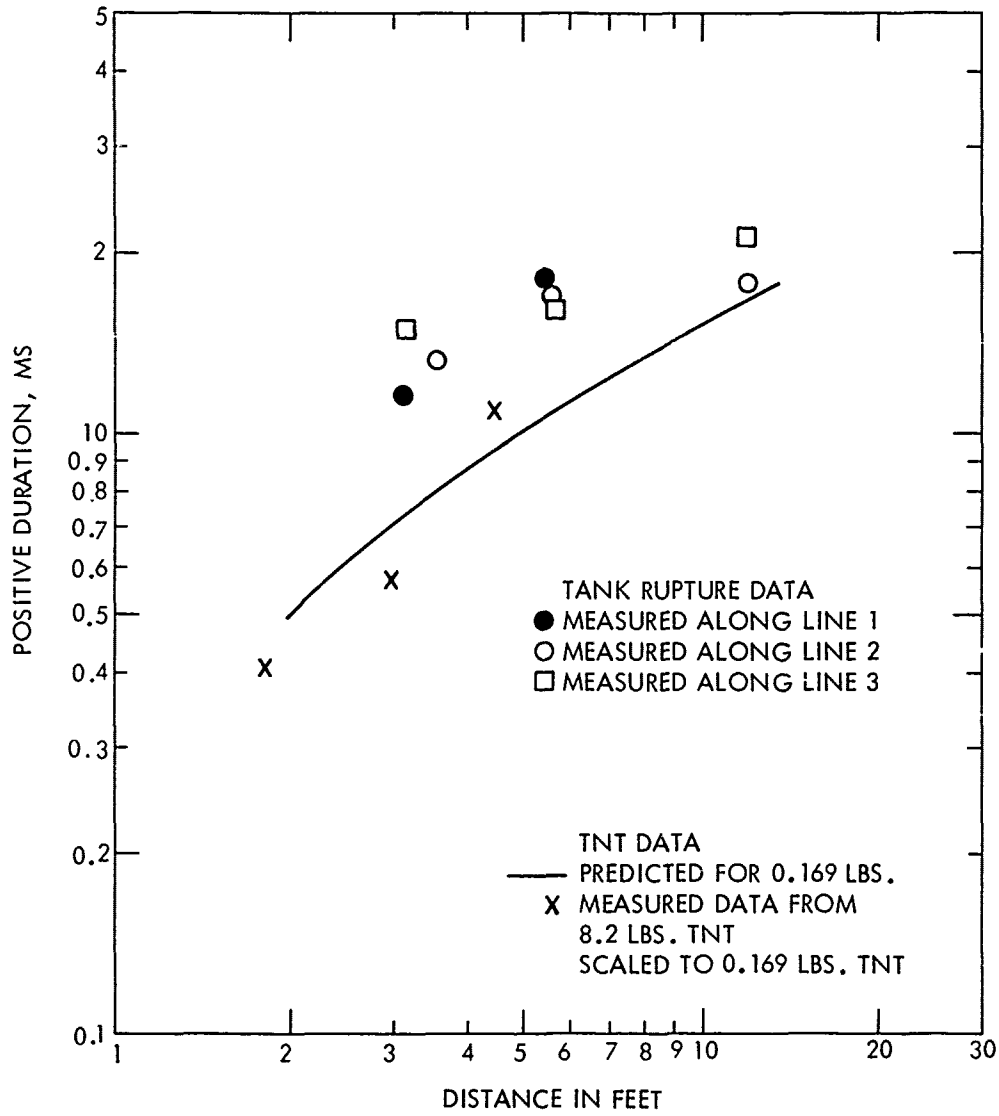

FIG. 3-17 SIDE-ON POSITIVE DURATION FROM TANK B; 1.68 FT^3

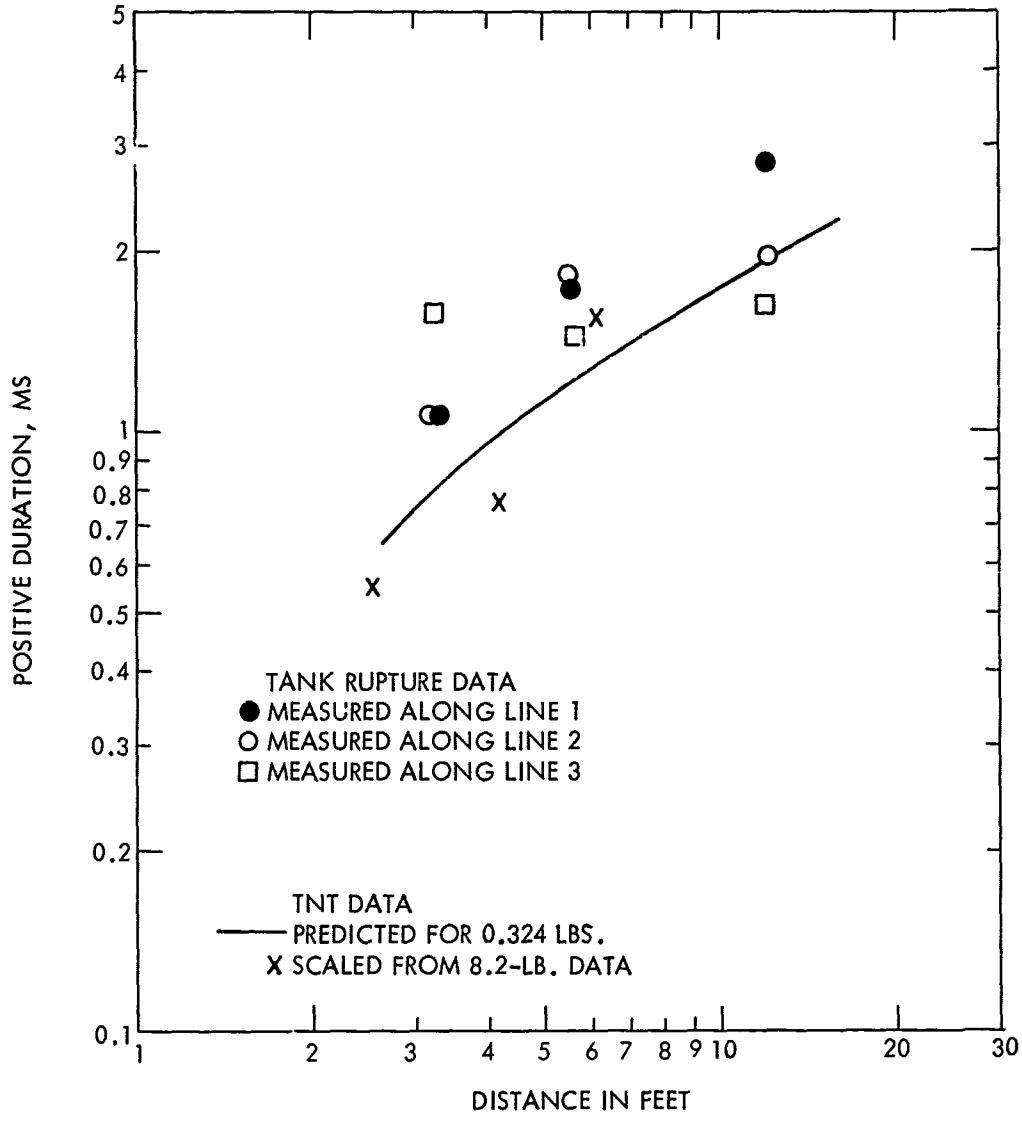

FIG. 3-18 SIDE-ON POSITIVE DURATION FROM TANK C; 0.235 FT^3

Figure 3.18 shows longer positive shock wave durations than those predicted for 0.324 lbs of TNT at the closer positions. Thus the tank rupture data generates a duration curve that has a flatter slope than does the curve generated by a conventional explosion.

3.5.3 Durations for Tanks D and E

Figures 3.19 and 3.20 present the side-on positive shock wave durations from the larger helium vessel rupture. The predicted TNT curve is generated from reference (6). These data were scaled to 10.1 lbs of TNT fired on the ground by assuming a ground reflection coefficient of 1.5. The experimental TNT values are those measured from the 8.2-lb TNT charges scaled to 10.1 lbs.

At the 18 ft gage position, the wall-reflected shock arrived back at the gages before the incident wave had decayed to zero (Figure 3.5). Therefore, positive durations for this position were obtained by extrapolating the incident pressure history to zero pressure.

The pattern of longer positive shock wave durations at the close-in gage positions was present in these two events as it was in all tank rupture cases.

3.6 Positive Shockwave Impulse

3.6.1 Impulse from Tanks A and B

Figures 3.21 and 3.22 present the positive shock wave impulse generated by the rupture of tanks A and B. The predicted TNT data are scaled from the reference (6) data using an assumed reflection coefficient of 1.5. Thus the one-lb TNT data from reference (6), both impulse and distance, are multiplied by 0.592 or 0.633, the scale factors developed in Section 3.4.1 for Tanks A and B respectively. The measured 8.2-lb TNT data were scaled to these tanks also. This was done by multiplying the measured distances and impulses by 0.256 or 0.275, the scale factors given in Section 3.5.1 for scaling the 8.2-lb data to Tanks A and B respectively.

The tank rupture data are higher than the predicted TNT data and except for the farther out position, higher than the measured TNT data.

Face-on positive impulses have not been plotted but are given in Tables 3.1, 3.2, and 3.6 for tanks A, B, and TNT respectively.

3.6.2 Impulse from Tank C

Figure 3.23 presents the positive shock wave impulse data from the rupture of tank C. The predicted TNT curve was scaled to 0.324 lbs from the data in reference (6) using an assumed reflection coefficient of 1.5. Thus the referenced distances and impulses were reduced by a factor of $(1.5)^{1/3}\ (0.324)^{1/3}$ or 0.79. The 8.2-lb TNT data were scaled to 0.324 lbs by reducing both distances and impulses by $\left(\frac{0.324}{8.2}\right)^{1/3}$ or 0.34.

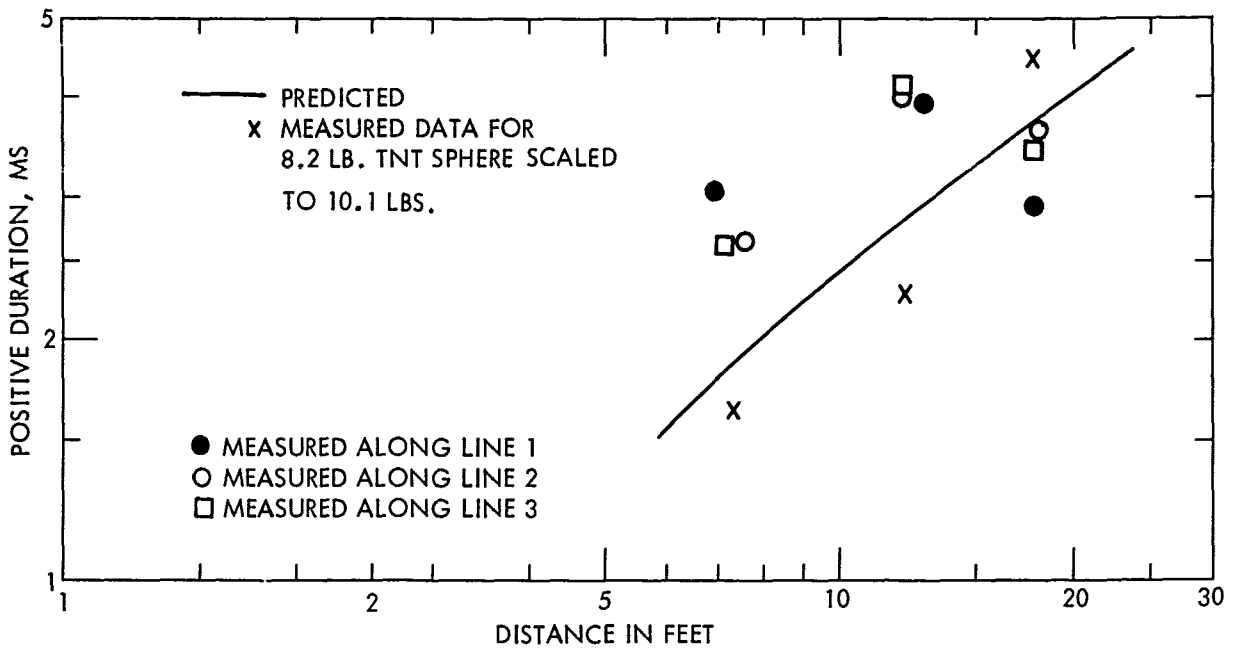

FIG. 3-19 SIDE-ON POSITIVE DURATION FROM TANK D; 6 FT^3

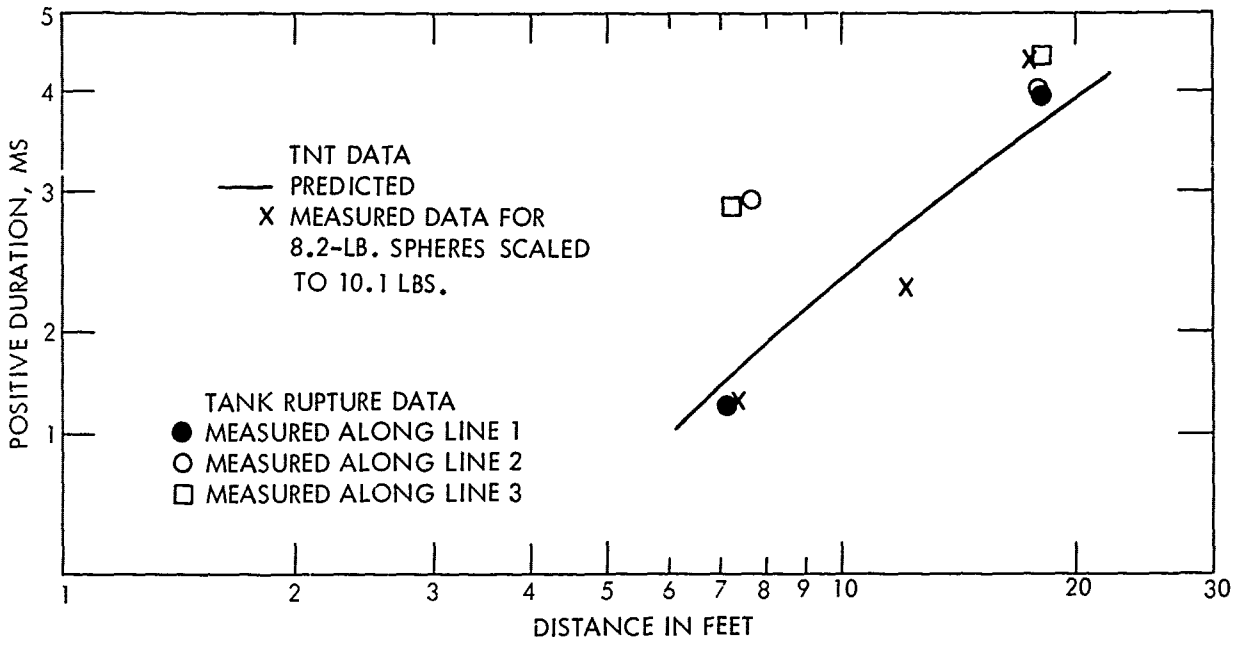

FIG. 3-20 SIDE-ON POSITIVE DURATION FROM TANK E; 6 FT^3

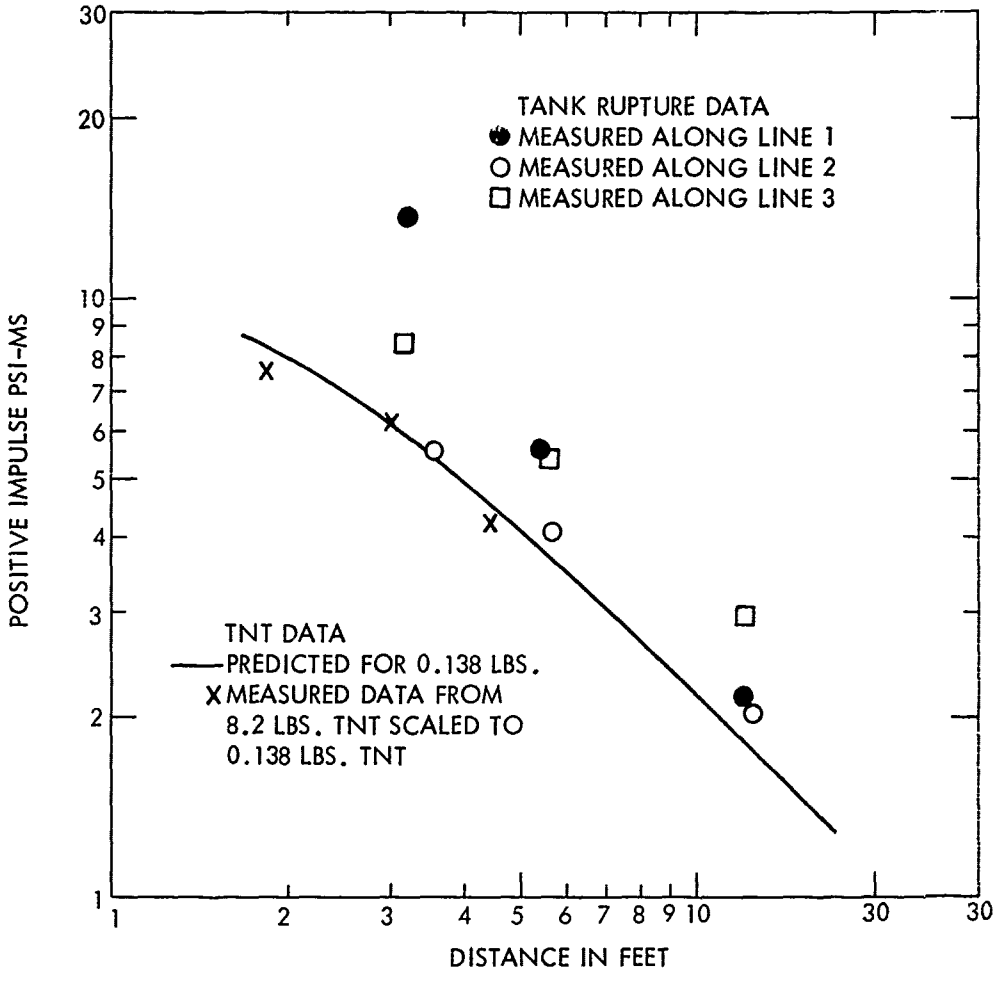

FIG. 3-21 SIDE-ON POSITIVE IMPULSE FROM TANK A; 1.34 FT^3

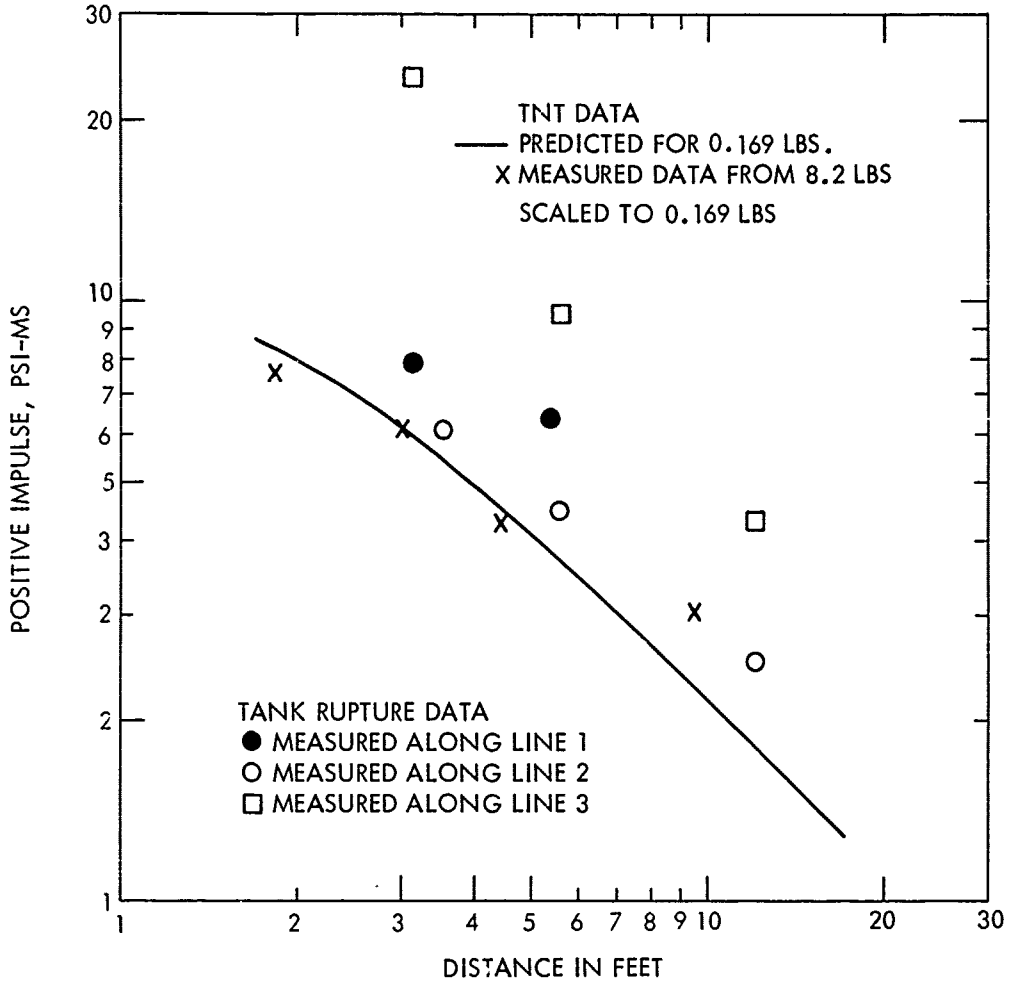

FIG. 3-22 SIDE-ON POSITIVE IMPULSE FROM TANK B; 1.68 FT^3

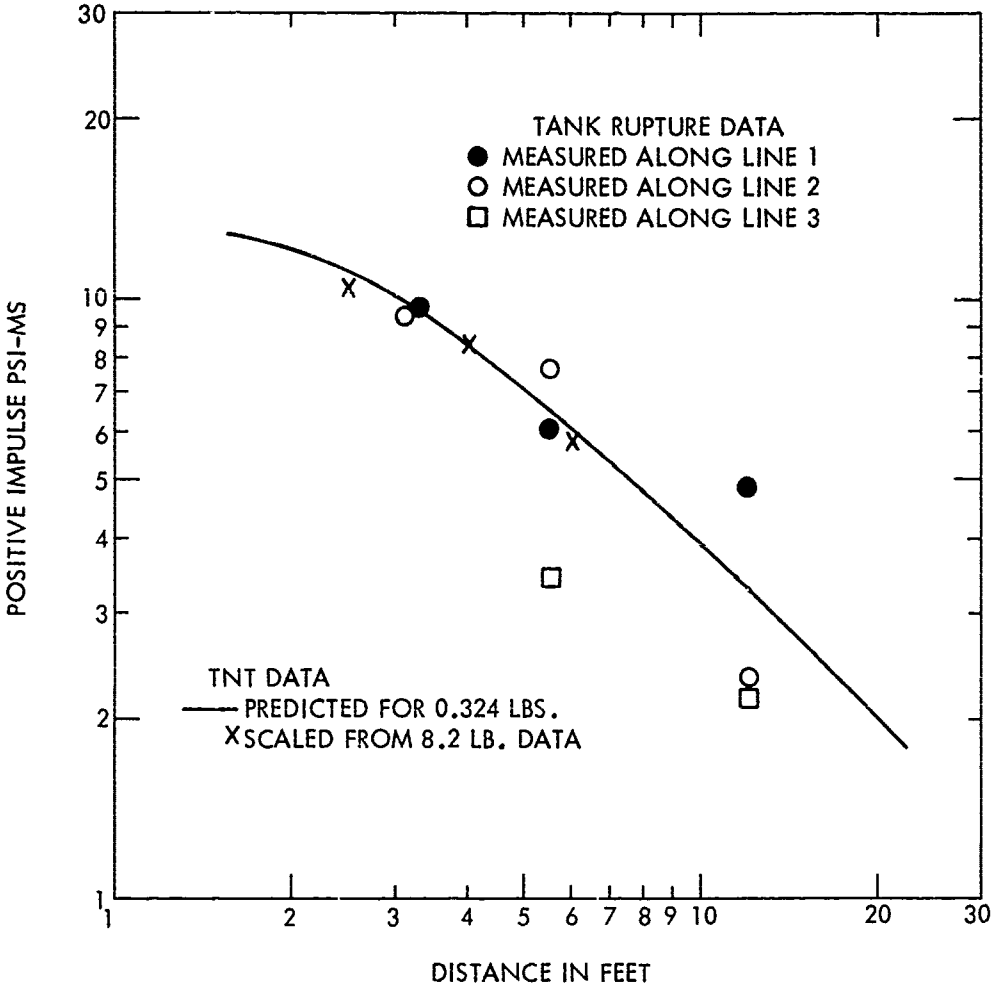

FIG. 3-23 SIDE-ON POSITIVE IMPULSE FROM TANK C; 0.235 FT^3

Side-on positive impulse from tank rupture seems to scatter about the predicted TNT data. Face-on positive impulse was not plotted but is given in Table 3.3.

3.6.3 Impulse from Tanks D and E

Figures 3.24 and 3.25 present the positive shock wave impulse data from the rupture of tanks D and E. The predicted impulse for TNT is generated from the 1-lb reference (6) data by assuming a reflection coefficient of 1.5. Thus the referenced data, both distance and impulse, were increased by $(1.5)^{1/3}(10.1)^{1/3}$ or 2.48. The measured 8.2-lb data scaled to 10.1 lbs is seen to compare quite well with the predicted curve.

The tank rupture data generally scatter about the predicted TNT curve. However, the impulse measured along line 1 for tank D (Figure 3.24) are quite low. The side-on pressures along this line for this tank, Figure 3.14, are also quite low.

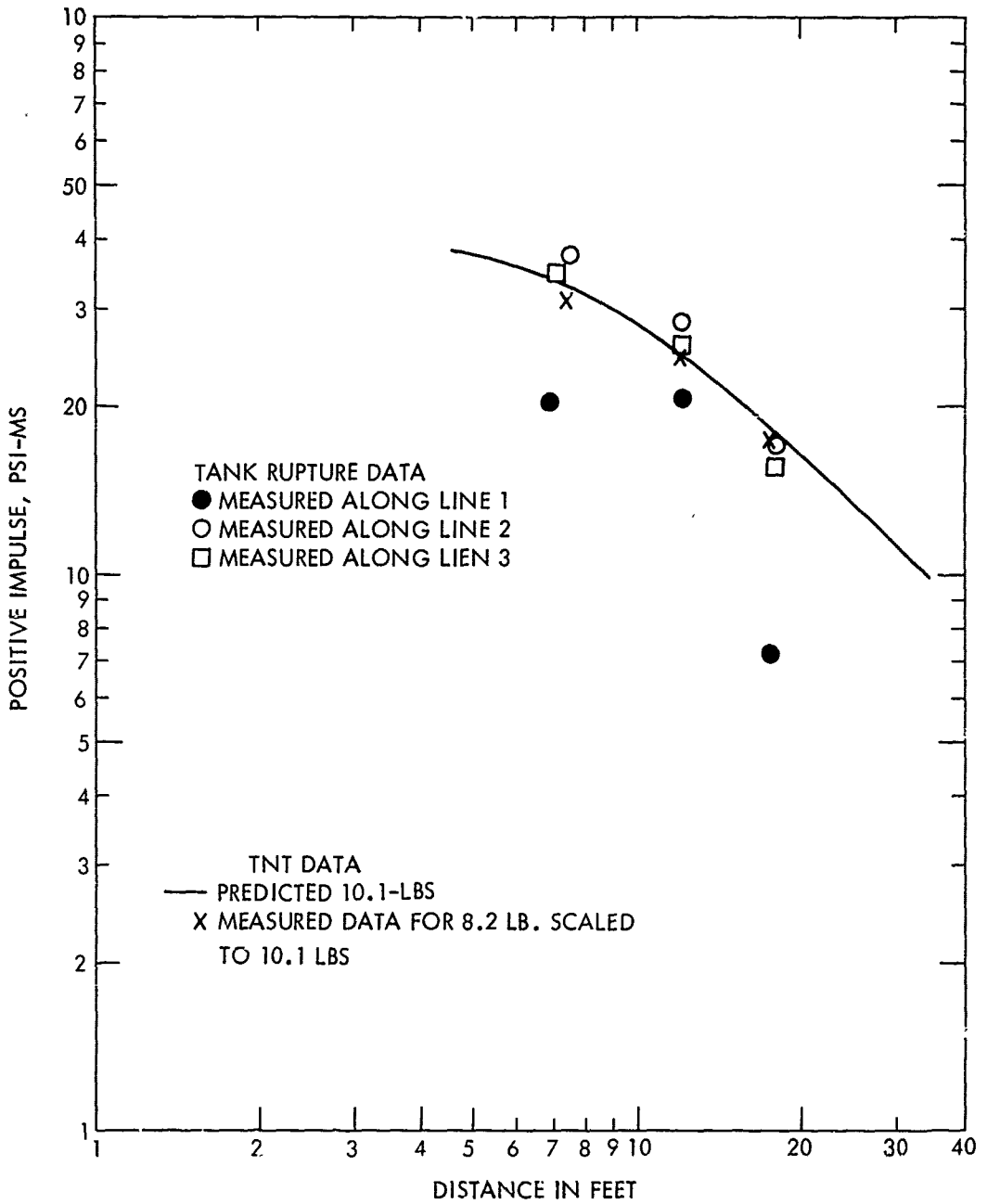

FIG. 3-24 SIDE-ON POSITIVE IMPULSE FROM TANK D; 6 FT^3

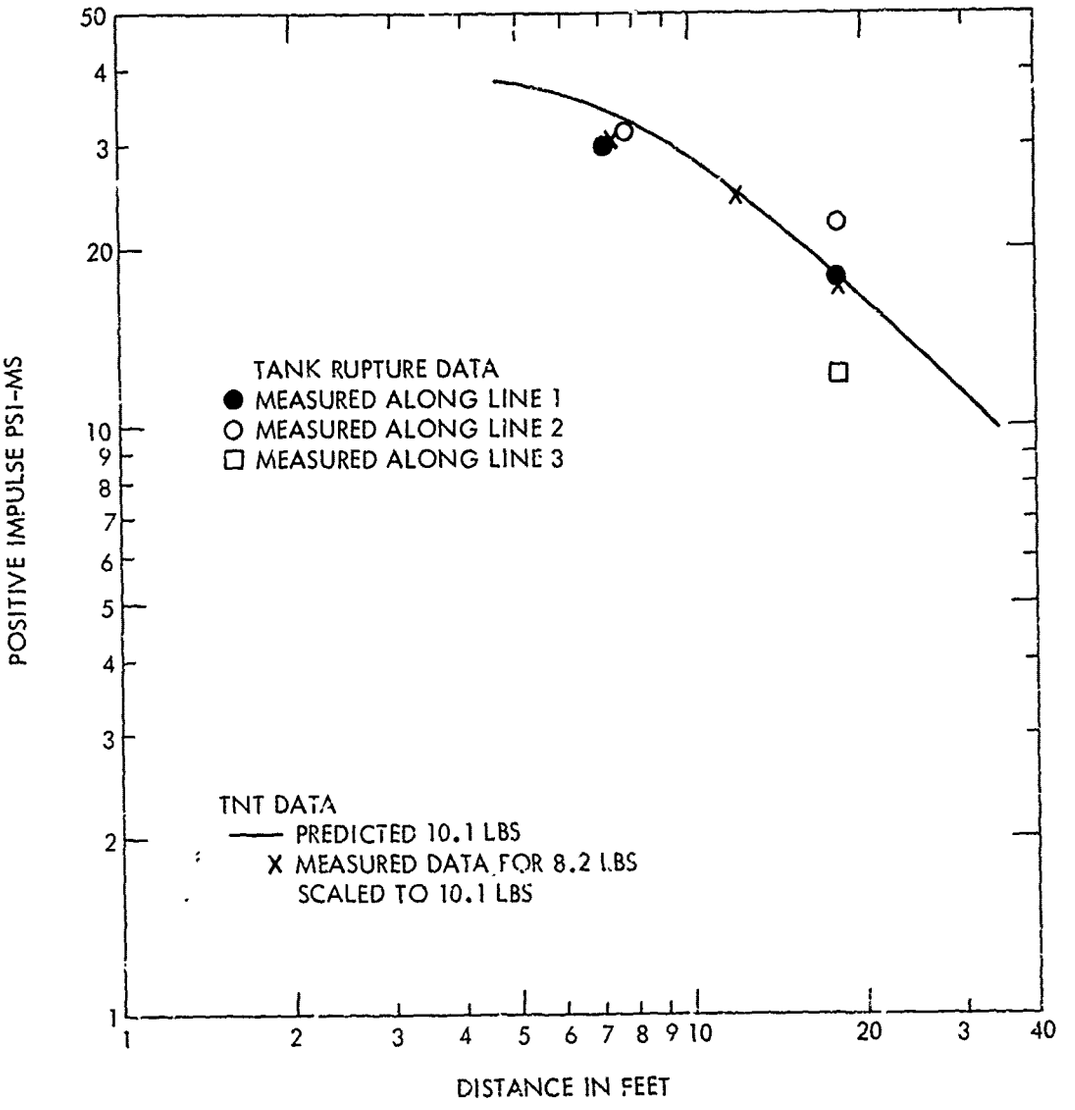

FIG. 3-25 SIDE-ON POSITIVE IMPULSE FROM TANK E; 6 FT^3

4. Fragmentation Results

4.1 Set up for Fragment Samples

An arena 40 ft in diameter was used to catch a sampling of the fragments. Arena walls were constructed of panels made from layers of 4' x 8' x ½" celotex wallboard.

The thickness of the panels (number of pieces in each wall) was calculated to stop most fragments. From reference (7), depth of fragment penetration can be calculated from the following empirical relationship:

$$dp = \left(\frac{VM^{0.94}}{1.129 \times 10^{5} A^{0.91} (\sec \theta)^{0.542}} \right)^{1.23},$$

where dp = penetration depth in inches normal to panel surface

v = fragment velocity in ft/sec

M = weight of fragment in grains

A = presented area of fragment in in^2

θ = angle between fragment trajectory and a normal to the panel surface

Not having factual fragmentation data available from rupturing pressure vessels, for our case we considered a fragment that is 1" x 1" x 0.3" striking the panel in such a manner as to present an area of about 0.5 in^2. The fragment weighs 330 grains and strikes the panel at a velocity of 1000 ft/sec. Since the greatest panel thickness is required when the trajectory is normal to the panel surface, sec θ was taken as 1.0. For the above conditions, the penetration depth is about 5.0". Based on this, panels 6" thick should be adequate to catch most fragments.

The total number of panels used for the 40 ft arena was $\frac{\pi D}{4} = 10\pi = 31.4$ panels. In practice, only 30 panels were used with the space equivalent to 1.4 panels (5.6') left open for an entrance and for a camera port. The thirty panels that made up the arena wall were numbered 1 through 30 starting at the arena opening and proceeding in a clockwise direction. The total number of celotex sheets used was 12/panel for 30 panels or 360 sheets. Details of arena construction are shown in Figure 2.2.

To complete the tank experiments in a rather restricted time frame, construction materials were ordered on the above preliminary information. Later and more accurate information proved that fragment material density was greater than that used in the calculations. Thus while the arena walls proved capable of stopping fragments

from the thin-walled cylindrical tanks, many of the fragments from the higher pressure tanks penetrated the arena walls. Some of those that penetrated the walls were recovered.

4.2 Fragment Recovery

4.2.1 Fragments from Tank A

A total of 36 fragments of tank A were recovered. These are shown photographed over a calibration grid in Figure 4.1. Grid line spacing in this and all fragment photographs is 2 inches. Fragment sizes range from about 10" x 12" to 1" x 2". Weights for each fragment are given in Table 4.1. Those fragments that were found imbedded in the arena walls are identified by the panel number in which they were found in Table 4.1.

Table 4.2 lists the number of hits on panels for each shot. A check shows that the number of panel hits for shot A does not correspond to the 10 fragments found in the celotex panels as listed in Table 4.1. The reason for this is that Table 4.2 lists the total panel hits, those fragments that remain in the panel and those that rebound; Table 4.1 lists only those fragments that remain in the celotex.

The remaining fragments listed in Table 4.1, except for 23, were found scattered about the arena. Fragment #23 was found 150 ft from GZ in a radial line with panel 6.

Prior to firing, the tank weighed 3850 grams. Total weight of the fragments found was 2837 grams, about 73% of the total weight. This recovery percentage may distort the fragment picture since the recovered items include the heavy tank parts listed in Table 4.1 and Figure 4.1, fragments 1, 34, 35, and 36. The amount of tank skin recovered weighed about 1349 grams. The total weight of the tank's skin based on a density of 4.41 and a thickness of 0.02 inches was 2390 grams. Thus about 56% of the tank's skin was recovered.

4.2.2 Fragments from Tank B

A total of 36 fragments from Tank B were recovered. These are shown in Figure 4.2. Sizes range from about 16" x 17" down to about 2" x $\frac{1}{8}$". (Fragments 2 and 33.) Table 4.3 gives the weight of each fragment. Fragment numbers correspond to those in Figure 4.2.

Table 4.2 indicates that a total of 15 fragments from Tank B hit the arena walls; of these, 10 were identified and are listed in Table 4.3.

The remainder of the fragments, except for #4, were found scattered about the arena floor. Fragment #4 was found about 100 ft from GZ and in line with panel 26.

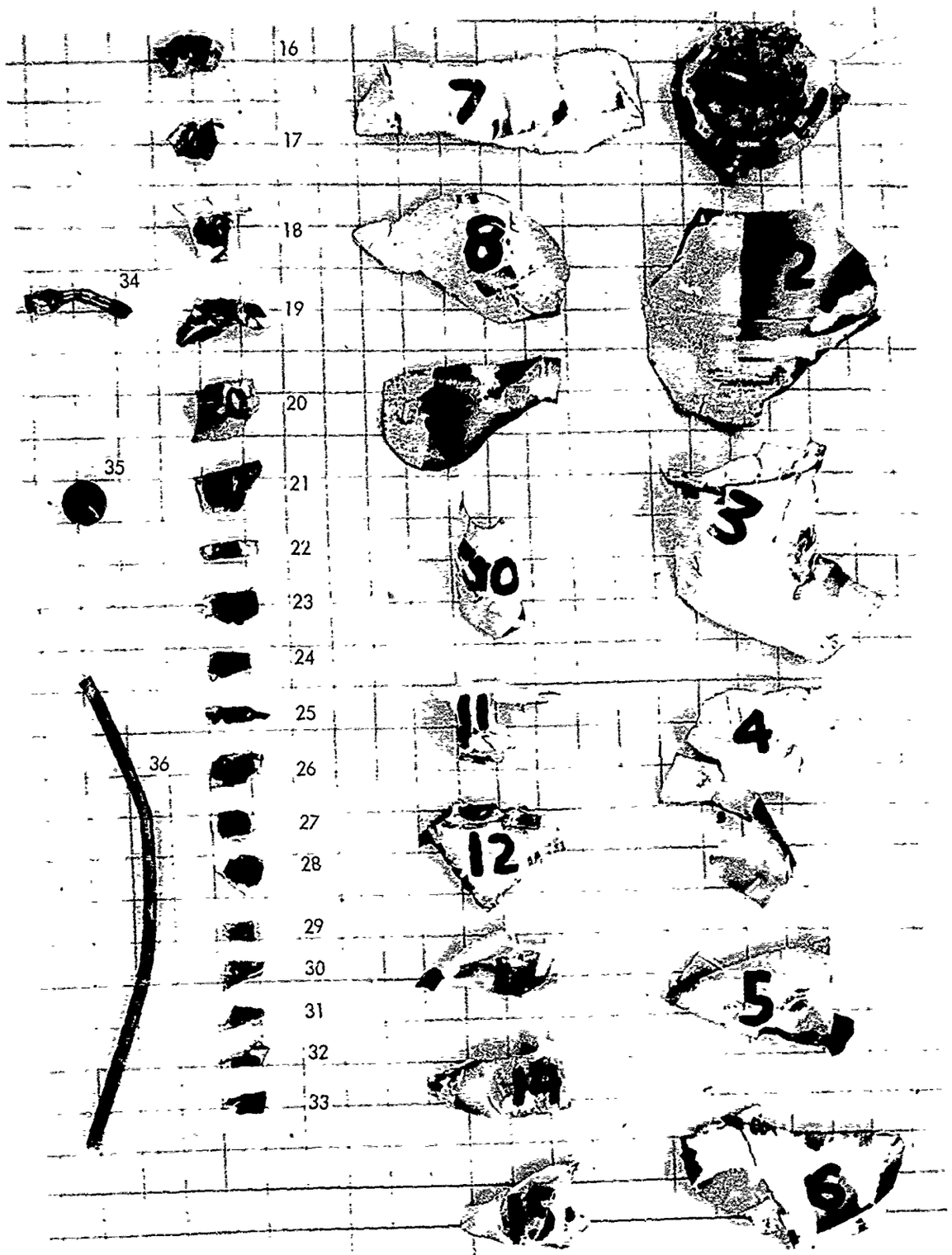

FIG. 4-1 FRAGMENTS FROM TANK A (2" LINE SPACING)

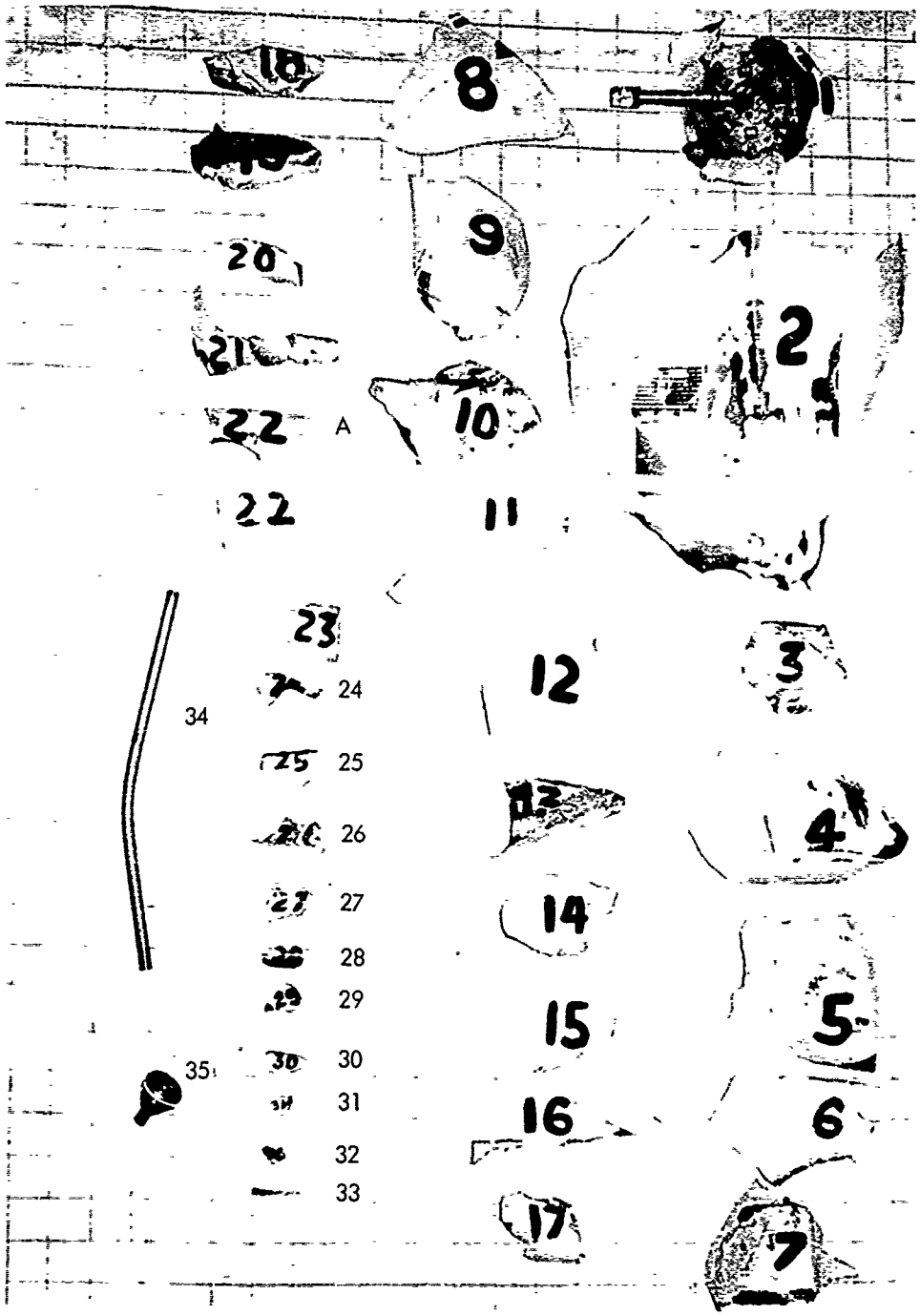

FIG. 4-2 FRAGMENTS FROM TANK B (2" LINE SPACING)

Prior to firing the tank weighed 4620 grams; total weight of the fragments found was 3300 grams--about 71% of the tank weight. Out of a calculated total skin weight of 2890 grams, we recovered 1774 grams or 61%.

4.2.3 Fragments from Tank C

The 8 fragments recovered from Tank C are shown in Figure 4.3. Fragment sizes range from about 4" x 6" down to about 1" x 2". Weights for each fragment are shown in Table 4.4.

Three panel hits are shown for Tank C in Table 4.2. These three fragments were located and are listed in Table 4.4.

The total weight of fragments recovered for this tank was 617 grams. The tank weight at firing was 2860 grams. Thus only 21.5% of the total weight was recovered. The reason for the low recovery percentage may have been due to the ricochet of many of the fragments off the concrete pad on a trajectory that carried them over the arena wall.

4.2.4 Fragments from Tank D

Figure 4.4 is a photograph of the fragments from Tank D. Weights for each fragment are listed in Table 4.5.

As may be seen in Table 4.5, we recovered 21 fragments from Tank D. From Table 4.2, there was a total of 28 hits on the arena wall. Seven of these fragments remained in the walls, 8 were found outside the arena, and the other 13 were not located. The locations where fragments were found are shown in Figure 4.5.

Tank D weighed 171 lbs (77,600 grams) in a condition ready for inflation. The recovered fragments weighed 76 lbs (34531 grams). Thus the fragments recovered amounted to 45.5% of the total tank weight.

4.2.5 Fragments from Tank E

A photograph of the fragments from Tank E are shown in Figure 4.6. Table 4.6 lists fragment weights.

We recovered 25 fragments from Tank E. From Table 4.2, there were 28 hits on the arena walls. Ten of these fragments remained imbedded in the arena walls, 8 were found outside the arena, and the other 10 penetrated the wall at high velocity and were not recovered. The holes in the arena walls gave a general indication of the size of the unrecovered fragments. Certainly none were as large as the three largest fragments in Figure 4.4 or the five largest in Figure 4.6. Rather, the holes gave evidence of sizes similar to those represented by fragments 4 through 21 for Tank D and 6 through 24 for Tank E.

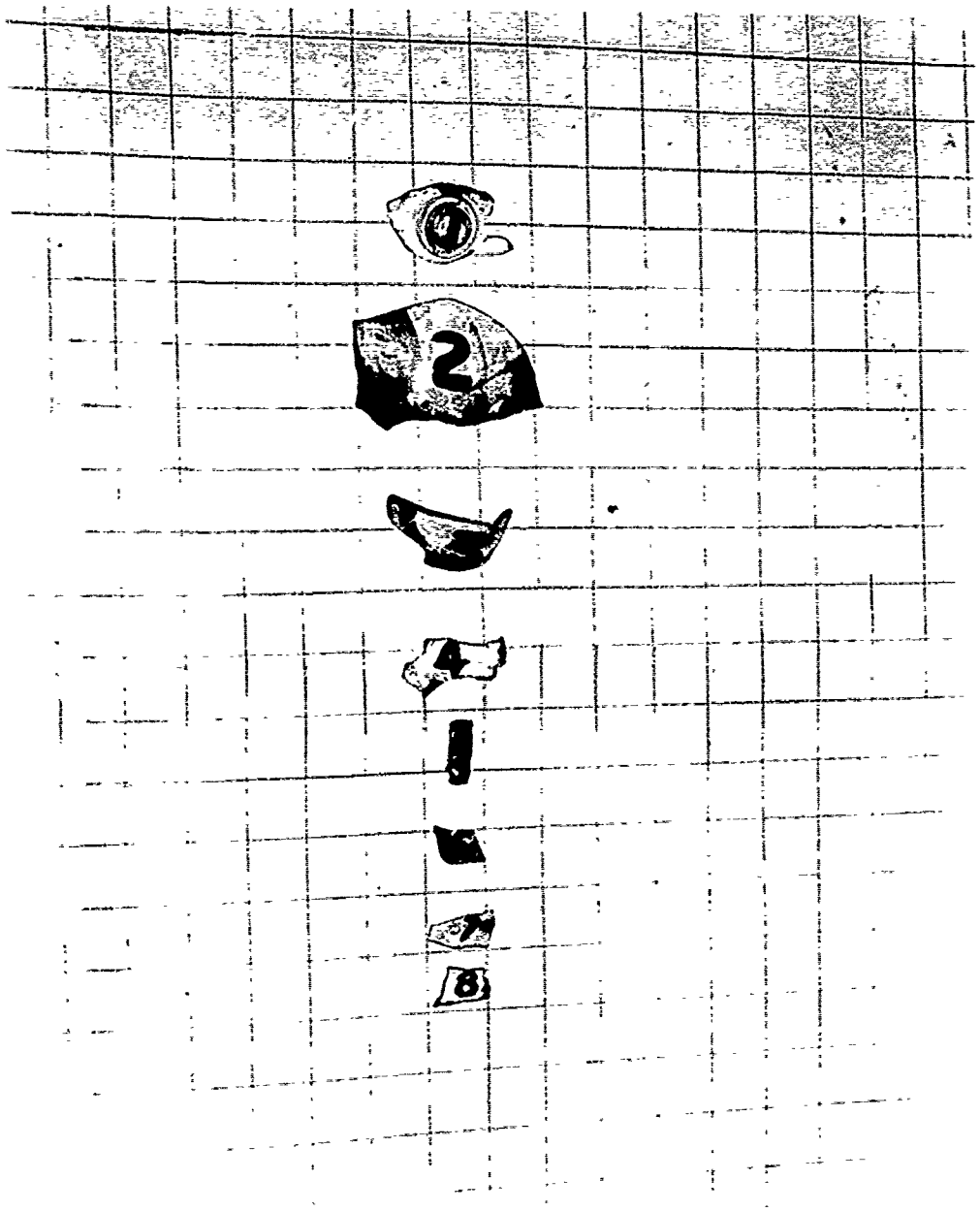

FIG. 4-3 FRAGMENTS FROM TANK C (2" LINE SPACING)

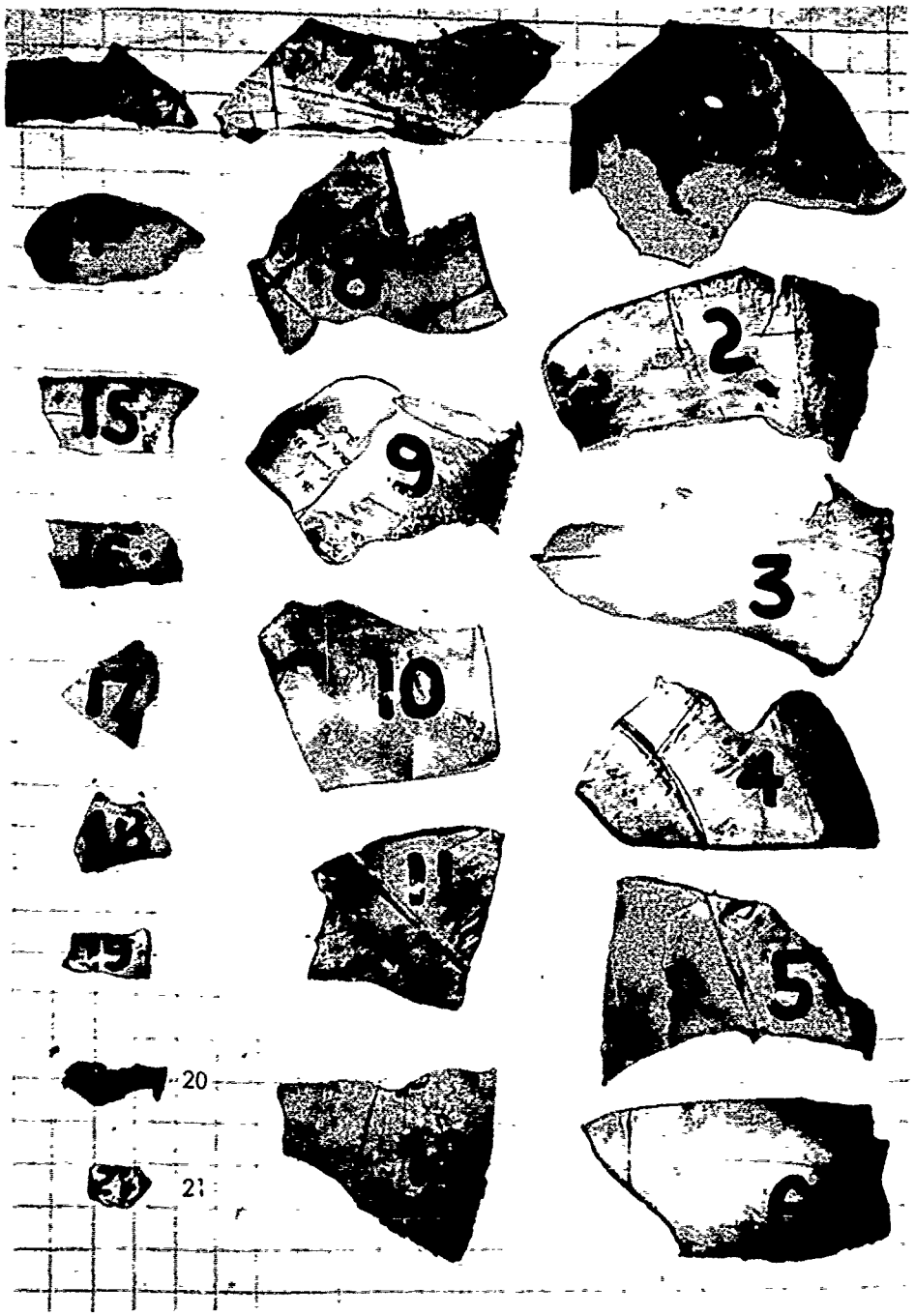

FIG. 4-4 FRAGMENTS FROM TANK D (2" LINE 50 CINC

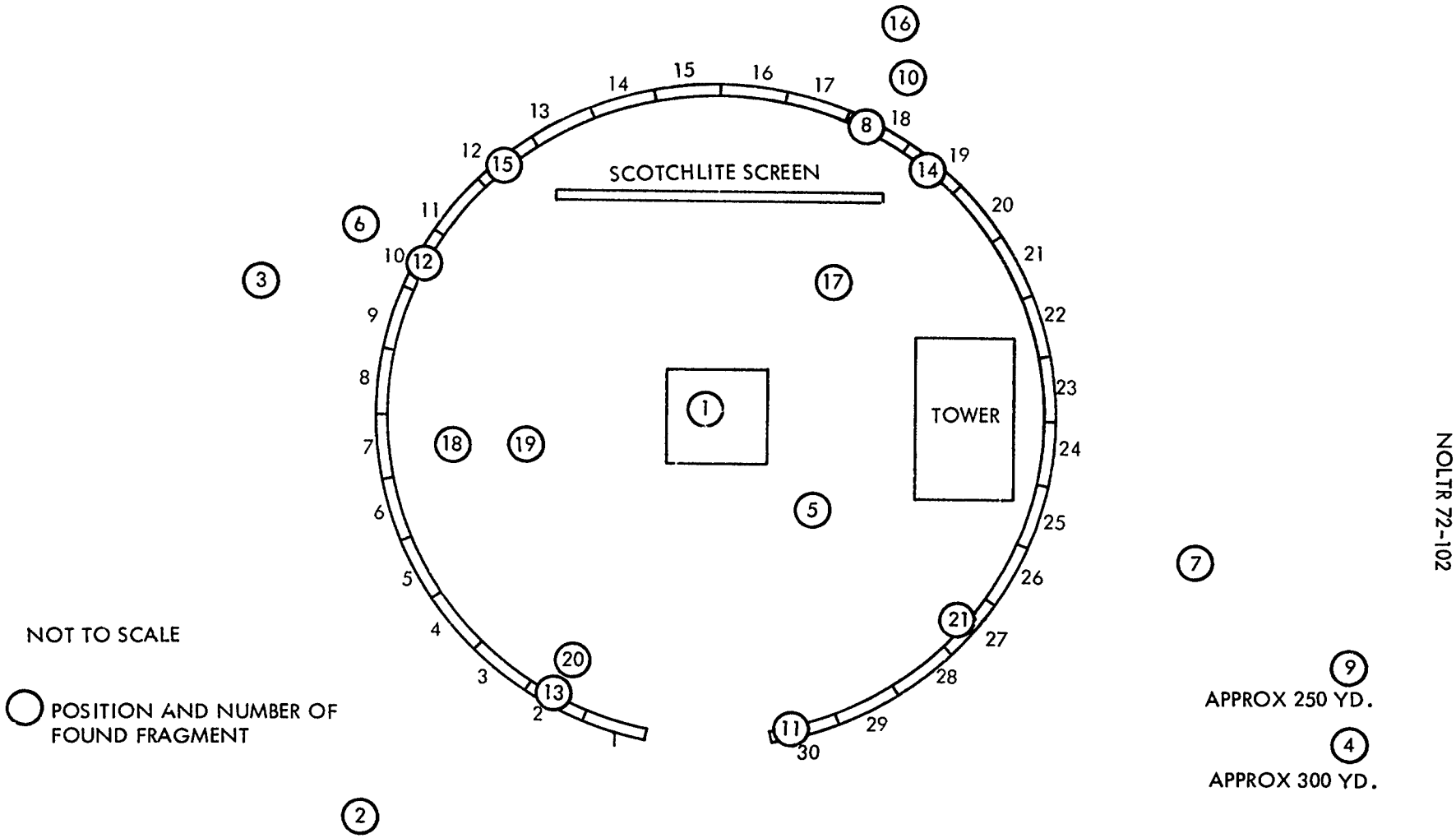

FIG. 4-5 APPROXIMATE LOCATION OF FRAGMENTS FOR TANK D

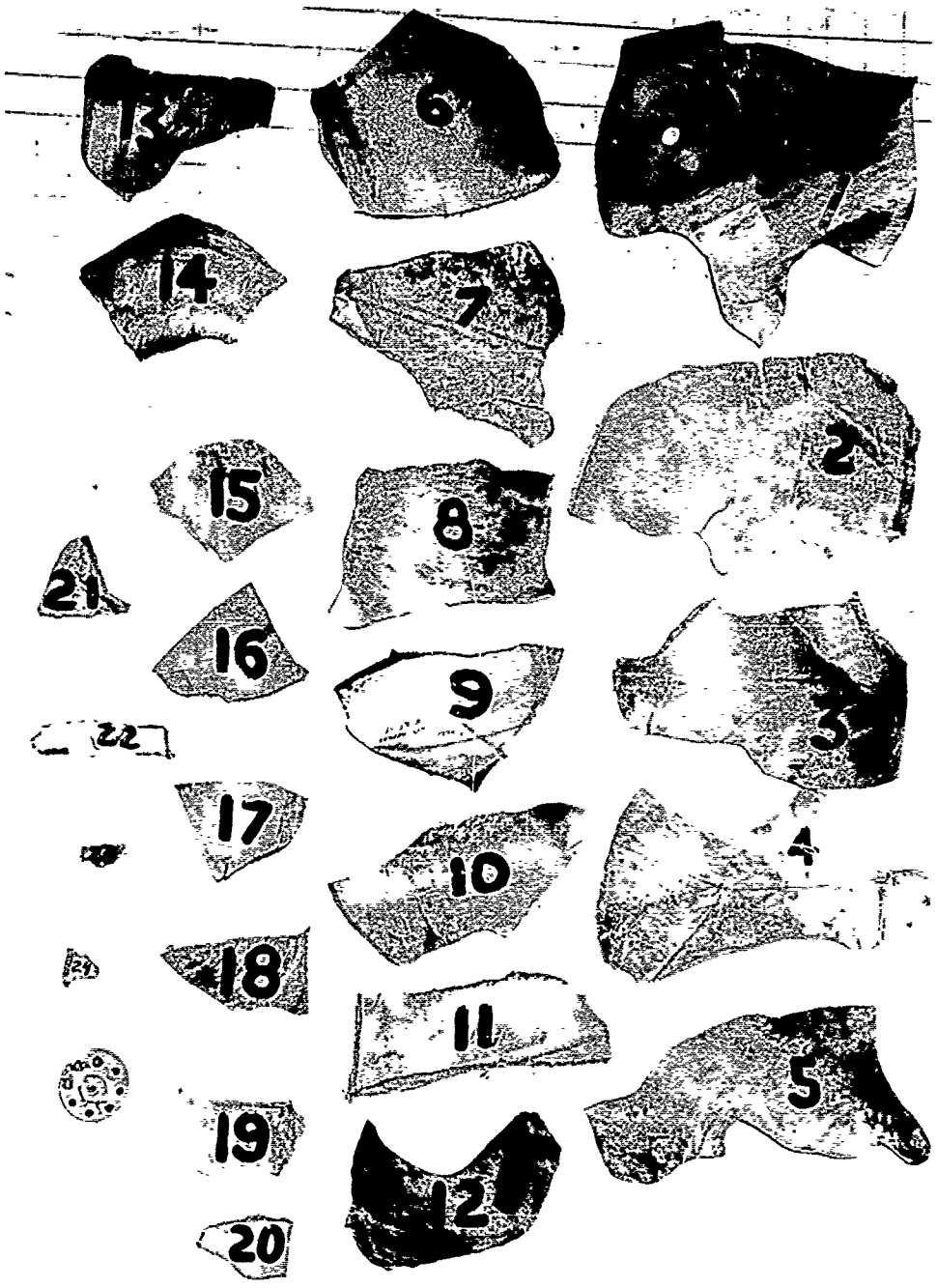

FIG. 4-6 FRAGMENTS FROM TANK E (2" LINE SPACING)

Locations where fragments were found are shown in Figure 4.7. The numbers inside the circles correspond to fragment numbers given in Table 4.6 and Figure 4.6. (Panel 30 was removed for tank E.)

Tank E weighed 170 lbs (77000 grams) at inflation. The weight of the recovered fragments totaled 87.7 lbs (39,809 grams). Thus the recovered fragments amounted to 51.6% of the total tank materials.

4.3 Fragment Velocities

The two methods for measuring fragment velocity are described in Section 2.3.2. While both systems did not operate on every test, one or the other did function. Therefore, fragment velocities were measured on every test. These results are presented below.

4.3.1 Velocities of Tank A Fragments

The breakwire system did not operate on this event. However, the strobe system yielded adequate pictures of the fragments in flight. Times at which the strobe flashes occurred are given in Table 4.7. Figure 4.8 shows the strobe picture with the reflective backdrop. The shockwave is clearly visible for the first three flashes and is labeled 1-S, 2-S, and 3-S. The shock labeled 1-S is at 0 time, i.e., the time at which the breakwire system signaled tank rupture. Obviously, the tank has burst and the shockwave formed by the time the wire in contact with the tank breaks. At 0 + 1.5 milliseconds, we photograph the shock labeled 2-S at its new position. Note that the shock is not symmetrical about the tank; it has traveled further on the right where rupture first occurs. The shock is not photographed by the 4th flash at 0 + 5 milliseconds since it is beyond the bounds of the scotchlite screen at this time.

The flashes seen on Figure 4.8 and 4.9 are self-illuminating collisions of fragments and pieces of the breakwire with solid objects. Since they are self-illuminating, we are unable to assign a time to their occurrence. Therefore, we cannot use them in velocity calculations.

In measuring fragment velocities, we assumed that the fragments traveled in straight lines. This may not be true since a large flat fragment traveling in a sailing mode would probably show some curvature. However, this assumption allowed velocity measurements when the fragment could not be identified on every flash. All fragments were assumed to emanate from the tank's equator parallel to the earth's surface. Fragment locations were determined from two mutually perpendicular coordinate systems described by camera fields of view and the tilt angles of the film plane. The tower camera geometry is shown in Figure 4.10.

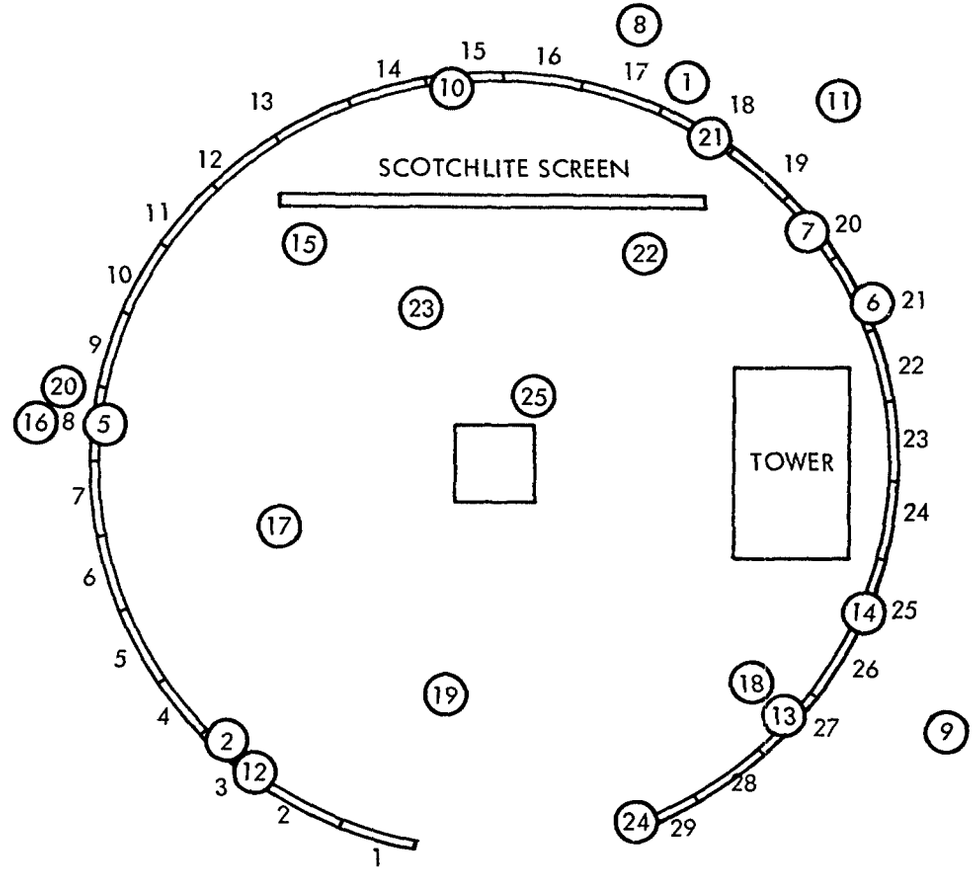

NOT TO SCALE

○ POSITION AND NUMBER OF FRAGMENT FOUND

FIG. 4-7 APPROXIMATE LOCATION OF FRAGMENTS FOR TANK E

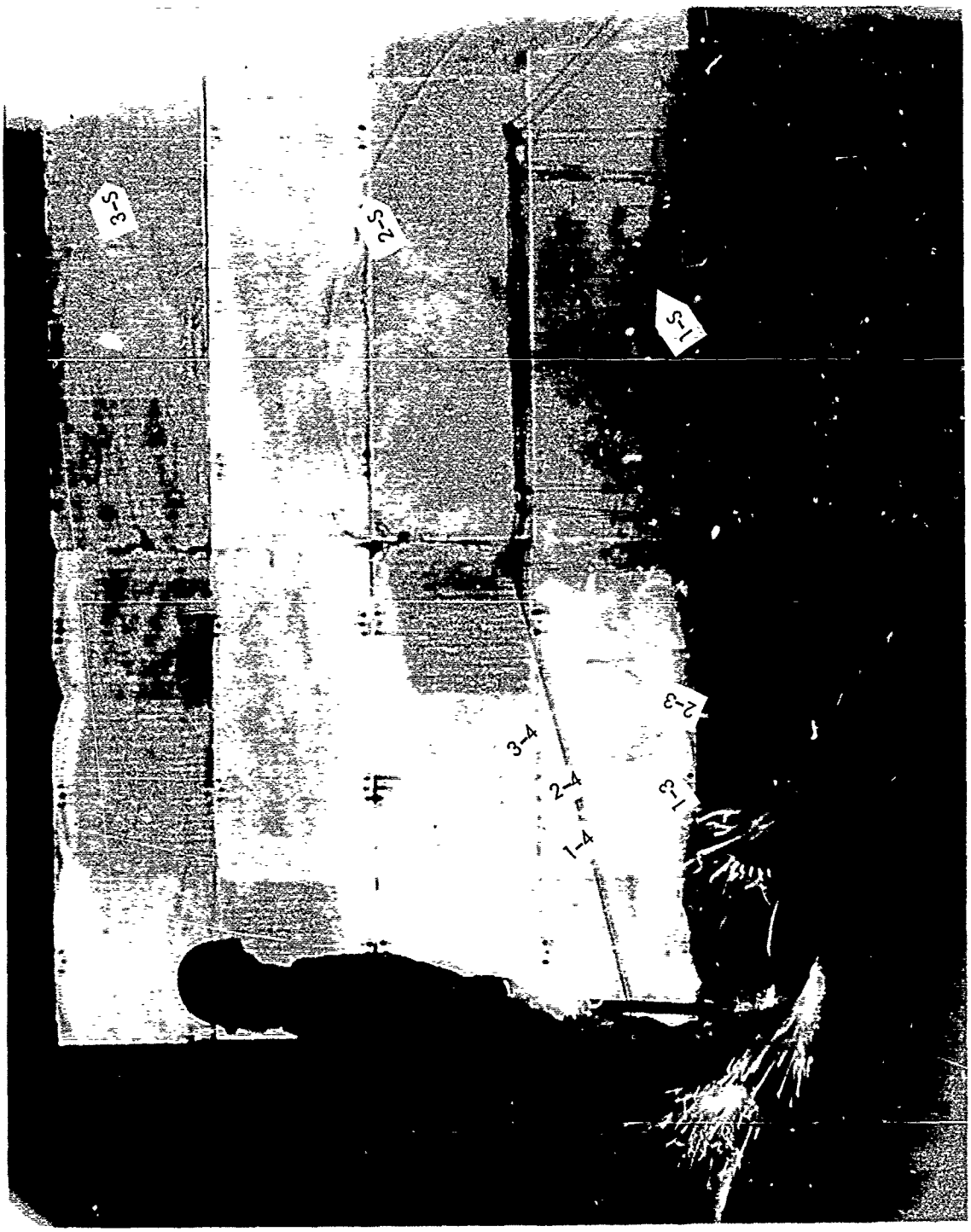

FIG. 4-8 GROUND CAMERA PHOTO OF TANK A RUPTURE
(SEE SECTION 4-3-1 FOR EXPLANATION OF NOTATION)

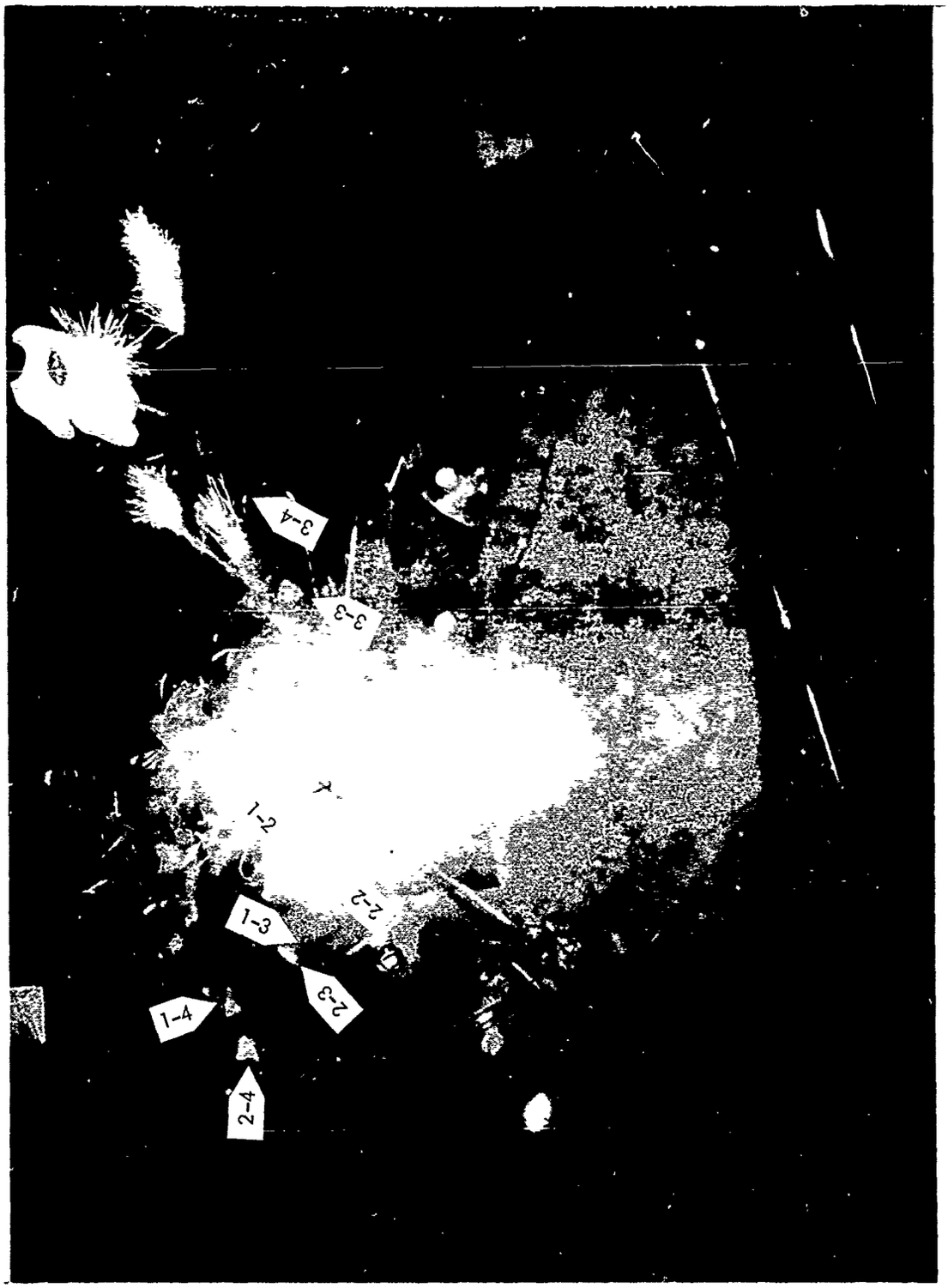

FIG. 4-9 TOWER CAMERA PHOTO OF TANK A RUPTURE
(SEE SECTION 4-3-1 FOR EXPLANATION OF NOTATION)

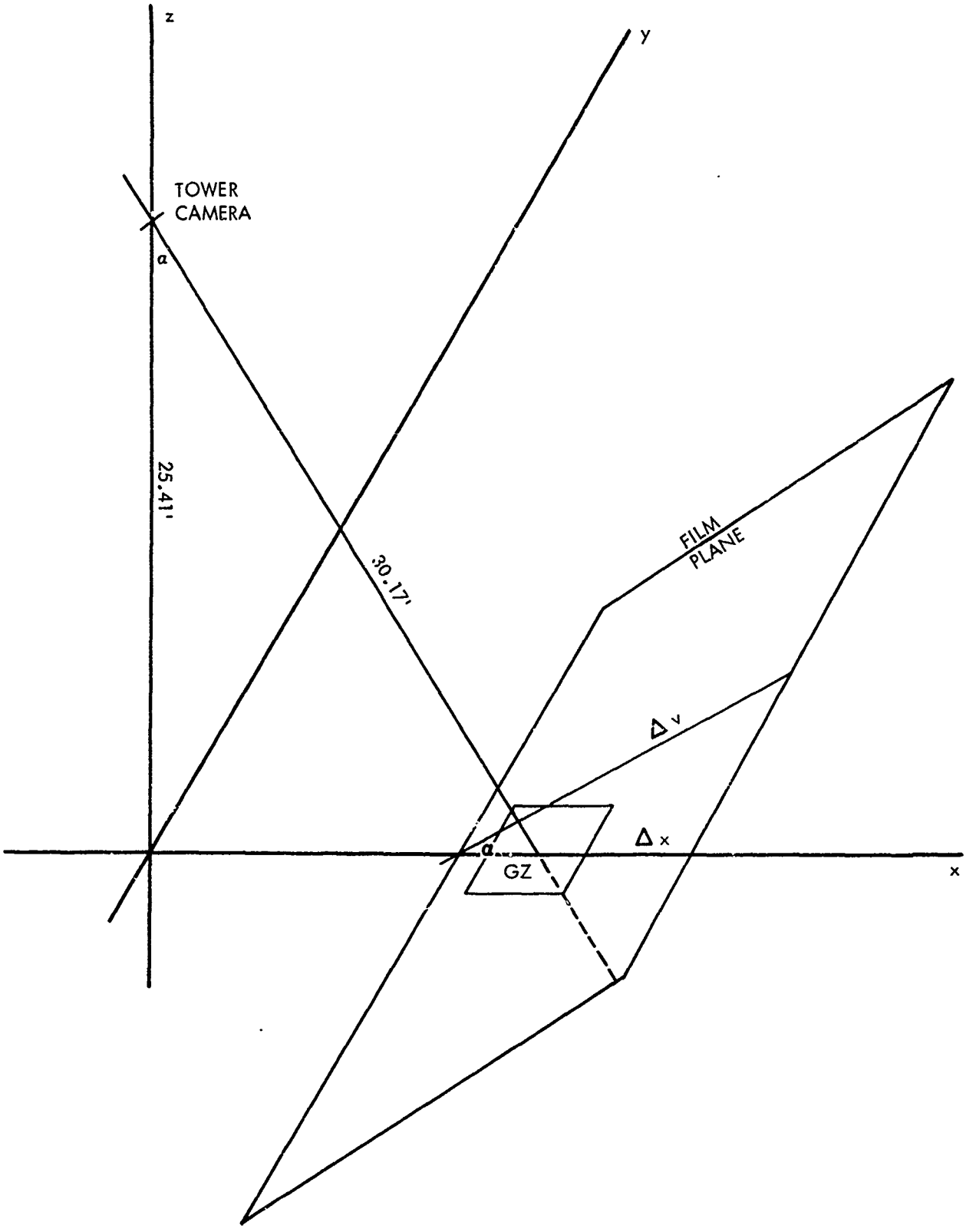

FIG. 4-10 TOWER CAMERA GEOMETRY

From Figures 4.8 and 4.9 we are able to get position-time information for selected fragments. For instance note the fragment labeled 1-2, 1-3, and 1-4. The first digit identifies the fragment. The second digit refers to the flash number. Thus, 1-4 refers to fragment #1 at the fourth flash or at 5.0 milliseconds. In the case of the three fragments chosen for obtaining fragment velocities, all could be located with sufficient accuracy to yield position-time data. These measurements are summarized in Table 4.8.

For Tank A, fragments 1 and 2 were identified at all four strobe flashes in Figure 4.9 and at the last two flashes in Figure 4.8. At 0 time the tank is assumed to be intact. The apparent increase in velocity for fragment 2 may be due to the fact that the fragment perimeter is not clearly identifiable in the condensation cloud formed by the expanding gas. Fragment 3 was identifiable on the last two flashes in Figure 4.9 but only on the last flash in Figure 4.8. Other fragments are visible in Figure 4.9 but cannot be found on Figure 4.8.

4.3.2 Velocities of Tank B Fragments

Both the strobe system and the breakwire system yielded velocity data for this event. Figure 4.11 shows that tank rupture has occurred and a shock marked 1-S is emerging from the upper end of the tank when the start signal occurs. (The shock is also seen on the second and third flashes and is marked 2-S and 3-S respectively.) At this time the distance between the tank perimeter and the stop wire support is 0.77 ft. The counter-measured time between the breakwire signals was 0.632 milliseconds giving an average fragment velocity of 1215 ft/sec. This value is not out of line with velocities measured by the photosystem.

Fragment velocity measurements were made from Figures 4.11 and 4.12. Unfortunately the 2 fragments labeled 2-4, 2-3, 1-4, and 1-3 in Figure 4.12 could only be identified for the third flash in Figure 4.11. From this we were able to obtain a trajectory and therefore some velocity information.

Fragment 1 travels a distance of 4.56 ft in 4.5 milliseconds for an overall velocity of 1010 ft/sec. Its travel time between the last two flashes is 1.5 milliseconds. It covered the distance between 3.06 and 4.56 ft or 1.5 ft. Average velocity over this interval is 1000 ft/sec.

Fragment 2 traveled a distance of 4.65 ft over 4.5 milliseconds an overall velocity of 1030 ft/sec. Its travel time between the last two flashes was 1.5 milliseconds. During this time it covered a distance of 1.35 ft for a velocity of 900 ft/sec. These measurements are summarized in Table 4.8.

FIG. 4-11 GROUND CAMERA PHOTO OF TANK B RUPTURE
(SEE SECTION 4-3-1 FOR EXPLANATION OF NOTATIONS)

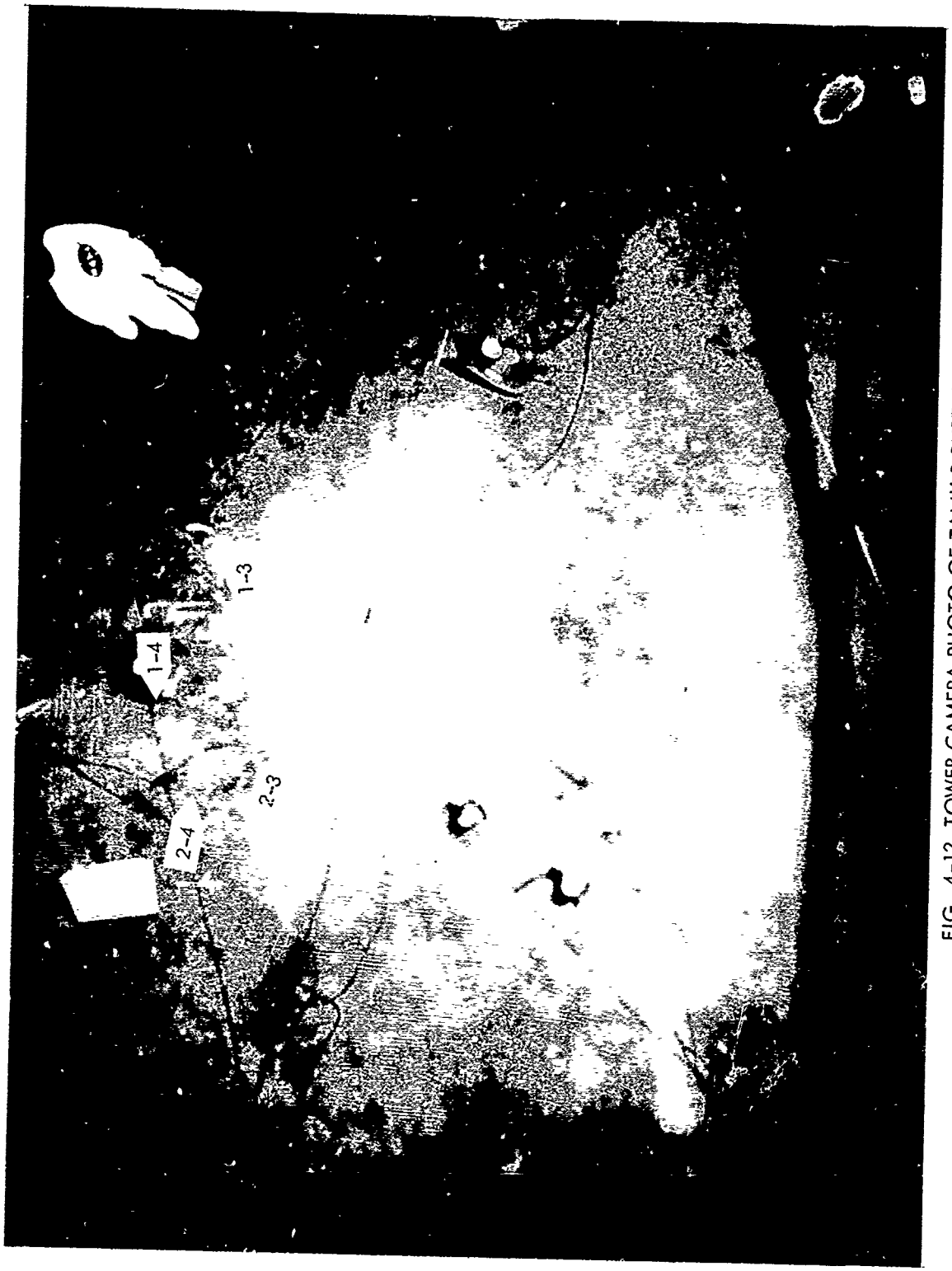

FIG. 4-12 TOWER CAMERA PHOTO OF TANK B RUPTURE
(SEE SECTION 4-3-1 FOR EXPLANATION OF NOTATION)

4.3.3 Velocities of Tank C Fragments

Fragment velocities for this tank were obtained from both the breakwire system and the strobe system. However, data from both systems require interpretation. For the breakwire system, the two electronic counters gave different readings. One counter gave a travel time for 12.5 inches of 0.876 milliseconds for a velocity equal to 1190 ft/sec. The other gave a travel time of 0.773 milliseconds over the same distance for a velocity of 1350 ft/sec.

The shutter for the ground camera did not close before the photofloods came on to illuminate the dummies. Therefore the film from this camera was overexposed (Fig. 4.13). While the shadows left by the shockwave were not washed out, we can identify only one fragment. Therefore, a fragment path is based on this and Fig. 4.14 to obtain velocity. From fragment 1 we get a total distance traveled of 5.20 ft in 4.50 milliseconds or an average velocity of 1150 ft/sec. Over the first 3.00 milliseconds, it traveled 3.60 ft or 1200 ft/sec. Over the final interval it traveled 1020 ft/sec.

4.3.4 Velocities of Tanks D&E Fragments

Both the strobe system and the breakwire system functioned during the rupture of these two large vessels. Because of the condensation cloud, no fragments could be seen in the photographs. Therefore, only the breakwire system yielded fragment velocities.

For Tank D the distance traveled was 0.97 ± 0.062 ft over the measured time interval of 0.689 milliseconds. The 0.062 ft is the accuracy we could maintain of the cage distance from the tank. This gives an average velocity of 1400 ft/sec over this interval.

The reason that no fragments could be clearly identified in the strobe photographs was that condensation at the front of the fill gas out ran and obscured everything behind it.

On Tank D, the strobe was flashed at 0, 0 + 1.5, 0 + 3.0, and 0 + 4.5 milliseconds. Figure 4.15 shows that the cloud has reached a distance of about 7 ft (distance to the first gages) in 4.5 milliseconds.

Figure 4.16 shows the shock at 0 + 1.5 milliseconds. No fragments are visible. However, the shock front has covered a distance of about 3 ft in the vertical direction during this period, an average velocity of 2,000 ft/sec. (Distances are given from the tank perimeter to the shock front.) To the right in Figure 4.16, the shock has traveled less than 2 ft for a velocity of 1300 ft/sec. No fragments are visible ahead of the condensation front. The multiple shock structure at the right may be due to fragment bow waves but is more probably due to the jetting of the N_2 at tank rupture.

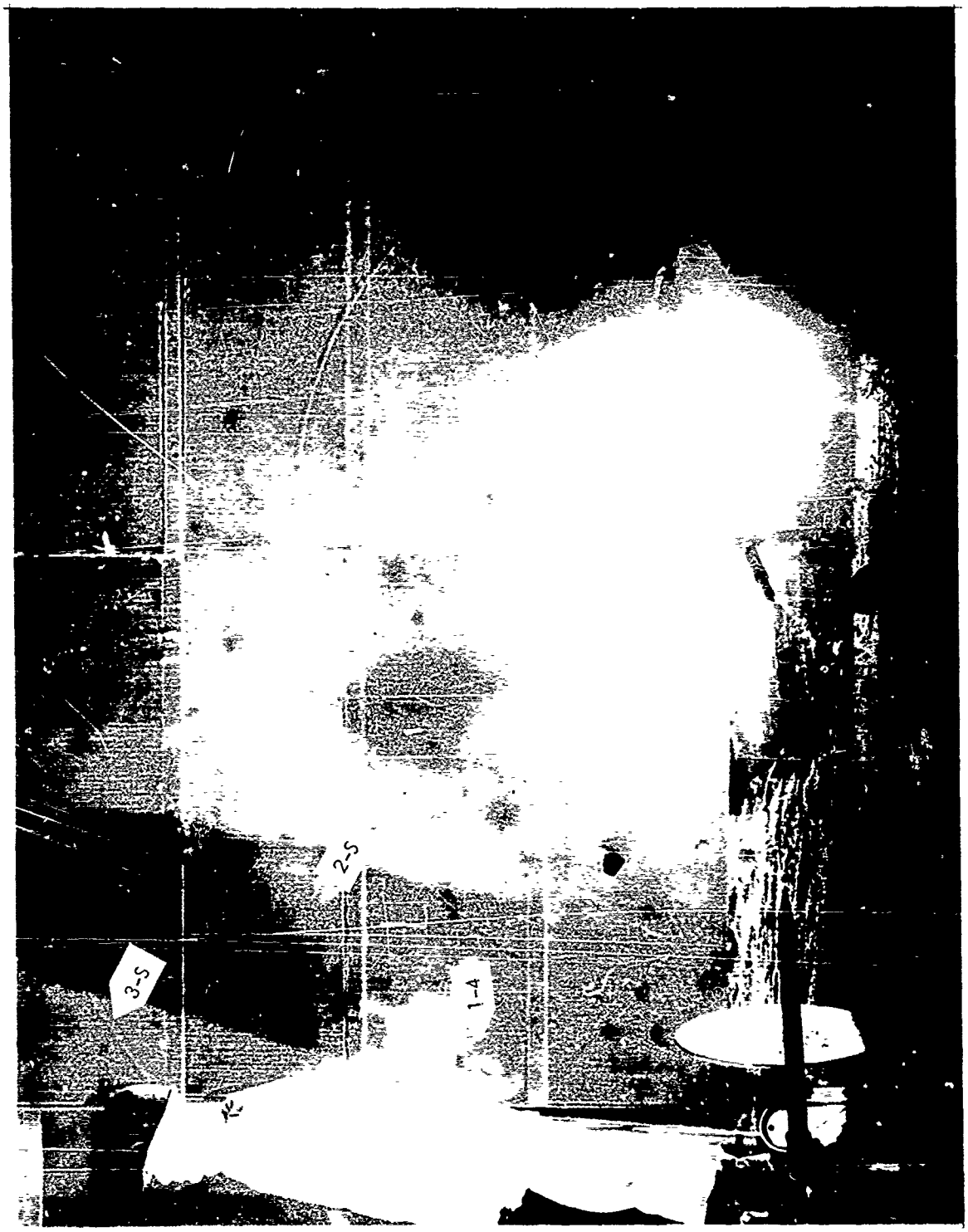

FIG. 4-13 GROUND CAMERA PHOTO OF TANK C RUPTURE
(SEE SECTION 4-3-1 FOR EXPLANATION OF NOTATION)

FIG. 4-14 TOWER CAMERA PHOTO OF TANK C RUPTURE
(SEE SECTION 4-3-1 FOR EXPLANATION OF NOTATION)

FIG. 4-15 TOWER CAMERA PHOTO OF TANK D RUPTURE

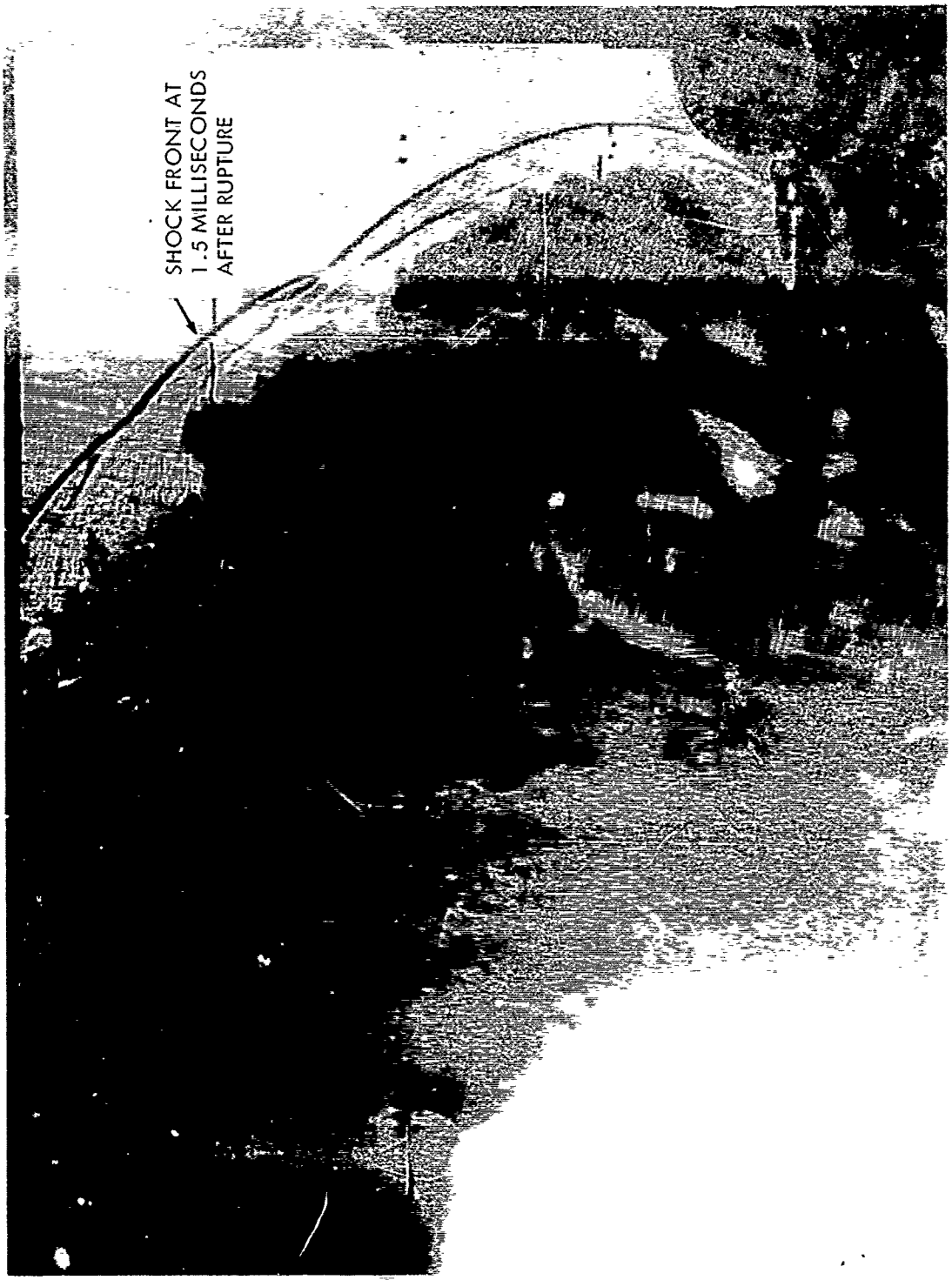

FIG. 4-16 GROUND CAMERA PHOTO OF TANK D RUPTURE

The strobe system was changed for Tank E in an attempt to photograph fragments. Height of the scotchlite screen for the ground camera was increased to 12 ft and width was increased to 24 ft. No scotchlite was used in the center of the screen since it was expected that the condensation cloud would cover this area. The strobe times were changed to flash at 0, 0 + 6, 0 + 7, and 0 + 8 milliseconds. It was hoped that the fragments would out-distance the cloud during this extended period. Fragments could be clearly identified above the cloud in Figure 4.17, the tower camera photograph but not in Figure 4.18, the ground camera photograph. Therefore, trajectory information was not available and no photo velocities could be calculated. Considerable flashing is evident in Figure 4.17 probably due to fragments encountering bits of the wire cage and other solid objects.

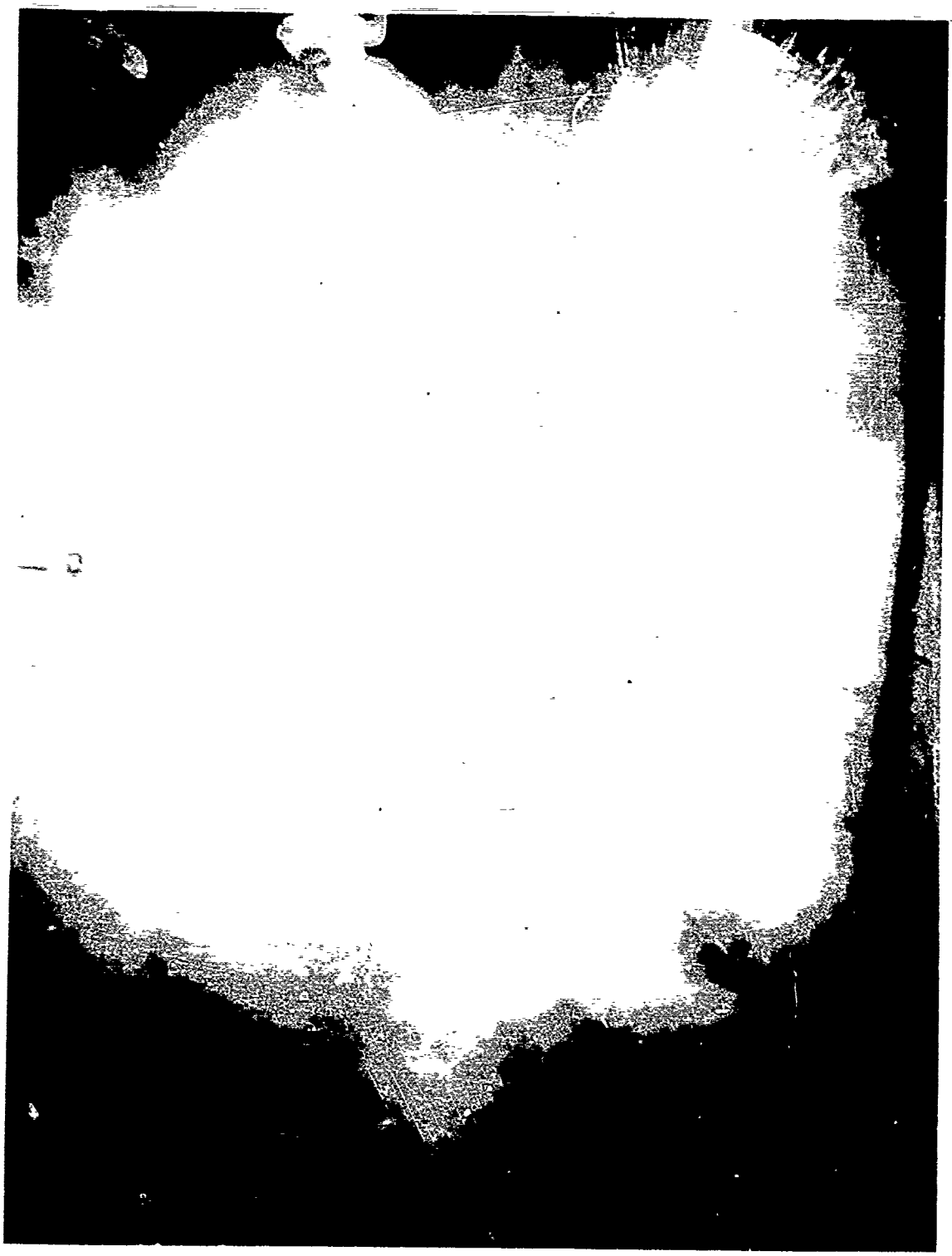

FIG. 4-17 TOWER CAMERA PHOTO OF TANK E RUPTURE

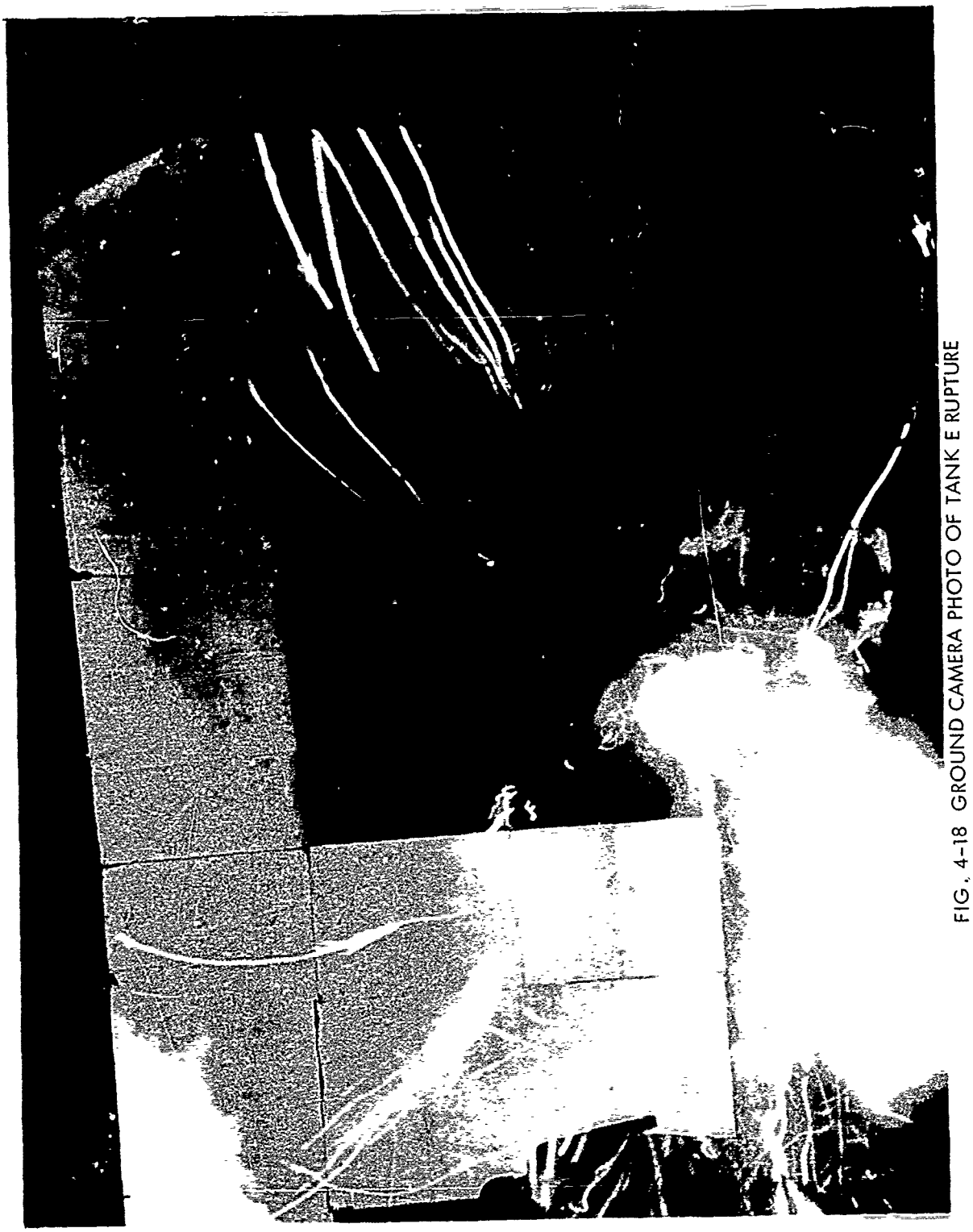

FIG. 4-18 GROUND CAMERA PHOTO OF TANK E RUPTURE

5. Anthropomorphic Dummies

For purposes of producing training films, anthropomorphic dummies were placed near the rupturing tanks. Motion picture photography recorded the visual effects of the blast waves on the dummies.

For tanks A, B, C, and D the three dummies were placed as shown in Figure 2.1. Tank to dummy distances for these four tests were 8.5, 12.8, and 13.7 feet. For the tank E test, the dummies were placed at slightly different relative positions. For this event, tank to dummy distances were 10.0, 14.5, and 15.2 feet. The dummies were supported in an upright position by 1" diameter aluminum pipes driven into the ground so that their tops were at waist level. They were placed in a manner such that the pipes offered little support against the blast.

None of the dummies were knocked over by the blast from any tank rupture, though some were knocked over by the collapse of the arena walls. For events A, B, and C, the closest dummy was in an area where a man would suffer ear drum damage -- side-on overpressures above 5.0 psi. For tanks D and E, all the dummies were in an area where ear drum damage would definitely occur. The closest dummy on event D was in the 25-psi region, a level where the onset of lung damage occurs.

It is unlikely that death would occur from blast alone. The fragments, however, could have proven lethal if a hit occurred in the right spot. On tank A, the closest dummy was hit in the buttocks by a large fragment, tearing out the seat of his coveralls. In addition to embarrassment, a man would have suffered severe lacerations. Another fragment from tank A sliced into and remained in the leg of the second dummy. A man's leg would have been severely cut, with a probable bone fracture. A fragment from tank D struck the leg of the second dummy edge on with sufficient force to bend the heavy metal I-beam in the leg in a right angle. A man's leg would have been severed.

All the tanks threw up dirt and gravel with sufficient force to penetrate a man's skin and to cause severe eye damage and probable blindness.

6. Discussion

6.1 Tank Pressurization

Tank pressurization results showed that none of the vessels burst at less than their rated burst pressure. The fuel tanks rated at 460 psig burst pressure actually burst at 625 psig for the aerozine fuel tank and at 600 psig for the oxidizer tank. The small helium tank, rated at 7,500 psig actually ruptured at 8,000 psig. The two large helium vessels were rated at 8,000 psig burst pressure. The first of these vessels burst at exactly 8,000 psig. The second tank was pressure cycled 55 times. This tank burst at 8,130 psig.

The tanks were radiographed prior to the tests to locate voids, flaws, sub-standard welds, or other defects. Dyepenetrate checks were also performed. No deficiencies were found. Indeed, tanks ruptured in what seemed a random manner. There were no patterns such as rupture along weldments.

There was no apparent residual effect from cycling the large helium tank. Its burst pressure was slightly but not significantly higher than that of the similar but uncycled tank. The pattern of fragmentation seemed unaffected. About the same total weight and number of fragments were recovered from both the large helium tanks

6.2 Blast Measurements

Side-on and face-on pressure measurements showed a lack of symmetry about GZ for the shock wave generated by tank rupture. The slope of the pressure distance curve was less for tank rupture data than for TNT data. For this reason, a single TNT equivalent does not characterize the TNT tank rupture data. Even so, tank rupture blast is a function of rupture pressure and tank volume. Therefore, we expect tank rupture airblast to scale geometrically. The pressure distance curves from such tanks coincide if distances are given in terms of tank radii. This is cube root scaling.

Shock overpressures from tanks C, D, and E have been averaged and are plotted as a function of tank radii in Figure 6.1. Therefore, this curve generalizes the pressure distance curve for similar tanks of any size burst at 8000 psig. Caution is recommended since tank rupture is asymmetric and shock overpressures that are 30% higher than those in Figure 6.1 may be encountered.

The TNT curve is based on the TNT weight whose blast energy is equal to the tank rupture energy for the tank size chosen where the fill gas is air or N_2. The TNT energy is taken as 1018 calories/gram. Based on the two curves of Figure 6.1, the equivalent weight of tank rupture in terms of TNT has been calculated and is plotted as a function of tank radius in Figure 6.2.

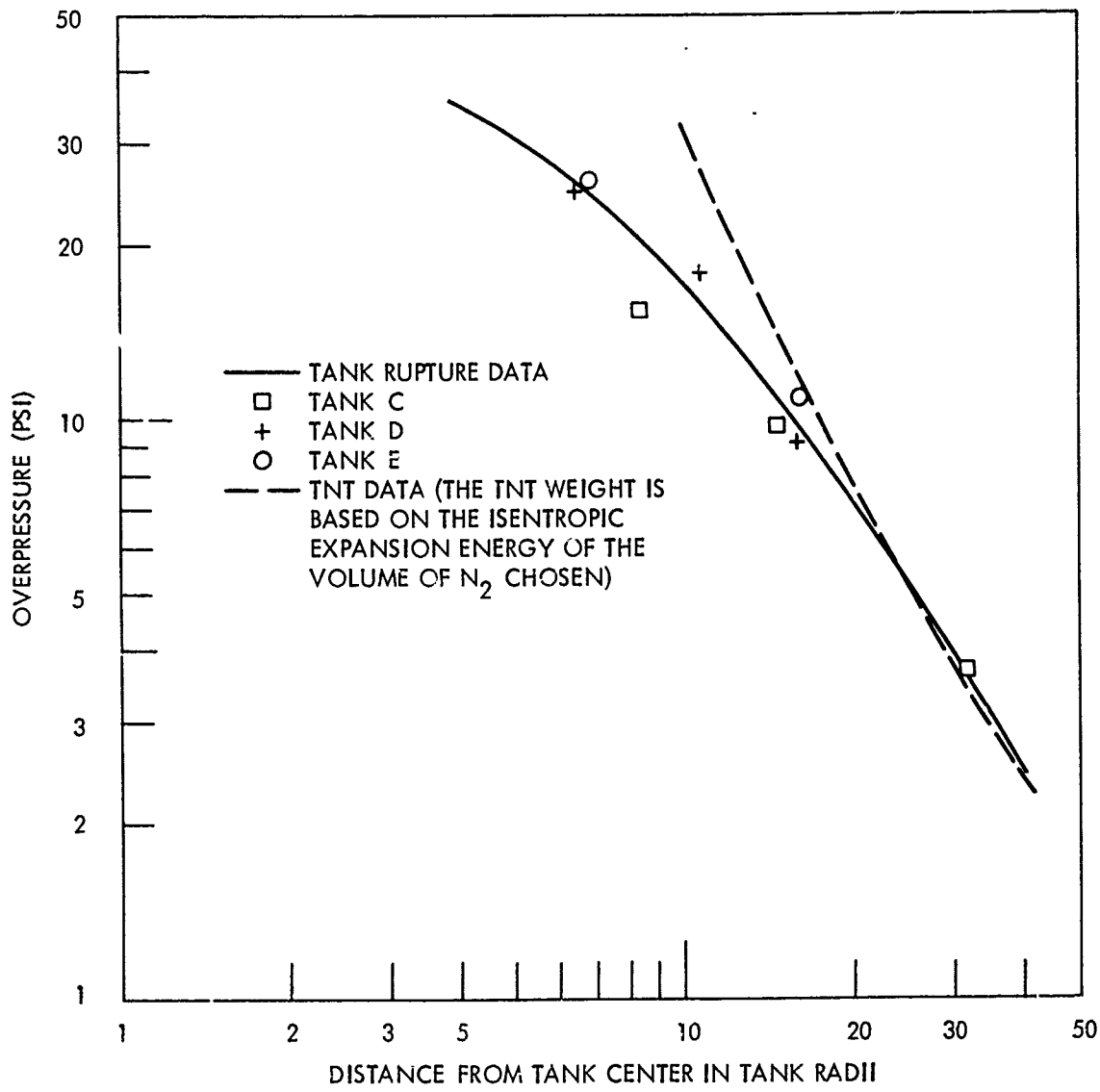

FIG. 6.1 PEAK AIRBLAST OVERPRESSURES FROM AN 8,000 PSIG TANK RUPTURE VS DISTANCE IN TANK RADII

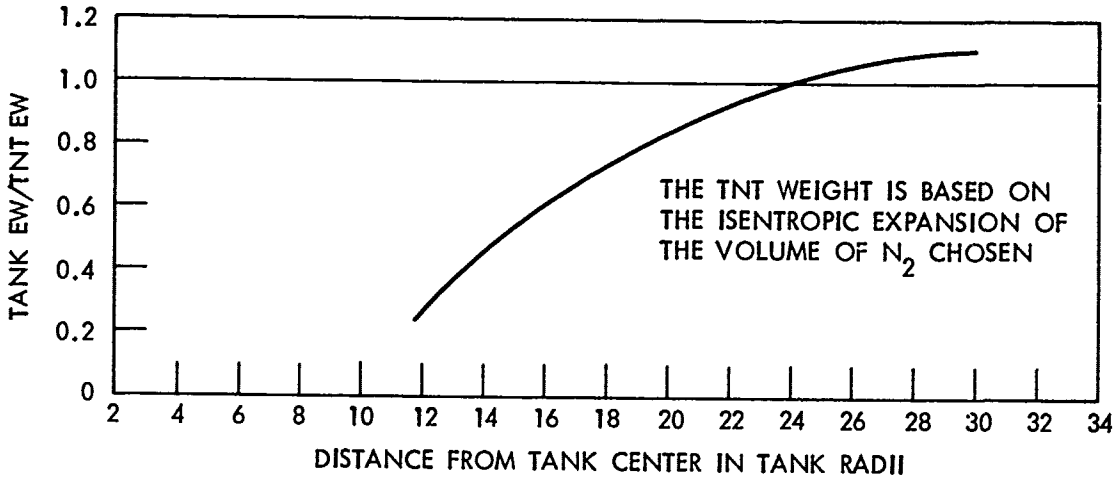

FIG. 6.2 TNT EQUIVALENCE OF THE AIR BLAST FROM AN 8,000 PSIG TANK RUPTURE BASED ON PEAK SHOCK OVERPRESSURE

The positive shockwave impulse from tanks C, D, and E have been combined and are shown in Figure 6.3. The curve is universal for similar spherical tanks burst at 8,000 psig. Again deviations from the curve may be 50% due to tank rupture blast wave asymmetry. We assumed that tank rupture equivalent weight based on positive shock wave impulse was constant based on TNT. From Figure 6.3, EW for tank rupture is about 0.76 x EW for TNT when the TNT weight is calculated on the basis of isentropic expansion.

The comparison of the airblast data from tanks C, D, and E with that from the TNT charges is correct in that both the tanks and TNT charges were spherical in shape. The comparison of the airblast data from tanks A and B with the spherical TNT charge data may be questioned since these tanks were cylindrical. Certainly the blast field generated by a spherical TNT charge would differ from that generated by a TNT cylinder of equal weight. (Reference (8)) Moreover, the pressure field generated by a cylindrical charge is dependent on the length to diameter ratio (L/D) and the point of detonation. The point of detonation determines the pattern of the detonation wave propagation which in turn determines the blast field about the cylinder.

In the case of the cylindrical tanks, there is no detonation wave. Therefore, comparing these airblast data with that from a cylindrical TNT charge has no more validity than comparing them with spherical TNT data. The similarity of the relationship between the cylindrical tank-spherical charge and the spherical tank-spherical charge data is seen in Figures 3.8 through 3.24.

Even if we used cylindrical charges of the same scaled shape, the blast field would still depend on the detonation scheme. Since we had no physical reason for choosing any one detonation scheme over another, no cylinders were fired.

Since the L/D of the cylindrical tanks was small (about 2/1) and the tanks had hemispherical ends, we treated them as equivalent volume spheres. To generalize, we plotted the mean peak shock overpressurer vs distance in tank radii for the two cylindrical tanks in Figure 6.4. (The radius is that of a sphere whose volume is equal to that of a cylinder.) The pressure distance curve in Figure 6.4 should be representative of that from similar tanks burst at 600 psig - with allowances of about 30% for blast wave asymmetry.

Based on the curves in Figure 6.4, tank rupture blast equivalence based on peak shock overpressure has been calculated and is shown as a function of tank radiis in Figure 6.5.

The positive shockwave impulse from the 600 psig tank ruptures have been combined and are shown as a function of tank radius in Figure 6.6. Again, this curve should be representative of the positive impulse from any sized similar tanks that burst at 600 psig. From Figure 6.6, the tank rupture TNT equivalence in terms of the weight of TNT as determined from isentropic expansion energy is considered a constant. In this case, the tank rupture EW/TNT EW averages about 1.78.

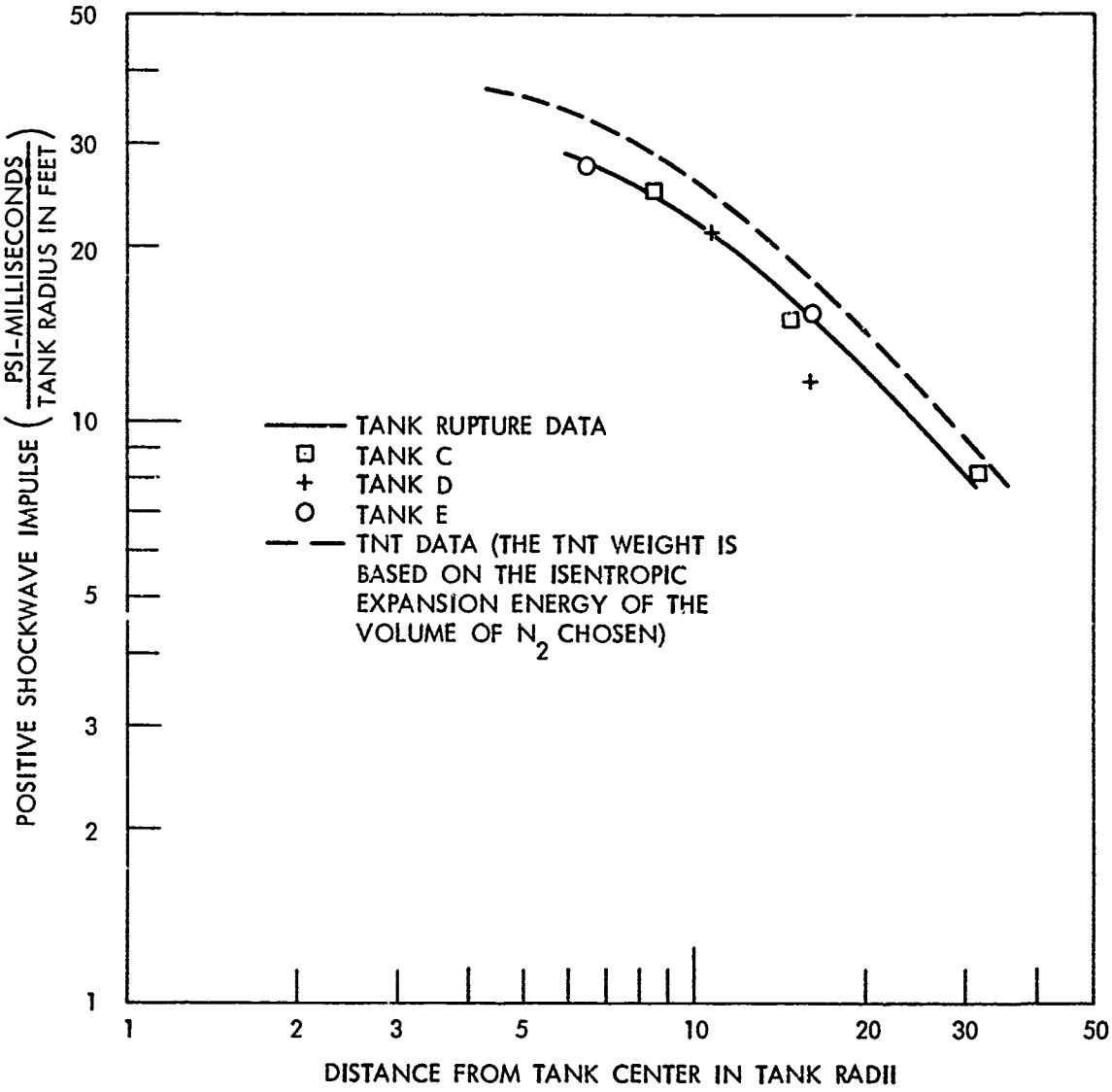

FIG. 6.3 POSITIVE SHOCKWAVE IMPULSE FROM AN 8,000 PSIG TANK RUPTURE VS DISTANCE IN TANK RADII

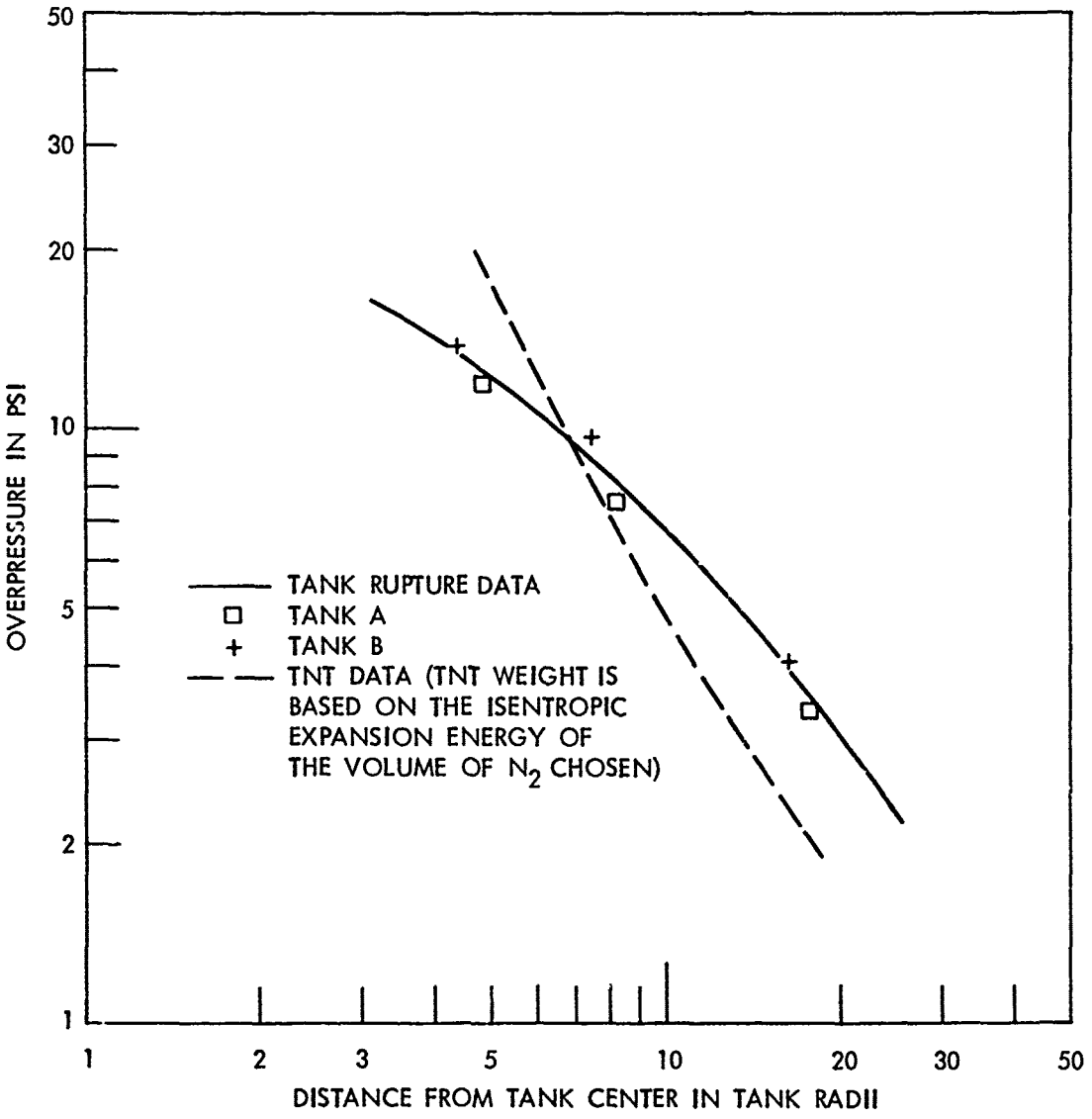

FIG. 6.4 PEAK AIRBLAST OVERPRESSURE FROM A 600 PSIG TANK RUPTURE VS DISTANCE IN TANK RADII

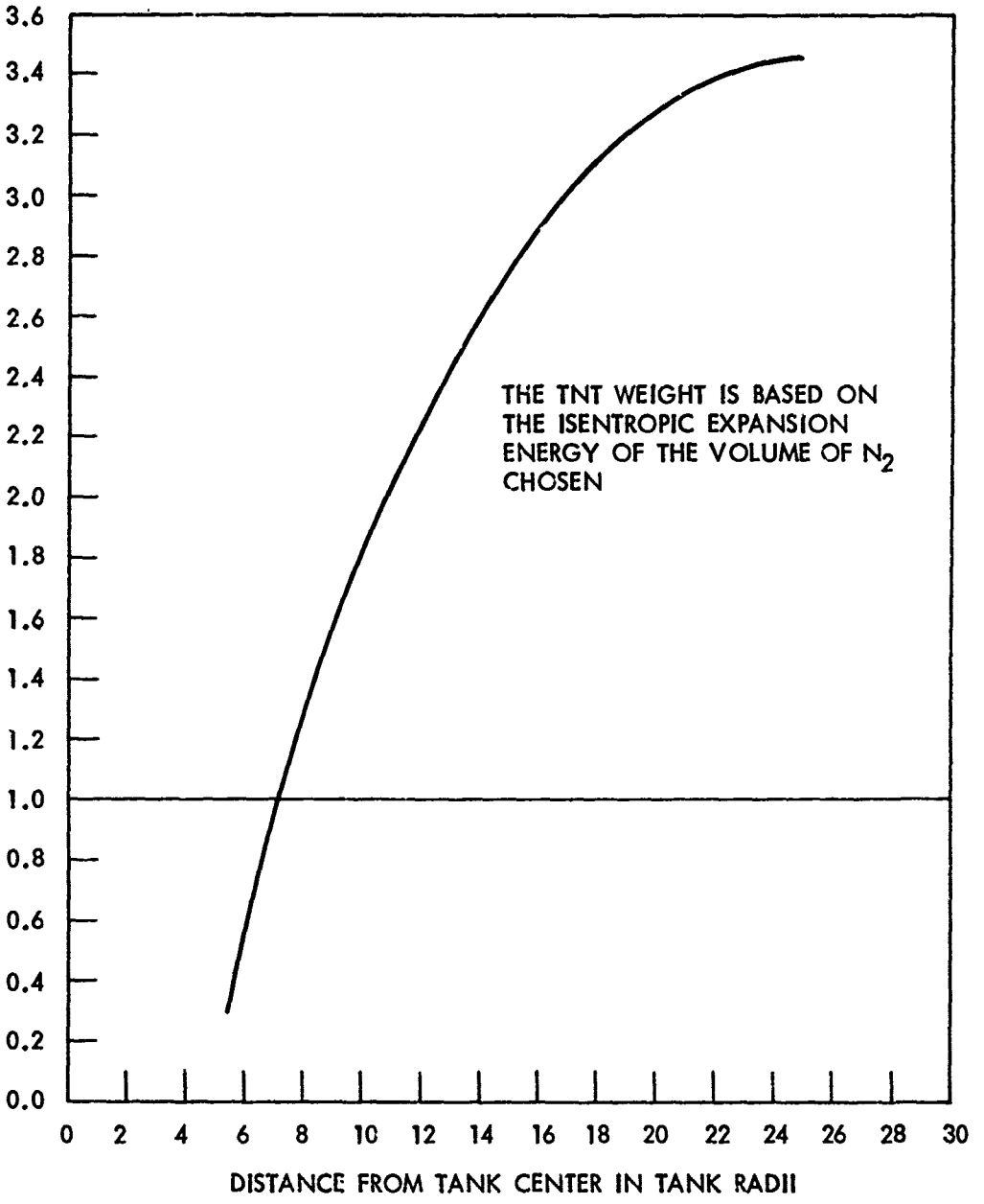

FIG. 6.5 TNT EQUIVALENCE OF THE AIRBLAST FROM A 600 PSIG TANK RUPTURE BASED ON PEAK SHOCK OVERPRESSURE

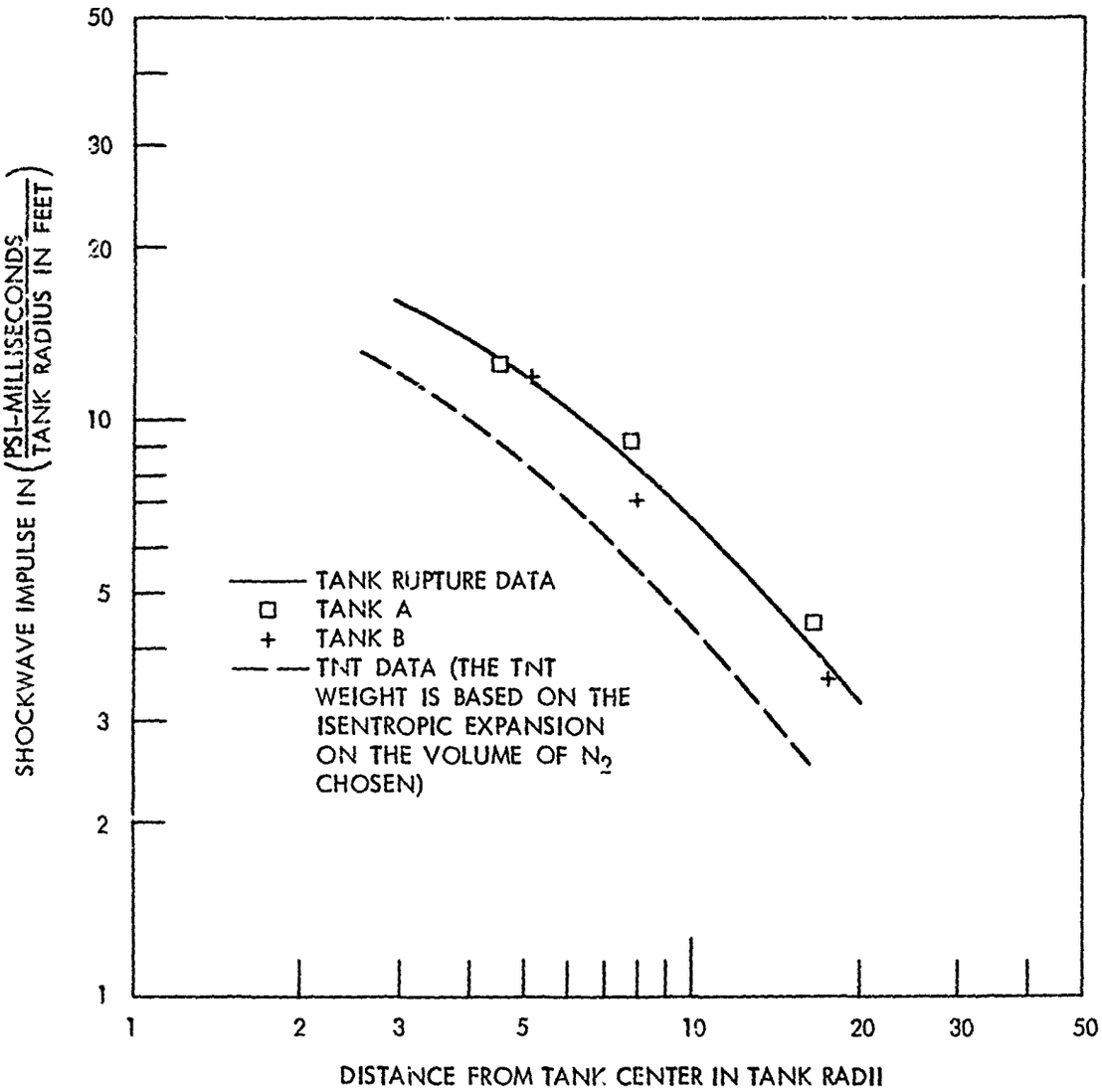

FIG. 6.6 POSITIVE SHOCK WAVE IMPULSE FROM A 600 PSIG TANK RUPTURE VS DISTANCE IN TANK RADII

Using the results of these experiments it is possible to predict the blast parameters generated by the rupture of similar tanks of different volumes providing rupture pressures are equal. It is not simple to predict the blast field for different rupture pressures. However, slight modifications to computer programs now being used at NOL would allow such predictions. The experimental data from this program would serve as a check on the validity of such calculations.

6.3 Fragmentation

6.3.1 Fragment Density

Procedures used for obtaining fragment size and distribution from munitions is misleading in the case of the tanks. The number of fragments from even a small bomb are orders of magnitude greater than the number from the tanks. Statistical treatments for munitions fragments are justifiable. In the case of the tanks, there were only three hits on a circular arena from one tank; this hardly leads to a statistical analysis.

A further complication in the tank case was the ricocheting fragments. In munitions work, a barricade is erected to intercept such fragments. In our case, we were unable to take this precaution because a barricade would have ruined blast measurements. A better technique is to estimate the total number of fragments based on the number and weight of those recovered.

In the case of tanks A and B, the number of heavy tank parts recovered could bias this estimate since with their weight added, we recovered about 70% of the tanks by weight. Since all the heavy parts were recovered, the unrecovered fragments consisted of the tank walls only.

We actually recovered 56% of the material making up the tank walls. Of the 36 fragments recovered, 32 were of tank wall material. On this basis 32 fragments equal 56% of the material, therefore the total number of fragments estimated from tank A would be 57. With the heavy fragments, this makes a total of 61. We further assume that these fragments were scattered equally over a 360° solid angle.

For tank B, 61% of the tank wall material was recovered. This was divided into 33 fragments. The estimated total number of tank wall fragments then would be 54. Including the heavy tank parts, the total is 57.

There is a possibility that in some cases, the heavy wire frame supporting the second breakwire may have cut some of the larger fragments into many smaller pieces. Thus had the tank ruptured in an unencumbered environment, fewer fragments would have resulted.

For tank C, because of the richochet problem, only 21% of the tank was recovered. This consisted of 8 fragments. A wild estimate of the total number of fragments from tank C would be 38 fragments.

For tank D we recovered 21 fragments, 45% of the tank by weight. Based on this, 47 fragments were produced. For tank E we recovered 25 fragments making up 51.6% of the tank's weight. Based on this the total number of fragments from tank E would have been 48. In the above, the flange (fragment 25 in Figure 4.6) has been ignored since its accounting would not influence the estimate.

Of the 21 fragments recovered from Tank D, six were inside the arena. The other 15 were either in the arena wall or just outside the walls. From Table 4.2 there were 28 arena wall hits. The above accounts for 15 hits. Thus there were 13 more fragments with trajectories, either direct or by ricochet, that intercepted the arena wall. Assume that all the fragments that were recovered had trajectories that were below the arena walls. (This means that no fragments had trajectories near enough to the vertical to fall back in the arena.) With this assumption, we add the 13 fragments not found to those 21 found for a total of 34 fragments. This means that the trajectories of all 34, or 72% were below the arena walls. Yet the top of the arena walls defined an angle that covered 59% of the tank's surface.

Based on a similar argument for tank E, 35 fragments or 73% had trajectories below the top of the arena walls. Again the angle described by the arena walls intercepted only 59% of the tank's surface.

We are left with these conclusions: (a) Our method of estimating number of fragments is incorrect. (b) The fragment distribution is not homogeneous over a solid angle described by a spherical shell. (c) All the fragments found on the floor of the arena went straight up and fell back in the arena. (Fragments 15, 17, 18, 19, 22, 23, and 25 in Figure 4.7 for instance.) The most probable factor is that we are underestimating the number of fragments because of the influence of the fragment numbered one in Tables 4.5 and 4.6 on fragment distribution and average weight.

6.3.2 Fragment Velocities

To aid in experimental planning, a short computer program was devised to give "ball park" estimates of fragment velocities. These calculations are presented in Appendix B. Calculated fragment velocities tended to be 20 to 40% lower than those measured by the breakwire and photographic system.

The calculated values for the cylindrical tanks (tanks A and B) in Figure 5 of Appendix B were even lower. However, a later calculation using the correct burst pressure and density for the tank wall material yielded maximum fragment velocity closer to the measured value. (Figure 6.7) The rapid decay of the calculated velocity with time results from the model used for the calculations. In the model, the fragments are tied to the gas front in an arrangement somewhat as though they were on a rubber band. The significant thing, from the standpoint of damage, is that the fragments do not slow down rapidly.

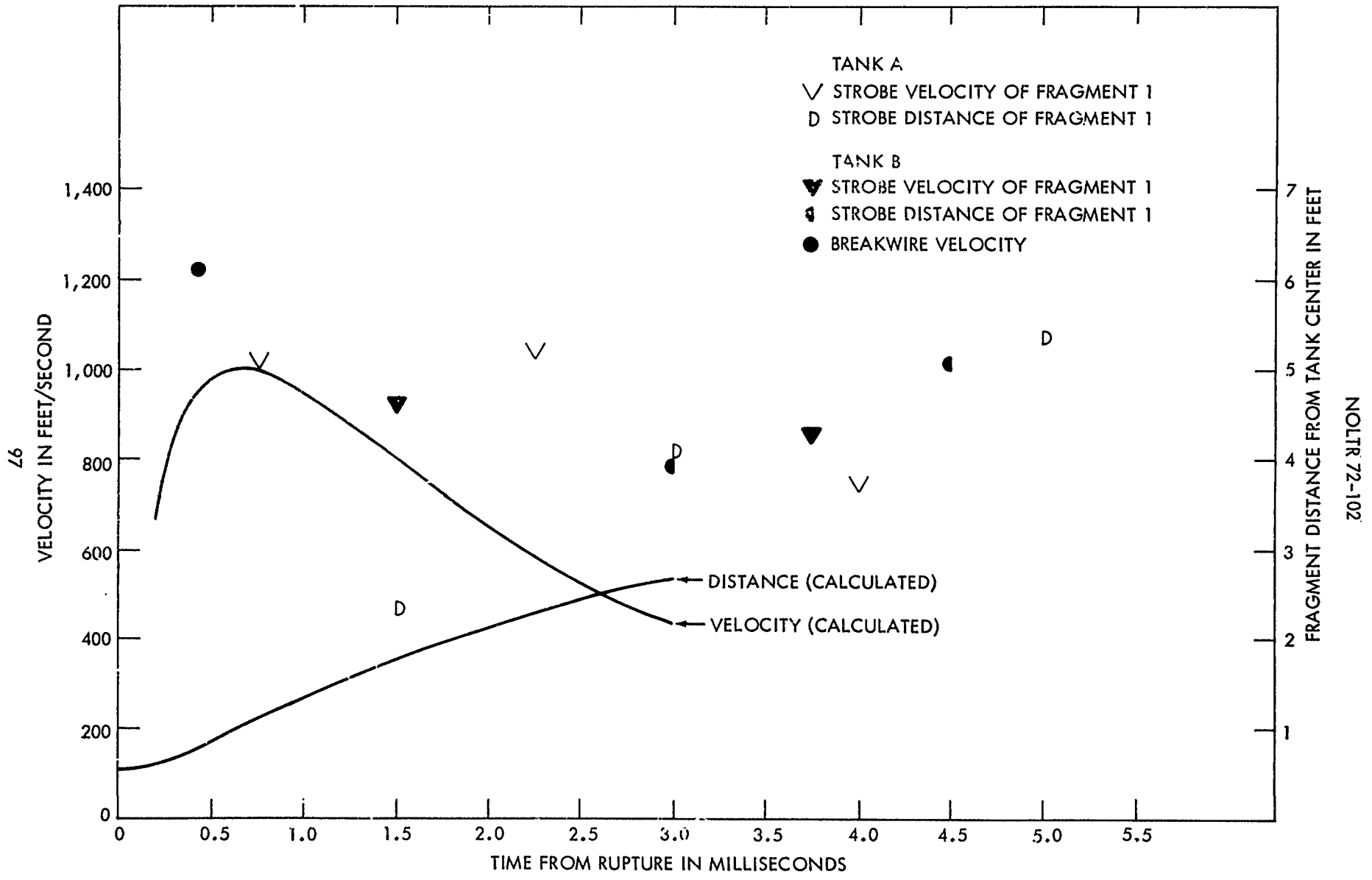

FIG. 6.7 CALCULATED AND MEASURED FRAGMENT VELOCITIES

NOLTR 72-102

In Figures 4.8 and 4.11, tank rupture is seen to have already taken place by the time the first flash occurs. The counter for velocity measurements started at the same time that the first flash occurred, within 5 microseconds. The question then arises, were fragments already in flight when the counters started? If so, then the breakwire system would yield a velocity greater than actually existed.

For tank A, the breakwire system did not operate. Therefore, we are unable to make a comparison. Note however, in Table 4.8, the average fragment velocity over the first 1.5 milliseconds of time as measured by the strobe system was slightly over 1000 ft/sec.

For Tank B the breakwire velocity was 1215 ft/sec. The strobe system did not yield fragment velocities over the first 1.5 millisecond time interval. However, velocities measured at later times by the strobe system were not greatly different from those of Tank A. For Tank C, the 1200 ft/sec fragment velocity measured by the strobe system over the first 3.0 milliseconds is not out of line with the 1270 $\pm$ 80 ft/sec measured by the breakwire system.

For Tanks D and E, the strobe system did not yield fragment velocities. However from Figure 4.15 we can put an upper velocity limit on the Tank D fragments. In Figure 4.15, no fragments are visible outside the condensation cloud at 0 + 4.5 milliseconds. Since the cloud is at a 7 ft radius at this time and the tank radius is 1.13 ft, the distance for a fragment to travel would be 5.87 ft. Therefore, no fragment has traveled at an average velocity greater than 1300 ft/sec over the first 4.5 milliseconds. In Figure 4.17, fragments from Tank E are clearly outside the condensation cloud at 0 + 8 milliseconds. Since the cloud is about 10.5 ft in diameter at this time, the fragments must have traveled a distance greater than 9.4 ft from the tank perimeter. Therefore the fragment velocity was greater than 1170 ft/sec averaged over 8 milliseconds.

6.4 Qualitative Damage

It was shown in Section 5 that the fragment hazard to personnel is severe from any of the tanks. Certainly people deployed as were our anthropomorphic dummies would have been maimed, possibly killed. The damage potential of heavy fragments -- several pounds -- traveling at supersonic velocities is awesome. These fragments sheared off heavy 3" pipes, passed through 6" of panel broadside on, and were found over 300 yards from Ground Zero!

Even the blast from any of the tanks would rupture eardrums and, in the case of tanks D and E, cause lung damage. More impressive, the blast from tanks D and E seemed to do things that would not be expected from 10 pounds of TNT. Specifically the blast from tank D drove the 4' x 4' x 1.5' concrete firing pad about 4 inches into the ground. The tank E rupture drove the pad another 5 inches into the ground. Both tanks caved in and collapsed the arena walls. The 8.2 pounds of TNT neither caved in the wall nor displaced the concrete pad any further, nor would the TNT be expected to do so.

Side-on overpressures and positive shock wave durations from tanks D and E were different from those for a TNT equivalent charge based on isentropic expansion; but they combined to give positive shock wave impulses quite comparable to those for the TNT. Nevertheless, blast from tank rupture, qualitatively at least, seemed more violent than that from TNT at comparable distances.

7. Conclusions

Our studies proved that no single TNT equivalent can be used to describe the blast generated by a rupturing pressure vessel. For instance, side-on pressures from tank rupture are lower than those for an equivalent TNT charge at blast pressures above 10 to 15 psi but are higher than those for TNT below 10 to 15 psi. However, the tank-rupture blast pressures combined with the positive shock wave durations yield positive shock wave impulse values whose impulse-distance relation was similar in slope to that for TNT. In the case of the large, high pressure vessels, impulse for tank rupture and for the TNT equivalent were not significantly different quantitatively.

The large, high velocity fragments generated by tank rupture will prove to be a significant hazard. Tanks A and B, similar cylindrical tanks, broke into about the same number of fragments and generated similar fragment velocities. The same reproducibility of number of fragments and similar velocities were recorded for the high pressure spherical vessels, tanks D and E.

We can make a general comparison of blast and fragment parameters generated by tank rupture and an equivalent TNT charge. Side-on pressures are higher for TNT above 10 to 6 psi and lower for TNT at pressures below these values. Face-on tank pressures show a similar relation to face-on TNT pressures. Positive shock wave durations are longer for tank rupture than for TNT. Impulse, both face-on and side-on, is similar for TNT and tank rupture. Damage, depending on distance, may be greater for tank rupture. Tank-rupture fragments were larger than would be expected from a cased TNT charge. Fragment velocities would be higher for a cased TNT charge than for tank rupture.

Further analysis of the tank rupture data and phenomena are required to correlate damage with the blast parameters.

The work reported here can be extended by calculations to other tanks with different shapes, volumes, and rupture pressures. The computational efforts in the appendices can be refined to handle such work.

REFERENCES

1. Tussing, R., "A Four Channel Oscilloscope Recording System", Naval Ordnance Laboratory, NOLTR 65-21, 18 May 1965

2. McLanahan, D., "Scotchlite® Photography Using Scotchlite Reflective Sheeting", Naval Ordnance Laboratory, NAVORD Rpt #6760, 4 March 1960.

3. Lehto, D. and Lutzky, M., "One-Dimensional Hydrocode for Nuclear Explosion Calculations", Naval Ordnance Laboratory, NOLTR 62-168, March 1965.

4. Lehto, D. and Larson, R., "Long Range Propagation of Spherical Shockwaves from Explosions in Air", Naval Ordnance Laboratory, NOLTR 69-88, 22 July 1969.

5. Porzel, F. B., Private communication.

6. Holland, N., Goertner, J., and Caudle, K., "Explosives Effects and Properties (U)", Naval Ordnance Laboratory, NOLTR 65-218, 21 Feb 1967 (C)

7. Malick, D., "The Calibration of Wallboard for the Determination of Particle Speed", Ballistic Analysis Laboratory, Rpt #61, May 1966.

8. Wisotski, J. and Snyer, H., "Characteristics of the Blast Waves obtained from Cylindrical High Explosive Charges", Denver Research Institute, DRI #2286, Nov 1965.

ACKNOWLEDGEMENTS

Many people contributed to the successful completion of this program. Within the Naval Ordnance Laboratory the following people gave their time as consultants and advisors: J. Petes, F. B. Porzel, and J. F. Proctor. The calculations needed to design the experiment were done by D. Lehto and R. Lorenz.

The people who worked so many nights to complete the program were: F. Bampfield, P. Peckham, C. Kelly, and E. Murray.

Outside of the Laboratory, CWO S. Moe of the Explosive Ordnance Disposal Facility at Stump Neck gave technical advice on the photographic system and supplied some of the photographic equipment.

The author is indebted to all the above people for their help and their cheerful enthusiasm.

Table 3.1

Blast data from 24" Cylinder; Tank A
Burst Pressure = 625 psi

Gage Position	SIDE-ON MEASUREMENTS R	P	AT	PD	I	Gage Position	FACE-ON MEASUREMENTS R	P	AT	PD	I
1B	3.20	14.4	1.61	1.46	10.3	1A	3.35		1.89	1.17	--
2B	3.53	8.07	2.43	1.51	5.55	2A	3.50	18.2	2.30	1.16	11.9
3B	3.15	13.2	1.81	1.34	8.50	3A	3.00	--	1.59	1.40	
1D	5.40	8.63	3.05	1.45	5.53	1C	5.42	16.9	3.64	0.89	9.37
2D	5.65	4.80	4.00	1.53	4.06	2C	5.75	13.0	4.00	1.23	8.46
3D	5.60	8.97	3.32	1.55	5.40	3C	5.35	15.7	3.30	0.92	9.47
1E	12.0	3.66	8.06	1.65	2.17						
2E	12.3	2.74	9.56	1.67	2.02						
3E	12.0	3.58	8.41	1.83	2.98						

R = Gage to tank center distance in feet
P = Maximum shockwave pressure in psig
AT = Arrival time in milliseconds
PD = Positive shockwave duration in milliseconds (ms)
I = Positive shockwave impulse in psi-ms

Table 3.2

Blast data from 29" Cylinder; Tank B
Burst Pressure = 600 psi

Gage Position	SIDE-ON MEASUREMENTS R	P	AT	PD	I	Gage Position	FACE-ON MEASUREMENTS R	P	AT	PD	I
1B	3.13	15.4	1.80	1.16	7.84	1A	3.30	26.1	2.07	1.05	
2B	3.51	8.83	2.39	1.34	6.01	2A	3.45	34.6	2.06	1.04	32.9
3B	3.17	16.7	1.37	1.59	23.7	3A	3.10	47.4	1.49	1.31	55.4
1D	5.40	9.35	3.27	1.82	6.37	1C	5.46	17.8	3.59	0.80	6.95
2D	5.60	7.13	3.79	1.69	4.46	2C	5.66	10.1	3.78	1.16	6.05
3D	5.62	12.4	2.86	1.61	9.58	3C	5.40	28.0	2.68	1.53	16.7
1E											
2E	12.2	3.54	8.92	1.79	2.49						
3E	12.0	4.51	7.72	2.13	4.30						

R = Gage to tank center distance in feet
P = Maximum shockwave pressure in psig
AT = Arrival time in milliseconds
PD = Positive shockwave duration in milliseconds (ms)
I = Positive shockwave impulse in psi-ms

Table 3.3

Blast Data From 0.235 Ft^3 Vessel; Tank C

Burst Pressure = 8000 psi

SIDE-ON MEASUREMENTS						FACE-ON MEASUREMENTS					
Gage Position	R	P	AT	PD	I	Gage Position	R	P	AT	PD	I
1B	3.35	17.5	1.61	1.06	9.77	1A	3.43	--	--	--	--
2B	3.22	16.9	1.52	1.06	9.38	2A	3.24	51	1.77	1.94	46.1
3B	3.22	11.7	1.83	1.58	--	3A	3.24	25.4	1.64	2.35	20.6
1D	5.58	9.70	2.92	1.77	6.10	1C	5.58	18.9	2.94	1.23	11.1
2D	5.53	12.2	2.76	1.82	7.69	2C	5.46	22.4	2.83	1.34	11.7
3D	5.68	7.15	3.52	1.44	3.45	3C	5.45	18.5	3.41	0.99	13.0
1E	12.10	5.36	8.2	2.78	4.82						
2E	12.05	3.08	8.08	1.96	2.34						
3E	12.10	2.60	8.95	1.63	2.17						

R = Gage to tank center distance in feet
P = Maximum shockwave pressure in psig
AT = Arrival time in milliseconds
PD = Positive shockwave duration in milliseconds (ms)
I = Positive shockwave impulse in psi-ms

Table 3.4

Blast Data From 6 ft^3 Vessel; Tank D

Burst Pressure = 8,000 psi

SIDE-ON MEASUREMENTS						FACE-ON MEASUREMENTS					
Gage Position	R	P	AT	PD	I	Gage Position	R	P	AT	PD	I
1B	6.92	20.8	4.00	3.08	20.3	1A	6.77	67.3	4.05	--	--
2B	7.59	27.1	4.30	2.62	37.6	2A	7.42	103	3.72	4.00	207.
3B	7.17	26.1	3.72	2.62	34.8	3A	7.12	110	3.73	3.62	148.
1D	12.17	14.6	7.51	3.97	20.6	1C	12.10	32.5	7.41	3.74	28.0
2D	12.22	19.7	6.35	4.00	28.3	2C	12.27	39.1	6.70	3.00	47.4
3D	12.07	19.4	6.75	4.16	25.5	3C	12.03	38.8	6.60	3.20	36.7
1E	17.77	7.25	9.98	2.93	7.1						
2E	18.12	10.5	10.8	3.68	17.0						
3E	17.95	9.30	10.6	3.42	15.5						

R = Gage to tank center distance in feet
P = Maximum shockwave pressure in psig
AT = Arrival time in milliseconds
PD = Positive shockwave duration in milliseconds (ms)
I = Positive shockwave impulse in psi-ms

Table 3.5

Blast Data from 6 ft cycled Vessel; Tank E
Burst Pressure = 8130 psi

SIDE-ON MEASUREMENTS						FACE-ON MEASUREMENTS					
Gage Position	R	P	AT	PD	I	Gage Position	R	P	AT	PD	I
1B	7.17	26.4	3.50	1.62	29.9	1A	7.01	111	3.38		
2B	7.64	31.0	3.62	2.92	31.7	2A } No records obtained					
3B	7.22	19.4	4.29	2.90	--	3A }					
1E	17.05	12.2	9.60	3.94	17.8						
2E	18.07	13.8	8.69	4.00	22.2						
3E	17.05	6.88	10.31	4.45	12.1						

R = Gage to tank center distance in feet
P = Maximum shockwave pressure in psig
AT = Arrival time in milliseconds
PD = Positive Shockwave duration in milliseconds (ms)
I = Positive Shockwave impulse in psi-ms

Table 3.6

Blast Data from 8.2-lb TNT Spheres

Shot No.	Gage Position	SIDE-ON MEASUREMENTS R	P	AT	PD	I	Shot	Gage Position	FACE-ON MEASUREMENTS R	P	AT	PD	I
555	1B	7.08	92.8	1.42	--	--	555	1A	--	--	--	--	--
555	2B	7.43	81.1	1.41	--	--	555	2A	7.10	773	1.39	--	--
555	3B	7.42	--	1.42	--	--	555	3A	7.10	549	1.39	--	--
556	1B	7.45	72.0	1.82	1.43	27.8	556	3A	7.20	--	1.70	--	--
556	2B	7.30	65.1	1.72	1.58	28.2	**Mean**		**7.13**	**661**	**1.49**		
556	3B	7.40	83.2	1.75	1.91	35.4							
Mean			78.8	1.59	1.64	30.5							
555	1D	12.35	22.2	3.86	2.19	19.7	555	1C	12.13	69.8	3.77	2.17	55.1
555	2D	12.02	29.5	3.72	2.30	24.8	555	2C	12.12	--	3.82	1.42	--
555	3D	11.90	40.1	3.73	2.14	26.8	555	3C	11.75	75.3	3.40	2.96	49.3
556	1D	12.65	20.9	4.38	2.50	26.1	556	1C	12.55	75.8	4.35	--	--
556	2D	11.70	24.8	3.80	2.90	31.3	556	2C	11.95	75.6	3.88	2.80	90.5
556	3D	11.95	29.1	3.81	1.80	20.3	556	3C	11.75	78.7	3.84	2.25	97.2
Mean		**12.10**	**27.8**	**3.88**	**2.30**	**24.8**			**12.04**	**75.0**	**3.84**	**2.32**	**72.5**

Table 3.6 (Cont'd)

SIDE-ON MEASUREMENTS

Shot No.	Gage Position	R	P	AT	PD	I
556	1E	18.35	11.2	7.80	4.07	14.8
556	2E	17.73	12.5	7.60	4.50	19.4
556	3E	17.80	12.3	7.58	4.90	--
Mean		17.96	12.0	7.66	4.49	17.1

R = Gage to tank center distance in feet
P = Maximum shockwave pressure in psig
AT = Arrival time in milliseconds
PD = Positive shockwave duration in milliseconds (ms)
I = Positive shockwave impulse in psi-ms

Table 4.1

Fragmentation Data from Tank A

Fragment Number	Weight Grams	Where Found (Panel)	Fragment Number	Weight Grams	Where Found (Panel)
1	1248	(note 1)	22	6.4	
2	177	6	23	5.5	
3	149		24	5.2	
4	109	(note 2)	25	5.2	
5	105	2	26	5.0	
6	100		27	3.7	
7	96		28	3.4	
8	78	(note 2)	29	2.7	12
9	53	5	30	2.5	
10	53		31	2.2	13
11	47		32	2.0	
12	46		33	1.9	
13	42		34	145.	
14	39		35	89.	
15	33		36	102.	
16	18	4	Total	2837.	
17	15				
18	14	1			
19	13	4			
20	11				
21	8.7	(note 3)			

Note 1: Found at GZ

Note 2: Found in camera shield at arena opening

Note 3: Found in leg of dummy

- Total tank weight ≅ 3850 grams
- Tank wall thickness ≅ 0.018" to 0.024"
- Material density ≅ 4.41 gm/cc

Table 4.2

Panel Hits

Panel	TANK A	B	C	D	E
1	1	1		2	
2	2	1			1
3					2
4	2	1			
5		1			
6	1	3			
7		3			
8					2
9				1	
10				1	
11					
12	2				2
13	2		1	1	3
14					
15			1	1	1
16				2	1
17					1
18				3	4
19					1
20			1		2
21					1
22				2	2
23				2	
24		1		3	
25		2		2	1
26		1		2	1
27		1			1
28				1	
29				2	2
30		1		3	
31*	2				
Total	12	15	3	28	28
Recovered	36	36	8	21	25

* 31 is protective wood shield in front of cameras at arena opening

Table 4.3

Fragmentation Data from Tank B

Fragment Number	Weight Grams	Where Found (Panel)	Fragment Number	Weight Grams	Where Found (Panel)
1	1503 (Note 1)		23	10	
2	397		24	6.6	
3	142	1	25	6.4	
4	125		26	6.2	
5	114	30	27	4.6	
6	100	24	28	3.2	
7	92	23	29	2.7	
8	72		30	2.0	
9	65		31	1.1	
10	63	5	32	0.4	
11	48		33	0.3	
12	44		34	101.	
13	38		35	70.	
14	33	25	Total	3300	
15	33				
16	32				
17	31				
18	31				
19	28				
20	26	6			
21	24	6			
22A	23	25			
22	20	6			

Note 1: Found at GZ

- Total tank weight ≅ 4100 grams
- Tank wall thickness ≅ 0.018" to 0.024"
- Material density ≅ 4.41 gm/cc

Table 4.4

Fragmentation Data from Tank C

Fragment Number	Weight (Grams)	Where Found (Panel)
1	300 (Note 1)	
2	167	20
3	67 (Note 2)	
4	30.9	
5	12.9	
6	13.1 (Note 3)	
7	15.6	
8	12.6	
Total	617.1	

Note 1: Found at GZ
Note 2: Through scotchlite at Panel 13
Note 3: Through scotchlite at Panel 15

- Total tank weight $\cong$ 2860 grams
- Tank wall thickness $\cong$ 0.108"
- Material density $\cong$ 4.44 gm/cc

Table 4.5

Fragmentation Data from Tank D

Fragment Number	Weight (Grams)	Where Found
1	7321	GZ
2	2923	Outside arena panel 3
3	2639	Outside arena panel 9
4	2497	Outside approximately 300 yards
5	2270	4' from GZ toward panel 27
6	2156	**Panel 10 low outside**
7	2156	Panel 25 outside
8	2157	Panel 18 outside
9	2043	**256 yards outside over panel 26**
10	2015	Panel 18
11	1731	Panel 30 low
12	1731	Panel 10
13	653	Base panel 2
14	624	Panel 19
15	482	Panel 12
16	454	Panel 18
17	227	10' from GZ toward panel 19
18	199	17' from GZ toward panel 7
19	85	14' from GZ
20	57	Base panel 2
21	111	Panel 27

Total weight 34,531 gms = 76 lbs
Average thickness 0.362 inches
Density 4.46 g/cc

Table 4.6

Fragmentation Data from Tank E

Fragment Number	Weight (Grams)	Where Found
1	8143	Panel 18 high
2	3802	Panel 3
3	3036	Outside arena behind panel 1
4	2610	Outside arena near camera station 2
5	2412	Panel 8 found at base
6	2270	Panel 21 high
7	2270	Panel 20 low
8	1873	Panel 17 low found outside
9	1759	Panel 26 low found outside
10	1674	Panel 15
11	1617	Panel 19 high found outside
12	1277	Panel 3
13	1022	Panel 27 middle
14	1050	Panel 25 low
15	738	Inside arena
16	624	Panel 8
17	539	Inside arena
18	454	Panel 27 base on ground
19	397	Inside arena
20	199	Panel 8
21	170	Panel 18
22	142	Inside arena
23	61	Inside arena
24	38	Panel 29 high
25	1532	GZ intake block

Total weight 39,809 gms = 87.7 lbs
Average thickness 0.365 inches
Density 4.46 g/cc

Table 4.7

Times of Strobe Flashes

(All times given in milliseconds after tank rupture)

Tank	1st Flash	2nd Flash	3rd Flash	4th Flash
A	0	1.50	3.00	5.00
B	0	1.50	3.00	4.50
C	0	1.50	3.00	4.50
D	0	1.50	3.00	4.50
E	0	6.00	7.00	8.00

Table 4.8

Measured Fragment Velocities

Tank	Breakwire Velocity	Strobe System Velocities			
		Fragment Number (1)	Time (2) Interval	Distance Traveled(3)	Velocity VA (4)
A	No Data	1	0 to 1.50	1.52	1010
			1.50 to 3.00	1.56	1040
			3.00 to 5.00	1.50	750
			0 to 5.00	4.58	918
		2	0 to 1.50	1.56	1040
			1.50 to 3.00	1.61	1070
			3.00 to 5.00	1.86	930
			0 to 5.00	5.03	1000
		3	0 to 3.00	3.10	1030
			3 to 5.00	1.73	865
			0 to 5.00	4.83	967
B	1215 ± 50	1	0 to 3.00	2.76	920
			3.00 to 4.50	1.29	860
			0 to 4.50	4.05	900
		2	0 to 3.00	2.96	986
			3.00 to 4.50	1.32	880
			0 to 4.50	4.28	950
C	1270 ± 80	1	0 to 3.00	3.60	1200
			3.00 to 4.50	1.53	1020
			0 to 4.50	5.20	1150
D	1400 ± 90	No Strobe Data			
E	1470 ± 100	No Strobe Data			

(1) Fragments identified in Figures 4.9 through 4.18
(2) Times in milliseconds
(3) Distance in feet
(4) VA - Average velocity in ft/sec over the time interval given

APPENDIX A

by

D. Lehto

Calculations of Blast from Exploding Pressure Vessels

Figure A-1 summarizes the results of a Wundy Hydrocode calculation for the explosion of a 6 ft^3 spherical tank filled with air at 15°C and burst at 8,000 psig. The air is assumed to act as an ideal gas with a gamma of 1.4. Tank mass is ignored; the container is assumed to disappear instantaneously like an ideal shock tube diaphragm. Table A-1 summarizes the initial conditions.

Figure A-1 compares the computed pressure-distance results for the tank explosion with those from a 10.1-lb TNT charge. (If one assumes that TNT energy is 1018 cals/gm, then 10.1 lbs is the TNT energy equivalent based on the isentropic expansion of the air contained in a 6 ft^3 air sphere compressed to 8,000 psig at 15°C.)

Figure A-2 shows the space-time paths for the main shock, the location of the first zero overpressure (end of the positive phase), and the contact surface position.

Figure A-3 shows predicted pressure-time records at positions 7-, 14-, and 18-ft from the tank center. Contact surface arrival distorts the tail of the 7 ft record.

Figure A-4 presents the predicted pressure-distance relation for a 1.34 ft^3 spherical, air filled tank burst at 460 psig. For comparison, a pressure-distance relation for a 0.125 lb TNT sphere is shown.

Table A-1

Calculations for Exploding Pressure Tank

Volume (cu ft)	= 6.0
Pressure (psia)	= 8.0×10^3
Gamma	= 1.400
Wt/Mole	= 28.964
Tank Volume (cu cm)	= 1.699×10^5
Radius (cm)	= 34.36
Compression Ratio	= 5.444×10^2
Initial Density (G/CC)	= 1.225×10^{-3}
Density in Tank (G/CC)	= 0.669
Mass in Tank (G)	= 1.133×10^5
Internal Energy (Erg/G)	= 2.068×10^9
E Loss on Expansion (Erg/G)	= 1.726×10^9
Total Energy Loss (cal)	= 4.672×10^6
TNT Equivalence (Grams)	= 4.589×10^3
TNT Equivalence (lb)	= 10.12

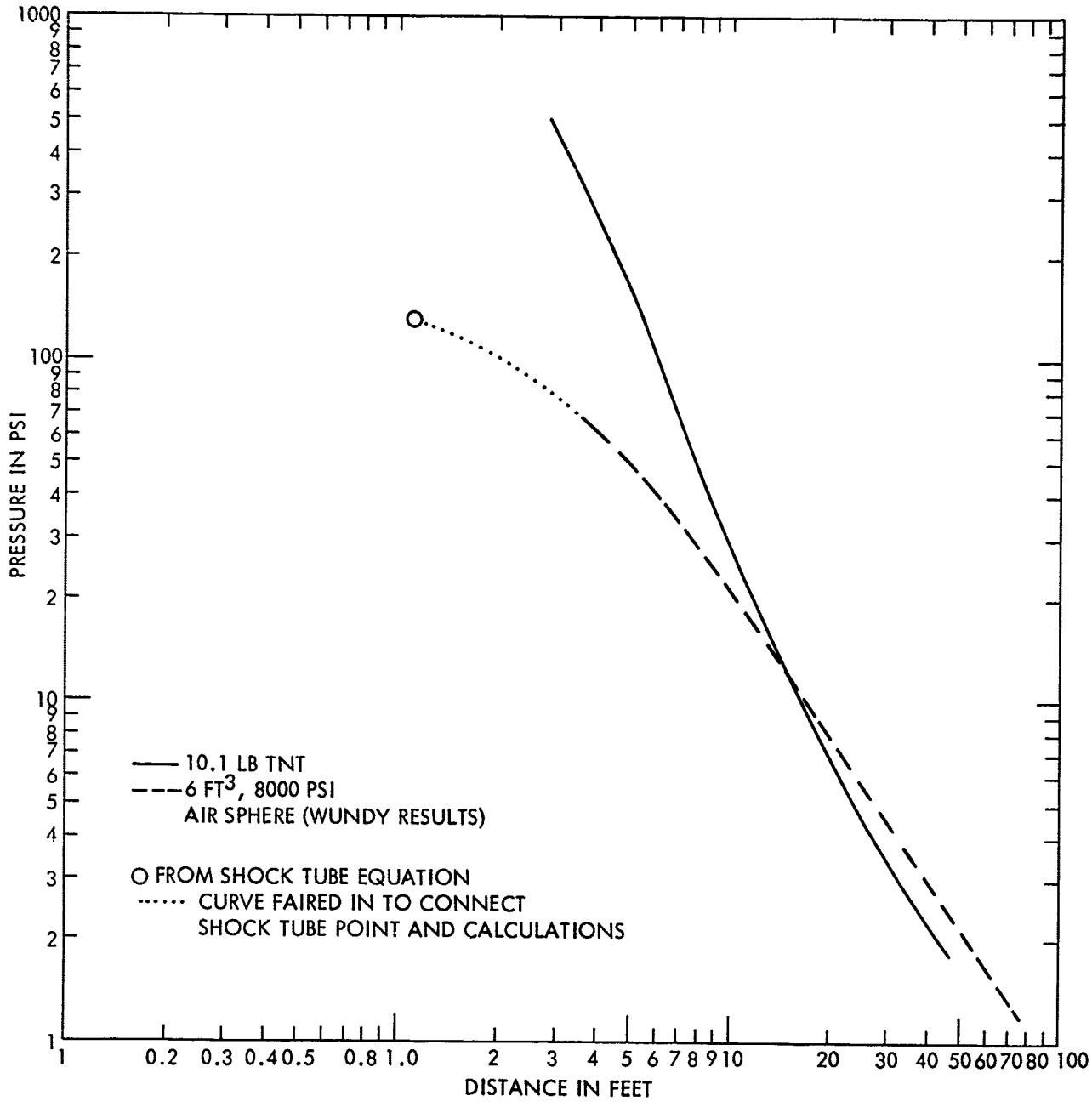

FIG. A-1 SHOCK OVER PRESSURE VS DISTANCE FOR EXPLODING PRESSURE VESSEL; 6 FT^3 AT 8,000 PSI

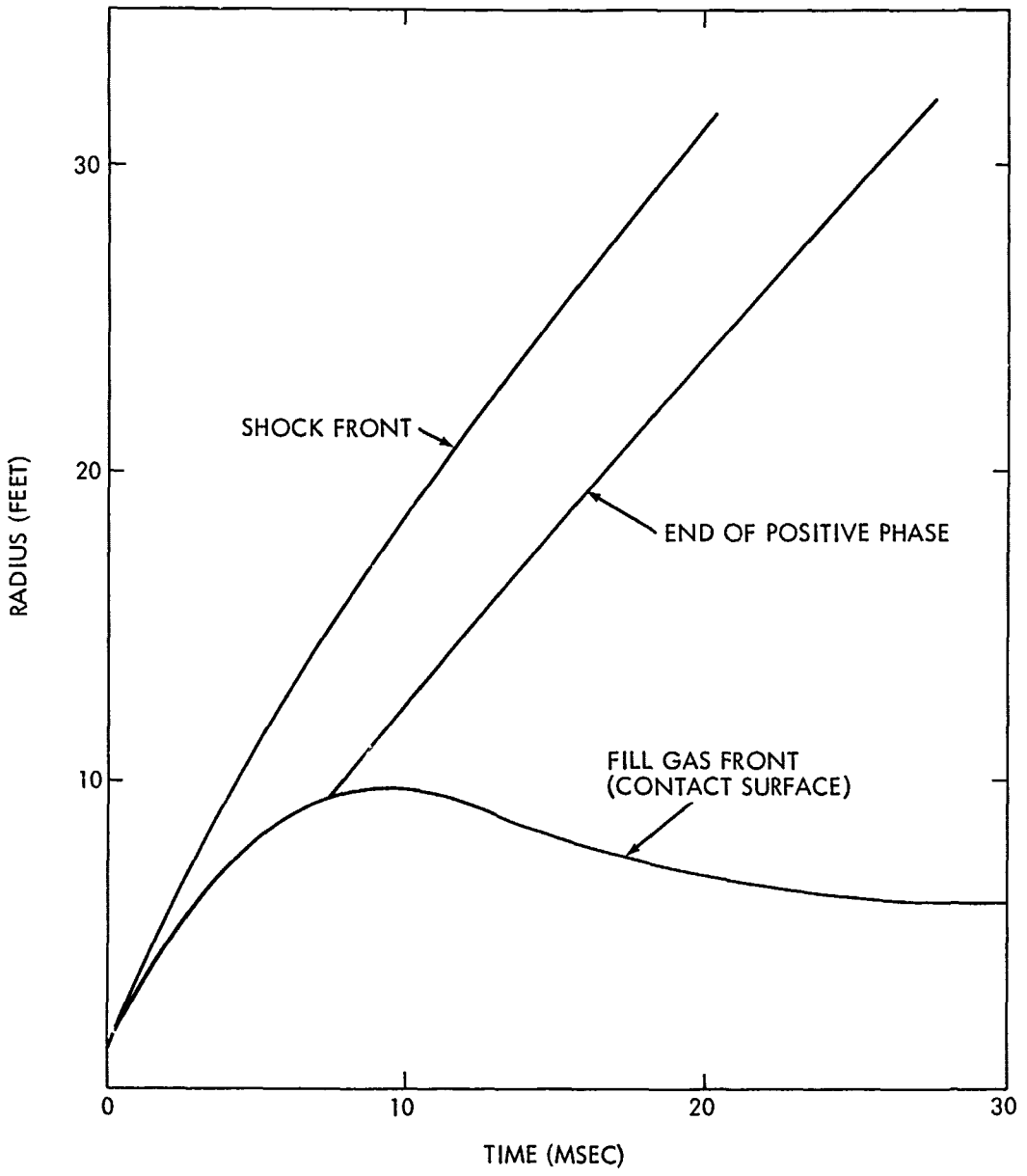

FIG. A-2 SPACE-TIME PATHS FOR EXPLOSION OF 8000 PSI AIR SPHERE

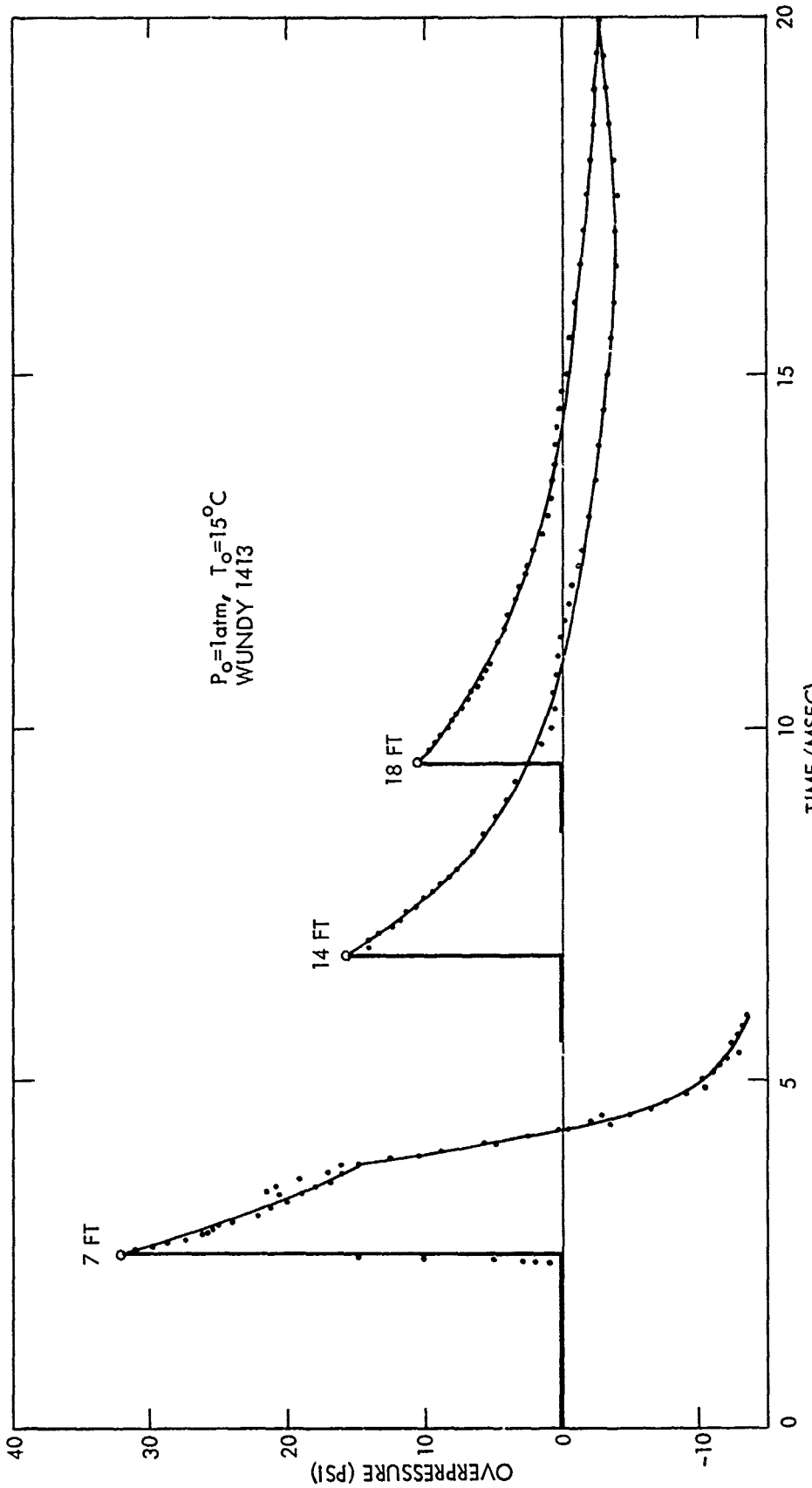

FIG. A-3 PRESSURE-TIME RECORDS FOR EXPLOSION OF 8000 PSI AIR SPHERE

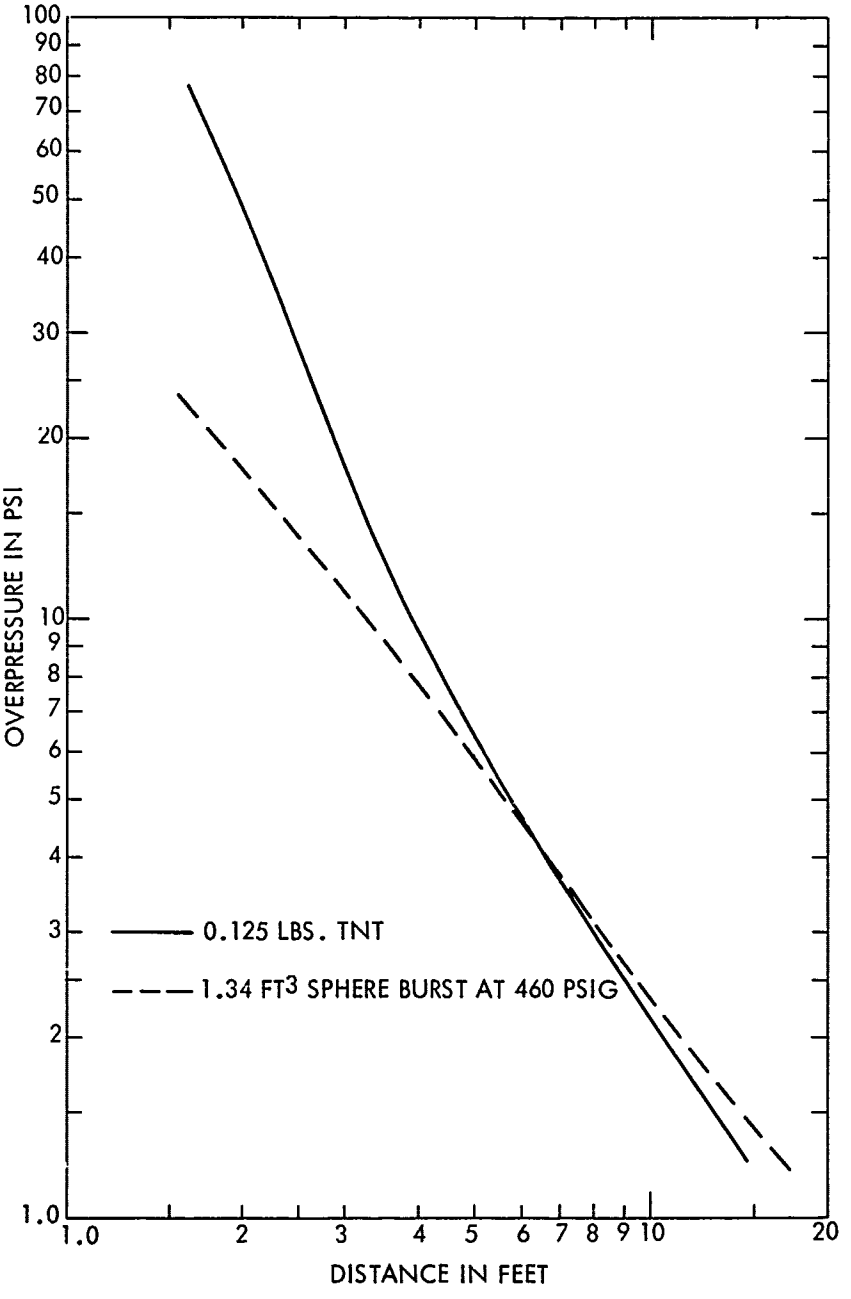

FIG. A-4 CALCULATED SHOCK OVERPRESSURES FROM 1.34 FT^3 TANK BURST AT 460 PSI

APPENDIX B

by

R. A. Lorenz

A Short Computer Code to Estimate the Early-Time Fragment Velocity and Position vs Time for a High Pressure Spherical or Cylindrical Tank Rupture

The work summarized in this report is the result of the need to predict the fragment velocity and position vs time while designing a series of high pressure tank rupture experiments.

The Spherical Model

The most important factors contributing to the motion of the fragments are:

(a) the driving pressure immediately behind each fragment
(b) the jetting of compressed gas between the fragments which results in a lower driving pressure, and
(c) the accumulation of compressed air ahead of the fragments and in the jets which absorb energy and tend to slow the fragments down.

In constructing a model to account for these factors and to keep the calculations as simple as possible, the following basic assumptions were made:

(a) The total area of all the fragments remains constant while their volume is negligible.
(b) Air turbulence and fragment tumbling are forbidden.
(c) At each instant, the pressure, internal energy, and density of the compressed gas is uniform throughout the volume of gas.
(d) The compressed gas inside the tank as well as the surrounding medium is a constant-gamma ideal gas.

The geometry used in the calculation (Fig. B-1) follows from assumption (a) above. Two regions are defined, one for the solid angle subtending the fragments, and the other for the jetting gas. As the fragments move outward in space, a larger fraction of the total solid angle becomes available to the jetting gas since the total area of the fragments remains constant. Note also that the outer surface of the jetting region is constrained to lie on a sphere.

The volume of the system is determined as follows, using the notation of Figure B-1:

$$\text{Volume of fragment region} = \left(\frac{r_o^2}{r_s^2}\right)\frac{4}{3}\pi r_1^3 \qquad (1)$$

$$\text{Volume of jetting region} = \left(1 - \frac{r_o^2}{r_s^2}\right)\frac{4}{3}\pi r_2^3 \qquad (2)$$

where r_o is the initial radius of the tank. These calculations are found in lines 420-425 of the program on page B-10. (See also lines 390 and 410-415.)

As a result of assumption (b) above, the motion of the system is restricted to radially outward motion. Therefore, the key velocities are: v_s, the velocity of the fragments; v_1, the velocity of the outer boundary of the fragment region; and v_2, the velocity of the outer boundary of the jetting region.

The uniform density of assumption (a) above, results in a simple expression for the velocity of the gas at any radius as a function of the velocity at the outer boundary. Consider first the time rate of change of the volume of an expanding sphere in general:

$$V = \frac{4}{3}\pi r^3$$

$$\frac{dV}{dt} = 4\pi r^2 v = \frac{3}{r}\left(\frac{4}{3}\pi r^3\right)v = \frac{3}{r}Vv \qquad (3)$$

where v is the velocity of the outer boundary of the sphere. Now consider the time rate of change of the density in that sphere:

$$\rho = \frac{m}{V}$$

$$\frac{d\rho}{dt} = -\frac{m}{V^2}\frac{dV}{dt} = -\frac{\rho}{V}\left(\frac{3}{r}Vv\right) = -\frac{3\rho v}{r}$$

where use has been made of Equation (3). But since ρ must be constant throughout the volume, then

$$\frac{1}{\rho}\frac{d\rho}{dt} = -\frac{3v}{r}$$

must also have the same value for any smaller sphere of constant mass within the original sphere. Therefore, it follows that

$$-\frac{3v(x)}{x} = -\frac{3v(r)}{r}$$

$$\therefore v(x) = \left(\frac{x}{r}\right) v(r) \qquad (4)$$

The kinetic energy of the gas in either region of Figure (B-1) can now be calculated by making use of Equation (4). First an expression for the spatial rate of change of mass inside a constant-density sphere is needed:

$$\frac{dm}{dx} = \rho\frac{dV}{dx} = \rho\, 4\pi x^2 \quad . \qquad (5)$$

Then the total kinetic energy, T, of the gas is found to be:

$$T = \int_0^r \tfrac{1}{2}\frac{dm(x)}{dx}\, v(x)^2 dx$$

$$= \int_0^r \tfrac{1}{2}\left(\rho\, 4\pi x^2\right)\left(\frac{x^2}{r^2}v^2(r)\right) dx$$

$$= \frac{2\pi\rho v^2(r)}{r^2}\int_0^r x^4 dx = \frac{2\pi\rho v^2(r)}{r^2}\left(\frac{r^5}{5}\right)$$

$$= \frac{2\pi\rho}{5} r^3 v^2(r) = \frac{3}{10}\left(\frac{4}{3}\pi r^3\right)\rho v^2(r)$$

$$T = \frac{3}{10} mv^2(r) \qquad (6)$$

where use has been made of Equations (4) and (5). Note that the result depends only on the boundary velocity and total mass within the region. The kinetic energy is calculated in lines 445-455 of the program.

The uniform pressure and internal energy assumption (c) together with the ideal gas assumption (d) allows the pressure to be calculated from the expression for the internal energy of an ideal gas, U, in terms of Pressure, P, and Volume, V,

$$U = \frac{PV}{\gamma - 1} \tag{7}$$

when the internal energy and volume are known. Equation (7) is also used to calculate the initial energy U_o of the system. The instantaneous internal energy of the system at any time is defined simply as

$$U = U_o - \text{(Total kinetic energy)} . \tag{8}$$

Equation (7) is employed in lines 195 and 465 of the program, while Equation (8) is used in Line 460.

Equations of Motion

In deriving the equations of motion, it is necessary to know the amount of mass incorporated into the system due to the outer boundaries of the regions sweeping up the ambient gas before them. This change in mass is given by

$$\Delta m = \rho_A \, \Delta V = \rho_A \, (4\pi r^2) \, \Delta r \tag{9a}$$

$$\text{or:} \quad \Delta m \approx 4\pi \, \rho_A r^2 \, v\Delta t \tag{9b}$$

where m is the mass of the gas in the region and r is the radius of the region's boundary. Equation (9a) is used in lines 335 and 375 in the program.

Considering the jetting region first, let P be the pressure of the compressed gas and P_A be the pressure of the ambient gas. Then the equation of motion for this region becomes:

$$\frac{d}{dt}(mv) = (P - P_A) \cdot 4\pi r^2$$

$$\frac{\overline{m\Delta v} + v\Delta m}{\Delta t} = (P - P_A) \cdot 4\pi r^2$$

$$\text{or} \quad \overline{m\Delta v} = 4\pi r^2 \left[(P - P_A) - \rho_A v^2 \right] \Delta t \tag{10}$$

where use has been made of Equation (9b). The left-hand side of the equation is the total change in momentum of the gas inside the region. Employing Equations (4) and (5), this term becomes:

$$\overline{m\Delta v} = \int_0^r \frac{dm}{dx} [(v_f(x) - v_i(x)] \, dx = \int_0^r \rho \, (4\pi x^2) \left[\frac{x}{r} v_f(r) - \frac{x}{r} v_i(r)\right] dx$$

$$= \frac{4\pi}{r} \rho \, [v_f(r) - v_i(r)] \int_0^r x^3 dx = \frac{4\pi}{r} \rho \, \Delta v \, (\frac{r^4}{4})$$

$$= \frac{3}{4} \, (\frac{4}{3} \pi r^3) \, \rho \, \Delta v$$

$$\overline{m\Delta v} = \frac{3}{4} \, m\Delta v \tag{11}$$

where Δv is the change in boundary velocity. It should be noted that the density ρ in the above derivation contains an appropriate constant factor to account for the fact that only a fraction of a total sphere is to be integrated over so that the m in Equation (11) is truly the total mass of compressed gas in the region. Using Equation (11), Equation (10) finally becomes:

$$\frac{3}{4} \, m\Delta v = 4\pi r^2 \left[(P-P_A) - \rho_A \, v^2\right] \Delta t \tag{12}$$

$$\Delta v = \frac{\frac{16}{3} \pi r^2 \left[(P-P_A) - \rho_A v^2\right] \Delta t}{m} \tag{13}$$

This calculation can be found in line 350 of the program.

A similar derivation can be made for the equation of motion for the fragment section except that the equation corresponding to Equation (11) must also include a term for the change in momentum of the fragments themselves. Thus the equation corresponding to Equation (12) becomes:

$$\frac{3}{4} \, m\Delta v + M_s \frac{r_s}{r_1} \Delta v = 4\pi r^2 \left[(P-P_A) - \rho_A v^2\right] \Delta t$$

$$\therefore \Delta v = \frac{\frac{16}{3} \pi r^2 \left[(P-P_A) - \rho_A v^2\right] \Delta t}{(m + \frac{4}{3} \frac{r_s}{r_1} M_s)} \tag{14}$$

where M_s and r_s are the mass and radius of the fragments. This calculation is made in lines 300-305 of the program.

The change in radius is given by the formula

$$r = r_o + vt + \tfrac{1}{2} v t^2$$

$$\text{or } \Delta r = (v + \tfrac{1}{2}\Delta v)\,\Delta t \qquad (15)$$

This calculation appears in lines 310 and 360 of the program.

Corrections

In order to conserve mass and energy, a few small corrections must be made to the above calculations. First consider the ambient gas which is compressed and incorporated into the system as the regions expand outward. The mass of the added gas has already been given by Equation (9a). If the gas is compressed adiabatically from ambient pressure P_A to the pressure P of the compressed gas, then

$$PV^{\gamma} = P_A V_A^{\gamma}$$

$$V = V_A \left(\frac{P_A}{P}\right)^{1/\gamma}$$

$$f4\pi r^2 \Delta r' = f4\pi r^2 \Delta r \left(\frac{P_A}{P}\right)^{1/\gamma}$$

$$\Delta r' = \Delta r \left(\frac{P_A}{P}\right)^{1/\gamma} \qquad (16)$$

where f is the fraction of solid angle occupied by the region, and $\Delta r'$ is the increase in radius due to the newly compressed gas. The results of Equations (15) and (16) must be summed to obtain the position of the region's new boundary. Equation (16) is used in lines 330 and 370 of the program.

Since the velocity is computed by Equation (13) or (14) for the old boundary, the velocity of the new boundary must be found using Equation (4). Therefore, the velocity of the new boundary will be somewhat greater than the value resulting from Equation (13) or (14). This calculation is found in lines 325 and 365 of the program.

An additional quantity of gas is being incorporated into the system simply because the jetting region is expanding sideways as well as outward. The mass concerned is represented by the shaded area in Figure (B-2). The added volume can be thought of as the volume of the shell between r_1' and r_2' multiplied by the fractional change Δf in solid angle of either the jetting or fragment region. Then the additional mass is given by

$$\Delta m = \rho_A \frac{4}{3}\pi (r_2'^3 - r_1'^3)\,\Delta f \qquad (17)$$

This calculation is included in line 395 of the program.

The final correction considered is the addition of the internal energy of the incorporated ambient gas to the total energy of the system. Using the results of Equations (9a) and (17) for the acquired mass Δm, the increase in internal energy becomes

$$\Delta U = \frac{P_A}{\gamma-1} (\Delta V) = \frac{P_A}{\gamma-1} \left(\frac{\Delta m}{\rho_A}\right) \qquad (18)$$

where use has been made of Equation (7). This calculations is performed in line 405 of the program.

Cylindrical Equations

For the cylindrical calculations, the same model is adopted as for the spherical calculations except that axial symmetry is to be used. Figures B-1 and B-2 remain valid for the new symmetry. The essential differences are that the volume is now $\pi r^2 h$ instead of $\frac{4}{3}\pi r^3$ and the surface area is $2\pi rh$ instead of $4\pi r^2$, where h is the height of the right circular cylinder.

The derivation of the cylindrical equations is similar to that of the spherical equations, so that only the results will be listed below with the equation numbers 100 greater than the corresponding spherical equation numbers. The position of the calculations in the cylindrical program is identical to their counterparts in the spherical program. An asterisk (*) following an equation number indicates that the form of the equation is the same for both symmetries.

$$\text{Volume of fragment region} = \left(\frac{r_o}{r_s}\right) \pi r_1^2 h \qquad (101)$$

$$\text{Volume of jetting region} = \left(1 - \frac{r_o}{r_s}\right) \pi r_2^2 h \qquad (102)$$

$$\frac{dV}{dt} = \frac{2}{r} Vv \qquad (103)$$

$$v(x) = \left(\frac{x}{r}\right) v(r) \qquad (104)^*$$

$$\frac{dm}{dx} = \rho 2\pi x h \qquad (105)$$

$$T = \tfrac{1}{2} m v^2(r) \qquad (106)$$

$$U = \frac{PV}{\gamma-1} \tag{107}*$$

$$U = U_o - (\text{Total Kinetic Energy}) \tag{108}*$$

$$\Delta m = \rho_A (2\pi rh)\, \Delta r \tag{109a}$$

$$\Delta m = \rho_A (2\pi rh)\, v\Delta t \tag{109b}$$

$$\overline{m\Delta v} = 2\pi rh\, [(P-P_A) - \rho_A v^2]\, \Delta t \tag{110}$$

$$\overline{m\Delta v} = \frac{2}{3}\, m\Delta v \tag{111}$$

$$\frac{2}{3}\, m\Delta v = 2\pi rh\, [(P-P_A) - \rho_A v^2]\, \Delta t \tag{112}$$

$$\Delta v = \frac{3\pi rh\, [(P-P_A) - \rho_A v^2]\, \Delta t}{m} \tag{113}$$

$$\Delta v = \frac{3\pi rh\, [(P-P_A) - \rho_A v^2]\, \Delta t}{(m + \frac{3}{2}\frac{r_s}{r_1} M_s)} \tag{114}$$

$$\Delta r = (v + \tfrac{1}{2}\Delta v)\, \Delta t \tag{115}*$$

$$\Delta r' = \Delta r \left(\frac{P_A}{P}\right)^{1/\gamma} \tag{116}*$$

$$\Delta m = \rho_A \pi h\, (r_2^2 - r_1^2)\, \Delta f \tag{117}$$

$$\Delta U = \frac{P_A}{\gamma-1} \left(\frac{\Delta m}{\rho_A}\right) \tag{118}*$$

No account has been taken of the motion of the cylinder ends or of the pressure release through them. Therefore, the calculations apply only to the central portion of the cylindrical tank where end-effects can be ignored. With this restriction in mind, h can arbitrarily be set equal to unity in the calculations since the relevant quantities become mass/length and volume/length.

Accuracy

The accuracy of the calculations will ultimately have to be determined by comparison with the experiments which have not yet been performed. All that can be said *a priori* is that when the driving pressure is much greater than ambient pressure, the defects in the model are expected to be negligible and therefore the calculated results (position and velocity vs time) should be good. As would be expected, the driving pressure becomes comparable to ambient pressure very soon after the fragment velocity reaches its maximum value. By this time, essentially all of the energy of the system has been transformed into the kinetic energy of the fragments and compressed gas. Therefore, as long as the fragment velocity is high, the momentum of the fragments will carry them along and the defects in the model can again be expected to be negligible. It is when the fragment velocity begins to drop significantly below the maximum value that the accumulated effects of the model defects should become noticeable.

The Programs

The programs are written in FORTRAN IV language for use on the CDC 6400 computer through the remote teletype units at NOL. The listings for the spherical and cylindrical programs are well annotated and are given in Appendices B-1 and B-2, respectively and are given starting on pages B-10 and B-13 respectively.

Input data are entered into the program between lines 104--155.

Each program contains running checks in the pressure and internal energy of the system and will terminate execution if the specified bounds are exceeded. The tests are made in lines 490--495 and lines 760--770 of each program.

In order to enable a user to abort a run and return to the SETUP mode of INTERCOM, the time-sharing system at NOL, a dummy READ statement is executed at lines 901, 906, and 911 of each program. Any alphanumeric character or set of characters may be entered after which the program will terminate normally.

Results

The calculated position and velocity vs time, as well as the input data, for the three pressure tanks are given in Figures B-3 through B-5. The burst pressure is listed on each figure, to which ambient pressure must be added before entering it into the program at line 115.

The same value of $\gamma = 1.4$ was used for the compressed and ambient gas in all three calculations. If the gas considered were air rather than ideal, the real value of γ for even the most compressed initial condition used would not be less than $\gamma_{min} \approx 1.36$.

Program Listing for Spherical Calculation

```
100 PROGRAM FRAG(INPUT,OUTPUT,TAPE5=INPUT)                    Initializati
105 R0=13.5 <----------Initial radius (inches)
110 R0=R0*2.54 <---------- "      "     (cm)
115 P0=8014.7 <---------- "    pressure (psi)
120 P0=P0/14.5E-6 <------- "      "      (dynes/cm**2)
125 SMASS=140. <-------- Mass of Tank (lbs)
126 SMASS=SMASS*453.5924 Mass of Tank (grams)
127 SMAS43=4.*SMASS/3.
130 DT=1.E-6 <----------Timestep (sec)
135 DTPRNT=.05E-3 <---- Print interval (sec)
137 TEND=3.E-3 <--------End of problem time (sec)
140 GAMMA=1.4
145 GAM1=1./GAMMA
150 RHOAMB=1.225E-3 <---- Ambient Density (gm/cc)
155 PA=1.01325E6 <------- Ambient Pressure (dynes/cm**2)
160 PI=3.14159265358979
165 PI4=4.*PI
170 PI43=PI4/3.
172 PI163=16.*PI/3.
175 RHOP4=RHOAMB*PI4
177 RHOP43=RHOP4/3.
180 PAGRHO=PA/(GAMMA-1.)/RHOAMB
185 V0=PI43*R0**3 <----------Initial volume (cc)
190 AMASS0=RHOAMB*V0*(P0/PA)**GAM1 <---Initial Mass of gas in tank (gm)
195 U=U0=P0*V0/(GAMMA-1.) <---------- "   Internal energy (ergs)
200 RS=R1=R2=R0 <---------- "   (area of tank)/4π (cm**2)
205 RS02=RS*RS
210 VELS=VEL1=VEL2=0.
215 F1=1. <---------- Fraction of sphere in fragment region
220 F2=0. <---------- "    "    "    "  jetting    "
225 AMASS=AMASS0
230 A1MASS=AMASS
235 A2MASS=0.
240 T=0. <---------- Time (sec)
245 TPRNT=-DT/2. <------- Printout time (sec)
247 TEND=TEND+TPRNT
250 P=P0
255 V=V0
260 PRINT 88, P0,PA,R0,V0,GAMMA,RHOAMB,U0,PAGRHO,SMASS,AMASS0,DT
265 88 FORMAT(/4H P0=1PE10.3,4X3HPA=E10.3,4X3HR0=E10.3,4X3HV0=E10.3/
270 + 7H GAMMA=0PF5.2,4X5HRHOA=1PE10.3,4X3HU0=E10.3,4X7HPAGRHO=E10.3/
275 + 7H SMASS=E10.3,4X7HAMASS0=E10.3,4X3HDT=E10.3/)
280 GO TO 200
```

```
300  100 DVEL1=F1*PI163*(R1**2)*((P-PA)-RH0AMB*VEL1**2)*DT
305  DVEL1=DVEL1/(A1MASS+(RS/R1)*SMAS43)
310  DR1=(VEL1+DVEL1/2.)*DT
315  RS=RS+DR1*(RS/R1)
320  PAPG1=(PA/P)**GAM1
325  VEL1=(VEL1+DVEL1)*(1.+(PAPG1*DR1)/(R1+DR1))
330  DR1=DR1*(1.+PAPG1)
335  DA1MAS=F1*RH0P4*(R1**2)*DR1
340  R1=R1+DR1
345  VELS=VEL1*(RS/R1)
350  DVEL2=(F2*PI163*(R2**2)*((P-PA)-RH0AMB*VEL2**2)*DT)/A2MASS
355  IF(A2MASS.EQ.0.) DVEL2=DVEL1
360  DR2=(VEL2+DVEL2/2.)*DT
365  VEL2=(VEL2+DVEL2)*(1.+(PAPG1*DR2)/(R2+DR2))
370  DR2=DR2*(1.+PAPG1)
375  DA2MAS=F2*RH0P4*(R2**2)*DR2
380  R2=R2+DR2
390  F1N=RS02/RS**2
395  DM=RH0P43*(R2**3-R1**3)*(F1-F1N)+DA1MAS+DA2MAS
400  AMASS=AMASS+DM
405  U0=U0+PAGRH0*DM
410  F1=F1N
415  F2=1.-F1
420  V0L1=PI43*(R1**3)*F1
425  V0L2=PI43*(R2**3)*F2
430  VN=V0L1+V0L2
435  A1MASS=AMASS*(V0L1/VN)
440  A2MASS=AMASS-A1MASS
445  T1=.3*A1MASS*VEL1**2
450  T2=.3*A2MASS*VEL2**2
455  TS=.5*SMASS*VELS**2
460  UN=U0-(T1+T2+TS)
465  P=P*(V/VN)*(UN/U)
470  V=VN
475  U=UN
480  T=T+DT
485  IF(T.GE.TPRNT) GO TO 200
490  IF(P.LE.PA.OR.P.GT.P0) GO TO 200
495  IF(U.LE.0.) GO TO 200
500  GO TO 100
700  200 AA=AMASS/AMASS0
720  PRINT 801, T,RS,VELS,P,V,AA
730  PRINT 802, F1,R1,VEL1
740  PRINT 803, F2,R2,VEL2
750  IF(T.GE.TEND) GO TO 700
760  IF(P.LE.PA.OR.P.GT.P0) GO TO 710
770  IF(U.LE.0.) GO TO 720
780  TPRNT=TPRNT+DTPRNT
790  GO TO 100
```

Eq. of motion calcs Fragment Region

Eq. of motion calcs Jetting Region

Increment total mass and energy

Reapportion the mass between the two regions

Calculate new pressure and internal energy

Test for Printout

Printout routine

Parameters are described on page B-3

```
900 700 PRINT 808
901 READ (5,807) AA
902 STOP 77
905 710 PRINT 808
906 READ (5,807) AA
907 STOP 11
910 720 PRINT 808
911 READ (5,807) AA
912 STOP 22
920 801 FORMAT(/1X1P5E13.5,0PF6.3)
930 802 FORMAT(4X3HF1=F6.4,1X1P2E13.5)
940 803 FORMAT(4X3HF2=F6.4,1X1P2E13.5)
950 807 FORMAT(A1)
960 808 FORMAT(//3H A=)
999 END
```

Program Windup

Dummy read for abort purposes

PRINTED OUTPUT

LINE 720

- T = Time (sec)
- RS = Radius of Fragments (cm)
- VELS = Velocity of Fragments (cm/sec)
- P = Pressure of Compressed Gas (dynes/cm^2)
- V = Volume " " " (cc)
- AA = Ratio of Mass of Gas to Original Mass

LINE 730

- F1 = Fraction of Solid Angle for Fragments
- R1 = Outer Radius of Gas in Fragment Region (cm)
- VEL1 = Velocity at Boundary of Fragment Region (cm/se

LINE 740

- F2 =
- R2 =
- VEL2 =

Same as LINE 730 but for the Jetting Region

Program Listing for Cylindrical Calculation

```
100 PROGRAM FRAG(INPUT,OUTPUT,TAPE5=INPUT)
105 R0=6.25 <---Initial radius (inches)                    Initialization
110 R0=R0*2.54 <--- "      "    (cm)
115 P0=474.7 <---Initial pressure (psi)
120 P0=P0/14.5E-6 <--- "      "      (dynes/cm**2)
125 SMASS=.31 <---Mass of Tank/Length (lbs/in)
126 SMASS=SMASS*453.5924/2.54 <-------Mass of Tank/Length (grams/cm)
127 SMASS2=3.*SMASS/2.
130 DT=1.E-6 <-------Timestep (sec)
135 DTPRNT=.05E-3 <-------Print Interval (sec)
137 TEND=3.E-3 <-------End-of-Problem Time (sec)
140 GAMMA=1.4
145 GAM1=1./GAMMA
150 RH0AMB=1.225E-3 <-------Ambient Density (gm/cc)
155 PA=1.01325E6 <---------- "    Pressure (dynes/cm**2)
160 PI=3.14159265358979
165 PI2=PI*2.
170 PI3=PI*3.
175 RH0P=RH0AMB*PI
177 RH0P2=RH0P*2.
180 PAGRH0=PA/(GAMMA-1.)/RH0AMB
185 V0=PI*R0**2 <-------------------------Initial Volume (cc)
190 AMASS0=RH0AMB*V0*(P0/PA)**GAM1 <-------"    Mass of Gas in Tank (gm)
195 U=U0=P0*V0/(GAMMA-1.) <---------------- "    Internal Energy (ergs)
200 RS=R1=R2=R0
205 RS0=RS
210 VELS=VEL1=VEL2=0.
215 F1=1. <----------Fraction of Cylinder in Fragment region
220 F2=0. <---------- "     "      "      " Jetting    "
225 AMASS=AMASS0
230 A1MASS=AMASS
235 A2MASS=0.
240 T=0. <----------Time (sec)
245 TPRNT=-DT/2. <-------Printout time (sec)
247 TEND=TEND+TPRNT
250 P=P0
255 V=V0
260 PRINT 88, P0,PA,R0,V0,GAMMA,RH0AMB,U0,PAGRH0,SMASS,AMASS0,DT
265 88 FORMAT(/4H P0=1PE10.3,4X3HPA=E10.3,4X3HR0=E10.3,4X3HV0=E10.3/
270 + 7H GAMMA=0PF5.2,4X5HRH0A=1PE10.3,4X3HU0=E10.3,4X7HPAGRH0=E10.3/
275 + 7H SMASS=E10.3,4X7HAMASS0=E10.3,4X3HDT=E10.3/)
280 GO TO 200
```

```
100 DVEL1=F1*PI3*R1*((P-PA)-RH0AMB*VEL1**2)*DT
105 DVEL1=DVEL1/(A1MASS+(RS/R1)*SMAS32)
110 DR1=(VEL1+DVEL1/2.)*DT
115 RS=RS+DR1*(RS/R1)
120 PAPG1=(PA/P)**GAM1
125 VEL1=(VEL1+DVEL1)*(1.+(PAPG1*DR1)/(R1+DR1))
130 DR1=DR1*(1.+PAPG1)
135 DA1MAS=F1*RH0P2*R1*DR1
140 R1=R1+DR1
145 VELS=VEL1*(RS/R1)
150 DVEL2=(F2*PI3*R2*((P-PA)-RH0AMB*VEL2**2)*DT)/A2MASS
155 IF(A2MASS.EQ.0.) DVEL2=DVEL1
160 DR2=(VEL2+DVEL2/2.)*DT
165 VEL2=(VEL2+DVEL2)*(1.+(PAPG1*DR2)/(R2+DR2))
170 DR2=DR2*(1.+PAPG1)
175 DA2MAS=F2*RH0P2*R2*DR2
180 R2=R2+DR2
190 F1N=RS0/RS
195 DM=RH0P*(R2**2-R1**2)*(F1-F1N)+DA1MAS+DA2MAS
200 AMASS=AMASS+DM
205 U0=U0+PAGRH0*DM
210 F1=F1N
215 F2=1.-F1
220 V0L1=PI*(R1**2)*F1
225 V0L2=PI*(R2**2)*F2
230 VN=V0L1+V0L2
235 A1MASS=AMASS*(V0L1/VN)
240 A2MASS=AMASS-A1MASS
245 T1=.25*A1MASS*VEL1**2
250 T2=.25*A2MASS*VEL2**2
255 TS=.5*SMASS*VELS**2
260 UN=U0-(T1+T2+TS)
265 P=P*(V/VN)*(UN/U)
270 V=VN
275 U=UN
280 T=T+DT
285 IF(T.GE.TPRNT) G0 T0 200
290 IF(P.LE.PA.0R.P.GT.P0) G0 T0 200
295 IF(U.LE.0.) G0 T0 200
300 G0 T0 100
700 200PAA=AMASS/AMASS0
720 PRINT 801, T,RS,VELS,P,V,AA
730 PRINT 802, F1,R1,VEL1
740 PRINT 803, F2,R2,VEL2
750 IF(T.GE.TEND) G0 T0 700
760 IF(P.LE.PA.0R.P.GT.P0) G0 T0 710
770 IF(U.LE.) G0 T0 720
780 TPRNT=TPRNT+DTPRNT
790 G0 T0 100
900 700 PRINT 808
```

Eq. of motion calcs fragment region

Eq. of motion calcs Jetting region

Increment total mass and energy

Reapportion the mass between the two regions

Calculate new pressure and interna energy

Test for printout

Printout routine

Parameters are described on page B-3

```
901 READ (5,807) AA
902 STOP 77
905 710 PRINT 808
906 READ (5,807) AA
907 STOP 11
910 720 PRINT 808
911 READ (5,807) AA
912 STOP 22
920 801 FORMAT(/1X1P5E13.5,0PF6.3)
930 802 FORMAT(4X3HF1=F6.4,1X1P2E13.5)
940 803 FORMAT(4X3HF2=F6.4,1X1P2E13.5)
950 807 FORMAT(A1)
960 808 FORMAT(//3H A=)
999 END
```

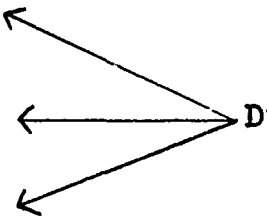

Program Windup

Dummy read for abort purposes

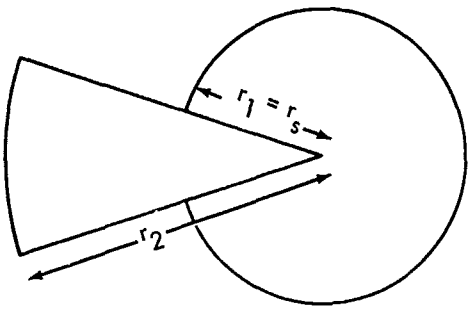

TYPICAL EARLY-TIME GEOMETRY

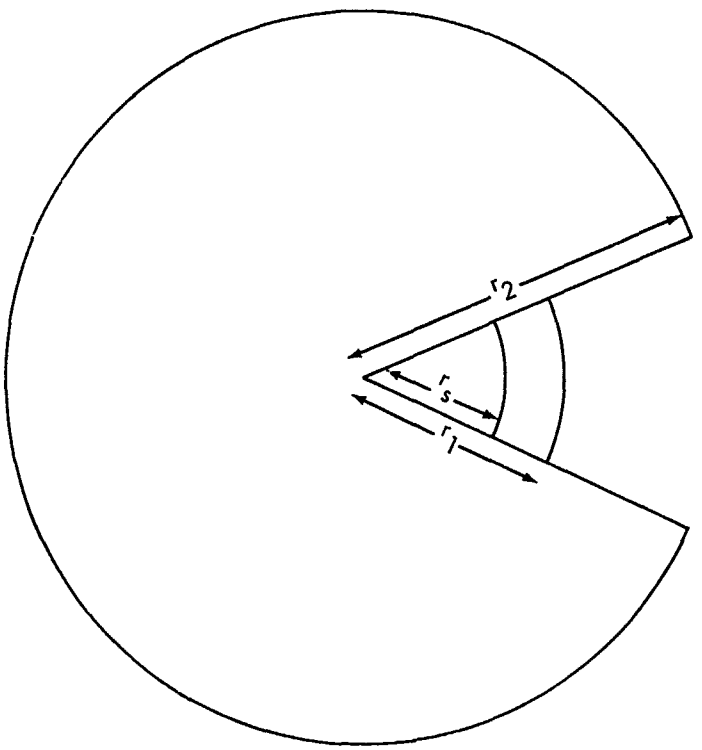

TYPICAL LATE-TIME GEOMETRY

r_s = RADIUS OF TANK FRAGMENTS
r_1 = RADIUS OF COMPRESSED GAS AHEAD OF FRAGMENTS
r_2 = RADIUS OF JETTING GAS

FIG. B-1. BASIC GEOMETRY FOR THE CALCULATIONS

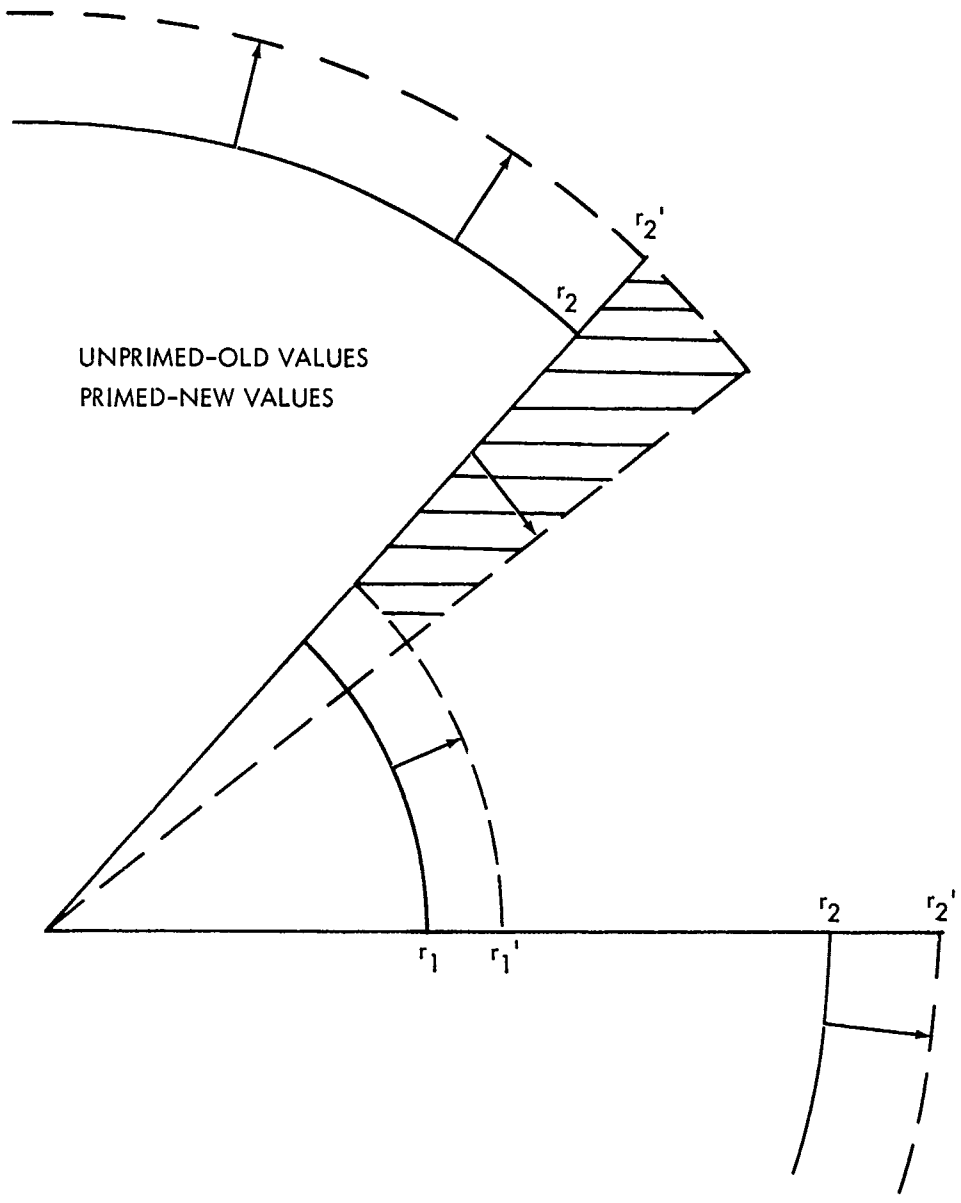

FIG. B-2. GEOMETRY FOR MASS CORRECTION

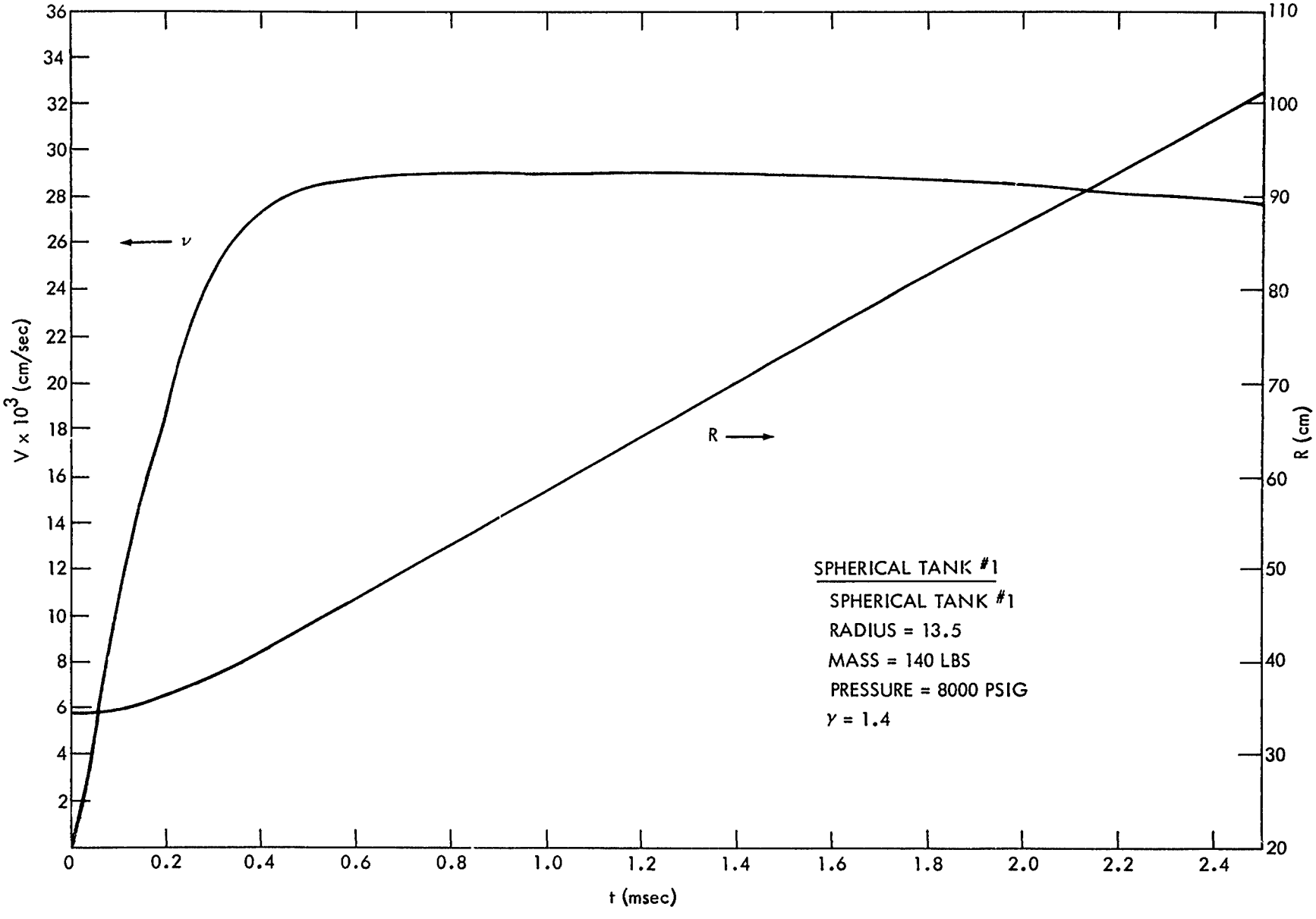

FIG. B-3. FRAGMENT RADIUS AND VELOCITY VS TIME

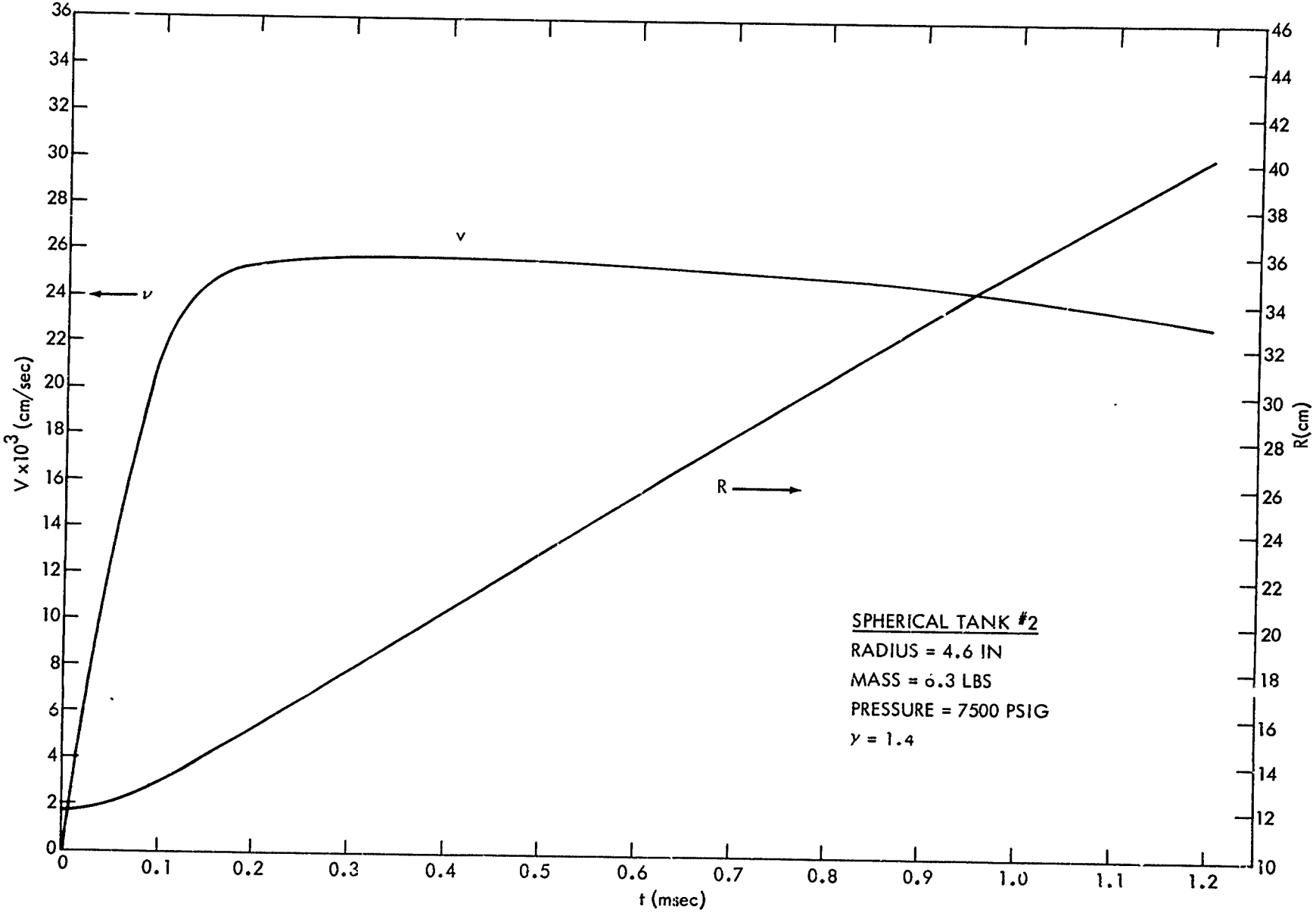

FIG. B-4. FRAGMENT RADIUS AND VELOCITY VS TIME

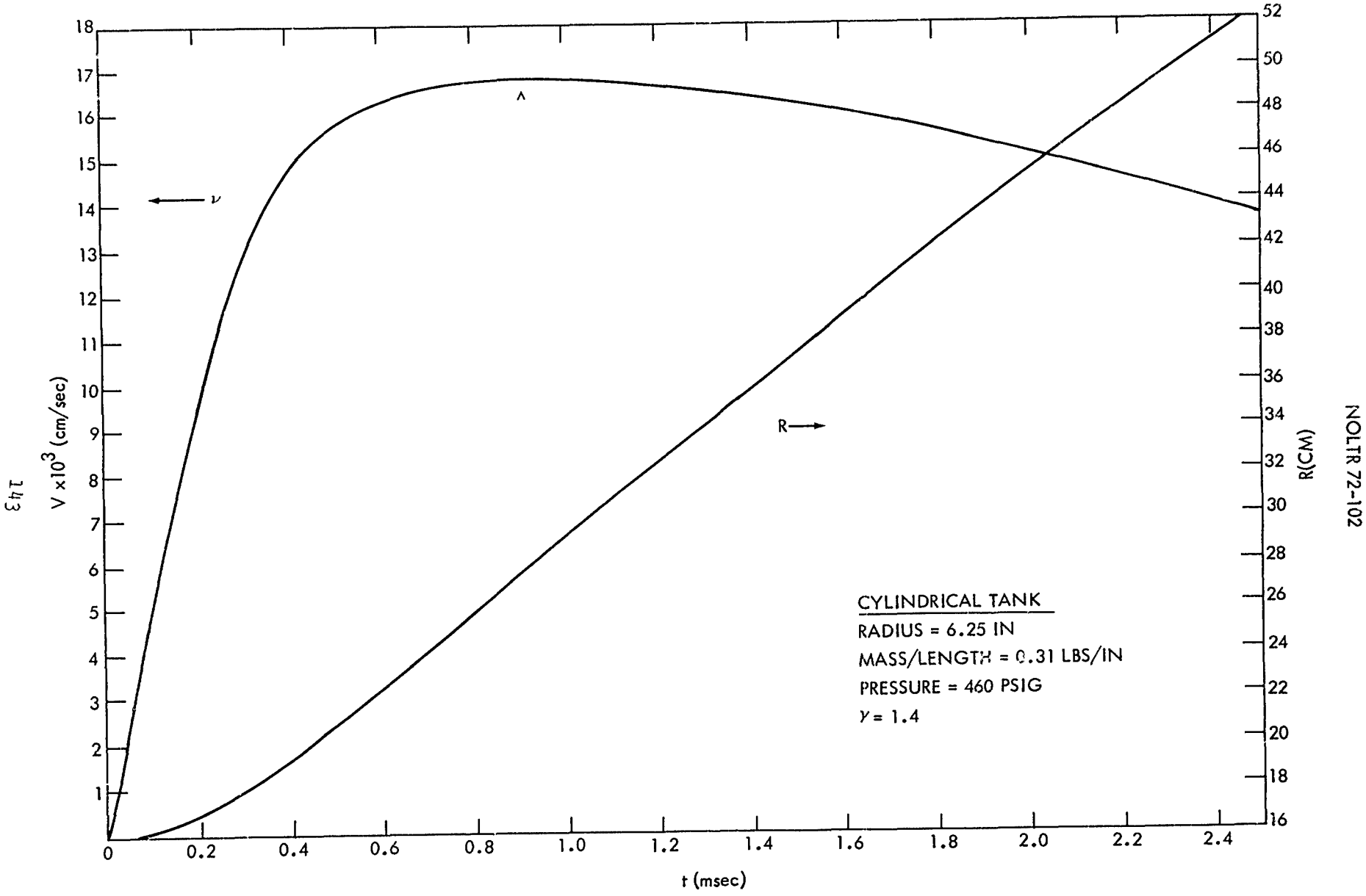

FIG. B-5. FRAGMENT RADIUS AND VELOCITY VS TIME

UNCLASSIFIED

Security Classification

DOCUMENT CONTROL DATA - R & D

Security classification of title, body of abstract and indexing annotation must be entered when the overall report is classified)

1 ORIGINATING ACTIVITY (Corporate author) Naval Ordnance Laboratory Silver Spring, Maryland 20910	2a. REPORT SECURITY CLASSIFICATION Unclassified 2b. GROUP

3 REPORT TITLE

Blast and Fragment Hazards from Bursting High Pressure Tanks

4 DESCRIPTIVE NOTES (Type of report and inclusive dates)

5. AUTHOR(S) (First name, middle initial, last name)

Joseph F. Pittman

6. REPORT DATE	7a. TOTAL NO. OF PAGES	7b. NO. OF REFS
17 May 1972	156	8

8a. CONTRACT OR GRANT NO. b. PROJECT NO NOL Task #577/NASA Work Unit X01 c. d.	9a. ORIGINATOR'S REPORT NUMBER(S) NOLTR 72-102 9b. OTHER REPORT NO(S) (Any other numbers that may be assigned this report)

10. DISTRIBUTION STATEMENT

Distribution limited to U. S. Government Agencies only; Test and Evaluation. Date statement applied 5/24/72. Other requests for this publication must be referred to NOL, Code 241.

11. SUPPLEMENTARY NOTES	12. SPONSORING MILITARY ACTIVITY National Aeronautics and Space Administration Kennedy Space Center, Florida

13 ABSTRACT

Five pressure vessels that are used in the flight hardware of spacecraft were inflated until they burst. Airblast and fragment parameters were measured to evaluate the hazards from the accidental rupture of such tanks during their handling, checkout, and use. Tank volumes ranged up to 6 ft^3, skin thicknesses up to 0.368 inches, and burst pressures up to 8,000 psi.

Airblast results showed that tank rupture generated shockwave overpressures and impulses at high enough levels to be a significant hazard to personnel and equipment. Rupture blast energy could not be equated to a single TNT blast yield. The tanks burst into as many as 60 fragments, some weighing several pounds. These fragments attained maximum velocities of about 1400 ft/sec.

DD FORM 1 NOV 1473 (PAGE 1)

S/N 0101-807-6801

UNCLASSIFIED

Security Classification

KEY WORDS	LINK A		LINK B		LINK C	
	ROLE	WT	ROLE	WT	ROLE	WT
Hazards from high pressure tank rupture Airblast from pressure release Tank fragment hazards						